nature communications

Article

https://doi.org/10.1038/s41467-024-45246-7

Molecular-level architecture of *Chlamydomonas reinhardtii's* glycoprotein-rich cell wall

Received: 12 December 2022

Accepted: 19 January 2024

Published online: 02 February 2024

Check for updates

Alexandre Poulhazan[1], Alexandre A. Arnold[1], Frederic Mentink-Vigier[2], Artur Muszyński[3], Parastoo Azadi[3], Adnan Halim[4], Sergey Y. Vakhrushev[4], Hiren Jitendra Joshi[4], Tuo Wang[5], Dror E. Warschawski[6] & Isabelle Marcotte[1]

Microalgae are a renewable and promising biomass for large-scale biofuel, food and nutrient production. However, their efficient exploitation depends on our knowledge of the cell wall composition and organization as it can limit access to high-value molecules. Here we provide an atomic-level model of the non-crystalline and water-insoluble glycoprotein-rich cell wall of *Chlamydomonas reinhardtii*. Using in situ solid-state and sensitivity-enhanced nuclear magnetic resonance, we reveal unprecedented details on the protein and carbohydrate composition and their nanoscale heterogeneity, as well as the presence of spatially segregated protein- and glycan-rich regions with different dynamics and hydration levels. We show that mannose-rich lower-molecular-weight proteins likely contribute to the cell wall cohesion by binding to high-molecular weight protein components, and that water provides plasticity to the cell-wall architecture. The structural insight exemplifies strategies used by nature to form cell walls devoid of cellulose or other glycan polymers.

Plants and algae are efficient producers of biofuel precursors, textile and paper fibers, pharmaceutical compounds, and food supplements[1–3]. A central source of these products is the carbohydrate-rich cell wall, commonly found in both land plants and microalgae, by which it regulates cell integrity and many other physiological processes such as stress response[4]. Microalgae are a low-cost green production platform with rapid growth and facile scalability, ease of genetic modification, able to grow under hetero- or phototrophic conditions. As eukaryotes, they also offer a wide post-translational modification machinery used for recombinant protein expression and synthetic biology[5,6]. However, to better exploit microalgae for industrial applications, we imperatively need an in-depth understanding of the molecular-level architecture of their cell wall[7].

Chlamydomonas reinhardtii is a freshwater microalga and stands out as one of the most abundantly studied. It is a model organism for directed mutagenesis applied to different research fields including biochemistry, physiology, and genetics[8,9]. In 2007, the fourth complete report of the *Chlamydomonas* genome revealed that it shares 706 protein families with humans[10]. The cell wall of *C. reinhardtii* has been investigated mainly from the 1970s to the late 2000s[11,12]. In contrast with the cellulose-based cell walls widespread amongst microalgae, that of *C. reinhardtii* is built on glycoprotein-rich layers reminiscent of extensins in higher plants[13]. Specifically, it is composed

[1]Department of Chemistry, Université du Québec à Montréal, Montreal, QC H2X 2J6, Canada. [2]National High Magnetic Field Laboratory, Florida State University, Tallahassee, FL 32310, USA. [3]Complex Carbohydrate Research Center, University of Georgia, Athens, GA 30602, USA. [4]Copenhagen Center for Glycomics, University of Copenhagen, Copenhagen, Denmark. [5]Department of Chemistry, Michigan State University, East Lansing, MI 48824, USA. [6]Laboratoire des Biomolécules, LBM, CNRS UMR 7203, Sorbonne Université, École Normale Supérieure, PSL University, 75005 Paris, France.
e-mail: wangtuo1@msu.edu; dror.warschawski@sorbonne-universite.fr; marcotte.isabelle@uqam.ca

 https://doi.org/10.1038/s41467-024-45246-7

of five dense glycoprotein-rich layers that form a protective shell, as seen by electron microscopy (EM)[14–17]. The water-insoluble core of the cell wall is made of three central layers, named W4/W6/W4, that contain fibrous material and denser objects described as granules[18,19] (Fig. 1a). According to previous studies, this central triplet comprises a large number of proteins, including high molecular weight hydroxyproline-rich glycoproteins (HRGPs), i.e., GP1 (~300 kDa), GP1.5 (170 kDa), GP2 (155 kDa, 110 kDa after deglycosylation) and GP3 (135 kDa, 65 kDa once deglycosylated)[16,20]. Low molecular weight proteins ranging from 30 kDa to 50 kDa referred to as "14-3-3" are also found and believed to act as cell wall cross-linking precursors[19–22]. These "14-3-3" proteins are rich in serine (Ser) and threonine (Thr), but not fully sequenced[22]. The remainder of the cell wall, also called the "insoluble cell wall" since it cannot be extracted even using chaotropic agents, is composed of a membrane-anchoring protein layer (W1), a dense layer with fibrillar proteins (W2), and an outer fibrillar surface (W7)[14,20]. The molecular mechanisms by which all these various glycoproteins interact are still unknown.

Previous investigations of *C. reinhardtii* cell wall provided a partial sequencing and composition of HRGPs by chromatography and mass spectrometry (MS), while EM revealed the layered architecture. HRGPs were shown to be glycosylated by short O-oligosaccharides containing 1–5 residues in which arabinose (Ara) and galactose (Gal) are the most abundant. These oligosaccharides would be linked to HRGP domains containing Ser or polyproline (PP) helices[19,23–25]. Traces of mannose (Man) were also reported, accounting for up to 7% of the overall glycan content, as well as β(1-2)-linked L-Arabinose (Ara) disaccharides substituted with galactofuranoses (Gal*f*) and O-methylation[26]. While O-glycosylation is the only post-translational modification described so far in the cell wall, an N-glycosylation pathway has also been described in *C. reinhardtii* that involved the linking of two N-acetylglucosamines (GlcNAc) and two Man to an asparagine (Asn)[27].

Here we use solid-state nuclear magnetic resonance (ssNMR) to determine the chemical nature and dynamics of the different water-insoluble but chaotrope-soluble cell wall constituents at the molecular level, without compromising its integrity since no extensive purification or digestion of the extracted cell wall is required. We establish the complete amino acid and glycan profile and reveal preferential contacts between carbohydrates and proteins. We also expose the presence of conformational domains and potential O- and N-glycosylation on the proteins, as well as the abundance of Man residues corresponding to low molecular-weight glycoproteins (LWGPs). We show that oligosaccharides are short, and reveal the segregation of glycan- and protein-rich domains with different hydration and dynamics. This work provides a molecular-level refinement of the complex protein-rich cell wall architecture of an aquatic microorganism in which glycans play a key role, and highlights the role of water in this superstructure.

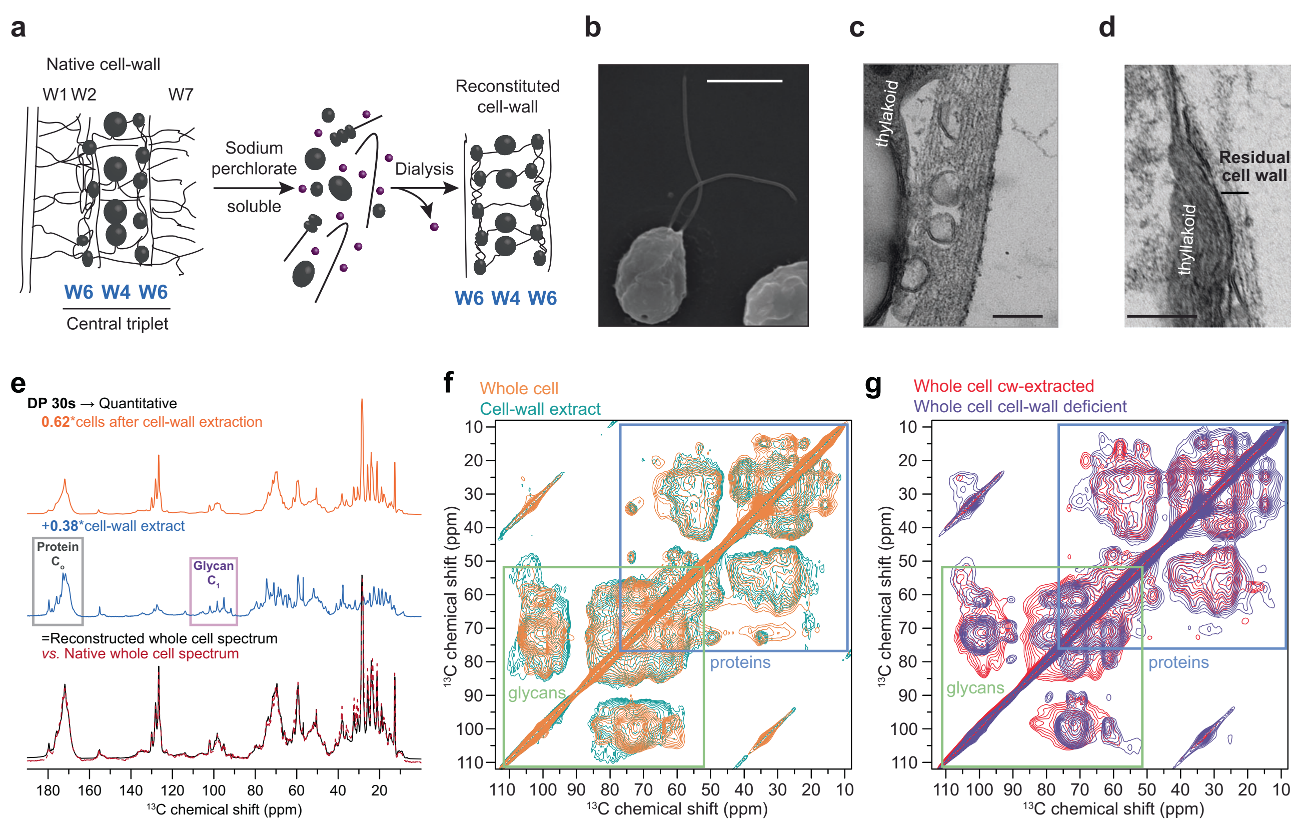

Fig. 1 | Cell wall extraction of *C. reinhardtii* preserves carbohydrates and cell surface. **a** Previously described layered organization and extraction protocol to reconstitute the native central triplet of the cell wall, based on the overall assembly observed by EM[19] (adapted from Goodenough et al.[19], used with permission of Rockefeller University Press; permission conveyed through Copyright Clearance Center, Inc). **b** SEM image of whole *wt C. reinhardtii* cells (scale bar: 5 µm). **c** TEM image of *C. reinhardtii* cell surface before cell wall extraction reveals a layered structure and large spherical components or cavities (scale bar: 200 nm). **d** TEM image after wall extraction shows remnants on the cell surface (scale bar: 200 nm). **e** 1D ^{13}C ssNMR of the cells after extraction (top; orange), cell wall extract (middle; blue), and intact cells (bottom; red dash line). The weighted sum (bottom; black) of the cell wall extract and the cell residual matches the spectrum of the intact cells, indicating no loss during the extraction protocol and that the cell wall accounts, here, for 38% of the overall intensity (matching sample reconstitution performed using Table 1). **f** Similarity of the intact whole-cell MAS-DNP (orange) and extracted cell wall (teal) spectra. **g** MAS-DNP spectra of *wt* cells after wall extraction (red) and cell-wall deficient *cw15* strain (purple) show that the central triplet, absent on the *cw15* strain, is extracted in the *wt* strain. MAS-DNP ^{13}C-^{13}C DARR experiments were recorded on a 600 MHz/395 GHz spectrometer at 100 K and 8 kHz MAS frequency. SEM/TEM (panels **b**–**d**) images were recorded in triplicate on independent biological replicates giving similar results.

https://doi.org/10.1038/s41467-024-45246-7

Results

Cell wall extraction retains the macromolecular core

We extracted *C. reinhardtii*'s water-insoluble (but chaotrope-soluble) cell wall constituents and verified if their composition was identical to intact cell walls. The cell wall was extracted with chaotropic agents, then slowly reconstituted after dialysis. We employed a milder protocol with fewer dialysis steps compared to the original method[18,20], to preserve the minor constituents of the cell wall (Fig. 1a). Scanning electron microscopy (SEM) (Fig. 1b) and transmission electron microscopy (TEM) (Fig. 1c) respectively show the intact microalga and the characteristic layered organization of the cell wall described in the literature. Cells were also undamaged after wall extraction, as demonstrated by the intact membrane bilayer and internal organelles such as thylakoids, partially visible in Fig. 1d. This was further confirmed by flow cytometry analysis, which revealed that about 80% of the cells remained alive and metabolically active after wall extraction.

The composition of the cell wall extract was also compared to intact cells using both the standard 1D ssNMR (Fig. 1e) and Magic-Angle Spinning Dynamic Nuclear Polarization (MAS-DNP) (Fig. 1f, g), which uses microwaves and a polarizing radical to provide a tremendous increase in sensitivity[28,29]. Here, we observed a 45-fold enhancement in NMR signals (Supplementary Fig. 1) but a loss in spectral resolution due to the low temperature required by this method. The weighted sum of the two spectra recorded on the cell wall extracts and the remainders after extraction correspond exactly to the spectrum of the intact cell walls (Fig. 1e), indicating no loss during our extraction protocol.

The 2D ^{13}C-^{13}C correlation spectra of both intact *C. reinhardtii* cells and extracts of cell walls exhibit a high degree of similarity. This is evident in the overlap of MAS-DNP spectra at 100 K, which show signals exclusively from the outer region of the cell (Fig. 1f), as well as in the data collected at higher temperature (283 K), which encompass all cellular components (Supplementary Fig. 2). This congruence confirms that the preservation of cell wall structure in the extract. It also suggests that the polarizing radical does not diffuse through the membrane but preferentially localizes in the cell wall. The minor differences can be ascribed to the fact that only the W4 and W6 layers were removed when extracting the cell wall, leaving the fibrillar W1, W2 and W7 layers attached to the cell surface (Fig. 1a). Because MAS-DNP only enhances and detects signals from the cell surface constituents, the intensity is thus improved, explaining for instance, the glycan-protein intermolecular contacts seen on Fig. 1f. This was also confirmed by the similarities between the MAS-DNP spectra of the cell-wall deficient strain (*cw15*) and the wild-type (*wt*) strain after cell-wall extraction (Fig. 1g). The *cw15* mutant has compromised cell wall synthesis[8]. The remaining wall components resemble the cell-wall outer layer[30], resist chaotropic extraction[31] and therefore likely correspond to the residual chaotrope-insoluble W1, W2 and W7 layers. The resemblance between the MAS-DNP spectra of *cw15* cells and the *wt* sample after cell-wall extraction further confirms that our extracts are composed of the cell wall central triplet.

Glycan composition of the cell-wall extract

We determined the complete glycan and amino acid profile in *C. reinhardtii's* cell wall extracts. We used the flagella-deficient *bald2* strain to avoid the occurrence of large flagella-associated proteins (~200 kDa) that could contaminate cell-wall extracts during the growth cycle. Our results were independent of the strain type, i.e., with (*wt*) or without (*bald2*) flagella, the growth conditions or cell differentiation (sexually competent, differentiated or not), as revealed by the protein composition of different cell wall extracts obtained using polyacrylamide gel electrophoresis (Fig. 2a) or ssNMR (Supplementary Fig. 3 and Supplementary Table 1). The amino acid profile of the protein bands separated by SDS-PAGE was also analyzed using HPLC on each cut band. The unlabeled and ^{13}C-labeled cell-wall protein profiles were also comparable using these methods.

Using fully relaxed 1D ^{13}C ssNMR spectra, we compared the integrals of peaks characteristic of carbohydrates (anomeric C_1) or proteins (carbonyl CO) (Fig. 1e; middle row). A 1:3 glycan/protein molar ratio was determined, indicating that a considerable part of the cell wall is composed of glycans, in agreement with the literature[27]. This ratio can reach 1:2 because of the large proportion of Gln/Glu and Asn/Asp - revealed by the amino acid analysis described below - that comprise two carbonyl groups. The composition of the cell wall extracts was then monitored using SDS-PAGE and compared to the literature[14]. The amino acid analysis of the SDS-PAGE bands of the native cell wall confirms that the high molecular weight proteins in cell wall extracts are rich in hydroxyproline (Hyp) and correspond to the reported HRGPs (Table 1). We found a higher abundance of low molecular weight proteins following our milder extraction protocol (Fig. 2a).

Quantitative analysis of the saccharide content and bonds of *C. reinhardtii*'s reconstituted cell wall using our protocol[32] was achieved using MS (Fig. 2b) and 2D ^{13}C-^{13}C ssNMR spectra (Fig. 2c and Supplementary Fig. 4). We found a majority of the residues being Man (52%), followed by Gal (15%), Ara (15%), GlcNAc (11%), non-modified glucose (Glc) (3%), rhamnose (Rha) (3%) and xylose (Xyl) (3%), as reported in Fig. 2d. A significant proportion of Glc is N-acetylated (GlcNAc), as previously but not quantitatively reported in *Chlamydomonas* cells[33]. One-third of anomeric carbons ascribed to Man and Gal have very low chemical shift values, and can therefore be assigned to non-reducing terminal groups of oligosaccharides (pink bars on Fig. 2d)[34,35]. Their abundance indicates the presence of short oligosaccharides, with approximately two glycan units followed by a terminal glycan. In addition, no Ara but almost all Gal are identified as terminal groups, confirming that most Ara oligosaccharides would be terminated by a Gal residue[26]. These results are supported by the high proportion of non-reducing terminal groups detected by semi-quantitative GC-MS (see t-X glycans on Fig. 2b).

The GC-MS analysis of glycan linkages demonstrates the high variety of glycosidic bonds in *C. reinhardtii*'s cell wall (Supplementary Table 2). It also helps evaluate the efficiency of our cell wall extraction protocol by comparing the glycan composition of whole cells (dominated by starch Glc), cells after wall extraction, and the extracted wall (Supplementary Table 7), showing that about 40% of the cell's glycans are contained in the cell wall, and that almost no sugar was lost or altered during the extraction and reconstitution (Supplementary Table 8 and Supplementary Fig. 2).

A striking finding is the high abundance of Man and GlcNAc in *C. reinhardtii*'s cell wall, which has been debated in the literature[27,36]. While Ara and Gal are generally presented as the most abundant glycans in HRGPs[11,26,37], earlier work showed that a water-soluble fraction of *Chlamydomonas* cell wall was rich in Man[38] and, more recently, that GP3 in the cell wall was heavily mannosylated[24]. The presence of glycoproteins rich in Hyp interacting with Man-rich lectin-like domains involved in the cell wall of *C. reinhardtii* has also been demonstrated in cell-differentiated zygotes[17]. Finally, recent work reported oligomannose glycans and 6-O-methylmannose in soluble and membrane-bound proteins of *C. reinhardtii*[36], as well as two putative mannosyltransferases, consistent with the presence of mannosylation[39]. The Man depletion after cell wall extraction and in the *bald2* mutant (Supplementary Tables 7 and 8), together with the MAS-DNP detection of Man signals in the intact cell walls, are strong indications that Man-rich glycoproteins are part of the cell wall, or at least strongly associated with it.

Amino acid composition and LWGP proteins

We then assigned and quantified the protein content using 2D ^{13}C refocused INADEQUATE spectra and HPLC methods (Fig. 3a,

https://doi.org/10.1038/s41467-024-45246-7

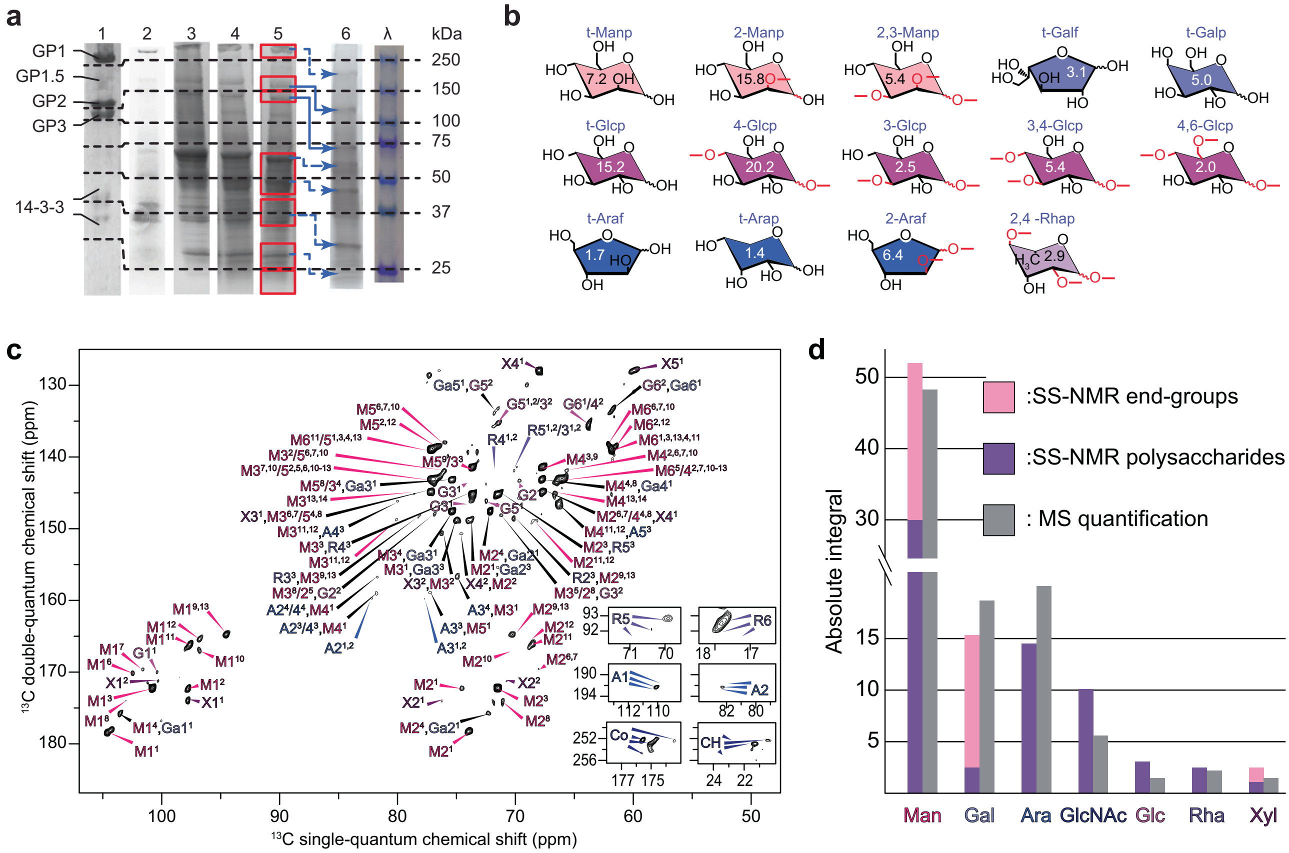

Fig. 2 | *C. reinhardtii* cell wall composition analyzed by electrophoresis, MAS and ssNMR. a SDS-PAGE (performed at least in triplicate and giving similar results) of cell wall extracts shows HRGPs and additional enrichment in low molecular weight proteins (<100 kDa). Lane 1: cell wall extract published by Goodenough et al.[14], used with permission; lane 2: cell wall extracted from the *bald2* strain; lane 3: cell wall extracted from sexually differentiated cells; lane 4: ^{13}C-labeled *wt* cell wall; lane 5: ^{13}C-labeled *bald2* cell wall used for ssNMR assays; lane 6: deglycosylated ^{13}C-labeled *bald2* cell wall with tentative molecular weight shift assignment; lane λ: molecular weight ladder. **b** Representative structures of glycosidic linkages identified by GC-MS (carbons involved in linkages shown in red). The numbers for each unit correspond to the percentage of such linkages obtained semi-quantitatively (Supplementary Table 2). **c** ^{13}C-^{13}C through-bond ssNMR INADEQUATE spectrum of extracted C. *reinhardtii* cell walls used for carbohydrate and amino acid identification and quantification. A XZ^Y glycan notation is used, where X is the type of sugar, Y the spin system number, and Z the carbon number (for example, Ga6[1] is the carbon 6 of the Gal unit number 1). Insets at the bottom right of the spectrum show the unique signals of Rha C_6 (top), Ara C_1 (middle), and acetyl/methyl group from GlcNAc (bottom). **d** SsNMR and GC-MS quantification of glycan units; End groups/oligosaccharides are in pink, and polysaccharides in purple, both differentiated by their C_1 chemical shifts (Supplementary Tables 3–6). Source data are provided as a Source Data file.

Supplementary Figs. 5–7 and Supplementary Tables 9–12). According to ssNMR, the most abundant amino acid residues in the cell wall extract are alanines (13%), followed by glutamines and glutamates (9% each), glycines (8%), asparagines and aspartates (6% each). We note that ~18% of the amino acids can be glycosylated. The relative abundance of the amino acids in the cell wall extract determined by HPLC, which is more sensitive and reproducible throughout different samples (Supplementary Table 12), is consistent with the ssNMR results for most amino acids (Table 1). No cysteine (Cys) or tryptophan (Trp) residues were detected by either technique, while histidine (His) or Hyp residues could not be detected by ssNMR, their abundance being below the 2% sensitivity threshold. Hyp was however detected using 2D ^{13}C-^{13}C-PDSD and MAS-DNP at low temperature (see below and Supplementary Fig. 8) but could not be quantified.

Table 1 and Fig. 3c reveal that Hyp is abundant (up to 22%) in GP1 to GP3, consistent with previous studies reporting that this residue constitutes up to one third of the total amino acid content in HRGPs[12,14,22,37,40,41]. Its overall proportion, however, is very low (~3%) in whole *C. reinhardtii* cell walls since HRGPs constitute only ~20% of the total protein content, based on SDS-PAGE image treatment (Figs. 2a and 3b, Table 1). This is also true for other amino acids, such as Ser for example.

To eliminate all glycan units from the cell wall extract without degrading the proteins, we performed a chemical deglycosylation since it allows removing both O- and N-linked glycosylations[42]. The deglycosylation led to a shift of all SDS-PAGE protein bands, proving that the low molecular weight proteins are also glycosylated (Fig. 2a, lane 5 *vs.* 6), to an approximate level of 20 % assessed by the change in molecular weight.

We were thus able to identify four new groups of low molecular weight glycoproteins (LWGPs) that we will refer to as GP4 to GP7, which contribute to almost 80% of the amino acids content in our reconstituted cell wall, and have a very low Hyp content. The molecular weights of GP4 (~50 kDa) and GP5 (~37 kDa) correspond to those reported for the "14-3-3" protein fraction[21,22]. GP4 and GP5 contribute *ca.* 35% of the amino acids, while the two lighter protein bands, GP6 (~25 kDa) and GP7 (<20 kDa), account for the *ca.* 45% left. LWGPs as well as "14-3-3" proteins, could be considered as "non-canonical cell-wall proteins"[43,44], but they do survive the extraction protocol, two dialysis steps, renaturing non-chaotropic conditions and centrifugation. They should therefore be considered either as part of the cell wall, or strongly interacting with it. The identification of a greater variety of glycoproteins in our cell wall extract, without any significant cell damage, confirms that our protocol is milder, and

Table 1 | Amino acid composition of the cell wall and specific proteins

			HRGPs			LWGPs			
	Total cell wall		GP1/1.5	GP2	GP3	GP4	GP5	GP6	GP7
	%mole		298/280 kDa	165 kDa	140 kDa	~50 kDa	~37 kDa	~25-20 kDa	<20 kDa
	ssNMR	HPLC	%mole	%mole	%mole	%mole	%mole	%mole	%mole
Gln	9.1	19.0 (0.3)	7.2	5.6	19.5	17.3	18.7	23.0	15.3
Glu	8.8								
Asn*	6.4	14.8 (0.3)	5.6/4.7/9.9	7.0/8.1	2.5/1.6	10.2	14.3	19.5	12.9
Asp	5.9								
Ala	13.1	10.9 (0.3)	9.4/10.1/8.4	10.5/8.5	15.4/10.2	8	9.9	11.9	8.7
Gly	8.5	8.0 (0.3)	11.6/6.6/23	7.8/8.5	10.7/11.0	8.2	10.3	6.5	10.8
Leu	8.0	5.5 (0.3)	3.7/2.9/5.1	7.5/7.0	0.2/7.0	10.2	4.8	4.6	8.4
Lys	6.2	5.3 (0.1)	2.7/3.6/4.2	3.0/3.0	7.1/4.5	5.8	6.5	3.4	8.2
Ser*	6.2	5.0 (0.2)	14.4/15.8/10.7	7.0/8.3	8.1/9.3	3.3	5	3.2	5.3
Pro	5.8	4.8 (0.2)	3.4/2.7/3.2	5.5/7.7	0.7/4.5	6.6	6.1	4.3	2.7
Val	5.7	5.6 (0.3)	3.4/4.4/3.0	7.3/5.7	5.3/5.9	9.7	4.1	4.3	5.1
Arg	5.1	3.5 (0.3)	1.9/1.7/2.7	3.4/3.0	3.6/2.1	3.8	4	2.4	5.5
Thr*	4.3	4.7 (0.4)	5.3/4.2/4.3	6.7/6.6	7.7/7.4	2.5	3.9	3.8	4.3
Met	2.5	1.6 (0.2)	1.1/0.8/0.5	1.6/1.0	1.4/0.9	1.6	2.7	1.3	1.9
Ile	2.2	3.1 (0.3)	3.2/3.3/2.3	4.2/1.3	2.2/3.2	5.9	3.1	4.0	2.9
Tyr	1.5	2.4 (0.2)	1.9/0.9/1.4	3.3/3.6	2.6/1.2	2	3.7	2.4	3
Phe	0.7	2.8 (0.4)	2.2/1.3/2.3	4.4/3.8	6.4/3.6	3.1	1.5	2.8	3.5
His	*NA*	2.0 (0.1)	0.6/0.8/1.5	0.8/0.2	1.0/1.0	1.4	1.3	1.5	1.4
Hyp*	*NA*	1.0 (0.1)	22.4/32.3/15.5	14.4/14.7	6.6/5.7	0.4	0.1	1.1	0.1
% SDS-page			5.3	7.2	9.3	10.6	24.3	35.1	8.3
			21.8			78.2			

Amino acid composition of the cell wall determined by ssNMR and HPLC (values in brackets correspond to standard deviation of three different HPLC samples) (see Supplementary Table 12 for replicates), and of specific proteins separated by SDS-PAGE and analyzed by HPLC. Published values are indicated for comparison and underlined[19,24]. Relative protein proportions (bottom two lines) were evaluated on Coomassie blue stained SDS-PAGE. The asterisk (*) symbol indicates amino acids that can be glycosylated.

is also an indication that its protein composition is closer to that of the native microalga.

To summarize, our results show that the amino acid content in the cell wall extract is dominated by Gln/Glu, Asn/Asp, Ala and Gly, with the lower weight GP4 to GP7 enriched in Gln/Glu and Asn/Asp. Interestingly, with the exception of Gln/Glu, these abundant residues have been reported to play an important role in plant cell walls[45]. Asparagine is known to be involved in N-linked glycosylation, while Ala-rich and Hyp-containing cell walls, possibly associated with arabinogalactan, have been reported in plants and fungi[46]. Also, Gly-rich proteins are involved in the formation of β-pleated sheet structures important for cell mechanical resistance in plant cell walls[47]. Altogether, *C. reinhardtii* probably shares some structural features with plants in terms of amino acid composition of cell wall proteins.

β-sheet domains, protein-glycan and inter-glycan contacts

The protein secondary structure was probed by analysis of the amino acids' ^{13}C chemical shifts, which are sensitive to the conformational environment. We could find no evidence of α-helices, but identified about half of the residues in β-sheet environments, mostly Ile, Lys, Thr and Val. The remaining chemical shifts were compatible with either random coils or PPII helices[20], principally for Asn/Asp, Gly, Pro and Ser (blue bars on Fig. 3a and Supplementary Table 9). No correlation could be established between the hydrophobicity or charge of the residues, or their secondary structure propensity. Our results do not clearly indicate but cannot rule out the presence of PPII that have been reported in HRGPs[23,48].

We then explored the role of glycans in the structuration of cell wall proteins by recording ssNMR spectra of deglycosylated cell walls. While the complete deglycosylation resulted in a total disappearance of the glycan signals in the 2D INADEQUATE (Fig. 4a) and DARR spectra (Supplementary Fig. 9), the amino acid chemical shift values remained almost identical, indicating no significant change in secondary structure of the proteins. However, Hyp and Thr signals were completely lost following deglycosylation, which could be explained by an increase in their mobility after deglycosylation, going from a "slow motion regime" to the ssNMR unfavorable "intermediate regime". This is a strong indication that, in addition to Hyp, Thr residues are heavily glycosylated to unidentified glycans in *C. reinhardtii* cell walls - another information that has never been reported before. It is possible, however, that Hyp- and Thr-rich regions could be structured before deglycosylation, but this change would not be detectable due to their signals' disappearance. Altogether, glycans appear to have almost no influence on the overall protein structure and dynamics, suggesting a model in which they are spatially isolated from the amino acids, in sugar domains outside or within protein segments. This information must be considered in building a new cell wall model.

We pursued the examination of glycan through-space connectivities using dipolar-based ssNMR methods. Multiple glycan-glycan contacts were revealed by the ^{13}C-^{13}C CP-PDSD spectrum of *C. reinhardtii*'s cell wall (Fig. 4b). For example, we detected inter-Man contacts between their $C_{2/3}$ (76 ppm) and C_1 of units 9, 13 (94.5 ppm), 2, 10 and 12 (97.2 ppm). We also identified inter-glycan contacts between Man C_1 (94.5 and 97.2 ppm) and Ara C_1 (109.8 ppm), C_2 (82.2 ppm) and $C_{3/4}$ (77.4 ppm). These units are probably not covalently linked[27], but spatially close.

The spin-diffusion driven experiments (PDSD and DARR) did not allow detecting specific glycan-protein contacts (Supplementary Fig. 11), probably because of fast relaxation or phase separation in dynamically distinct domains. The increased sensitivity provided by

https://doi.org/10.1038/s41467-024-45246-7

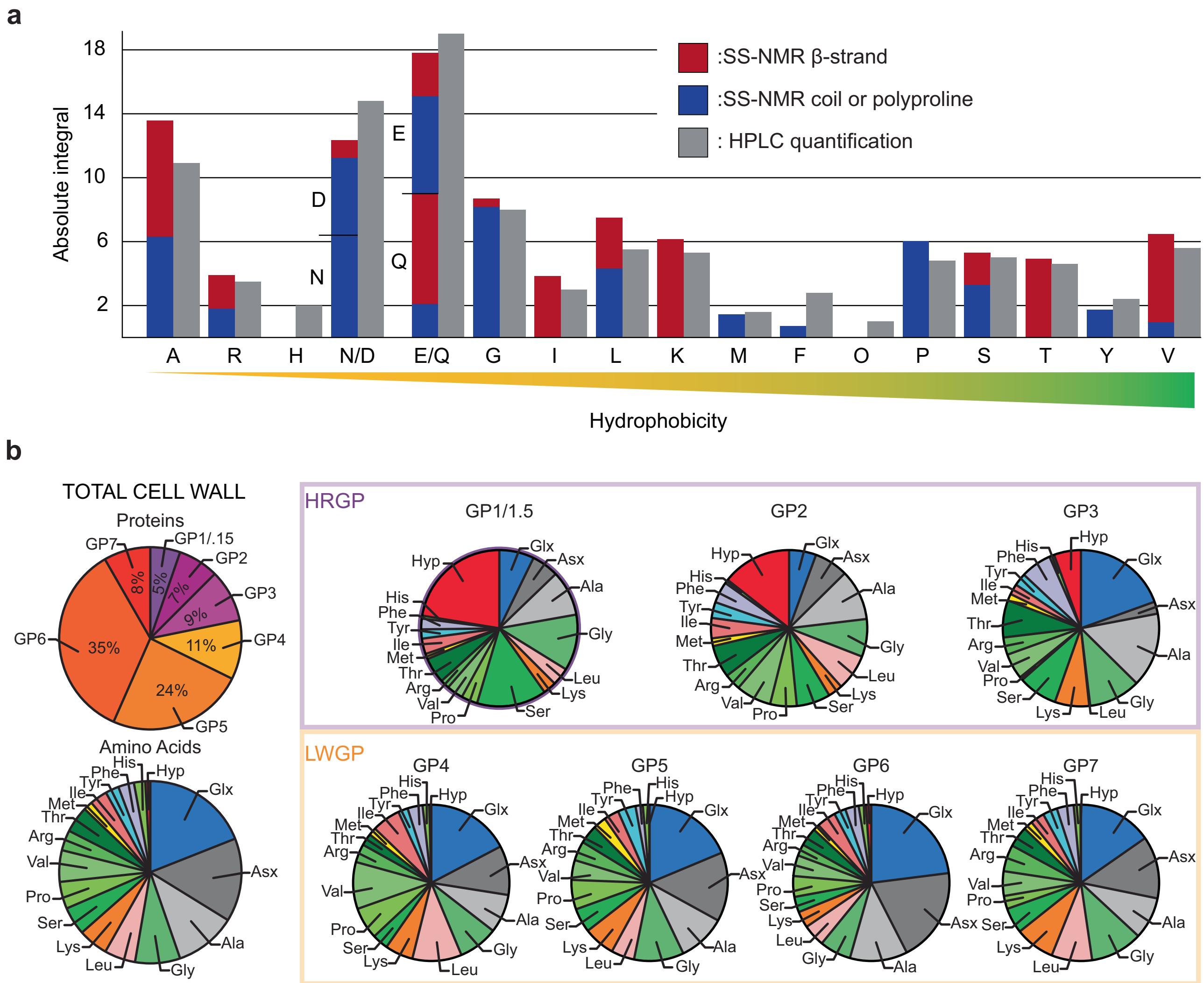

Fig. 3 | *C. reinhardtii* cell wall protein composition analyzed by electrophoresis and ssNMR reveal low Hyp relative abundance. a ssNMR (red/blue bars), and HPLC (gray bars, error <0.5% for all amino acids) quantification of amino acid units and ssNMR secondary structure prediction by TALOS+ (β-strands are in red, and random coils are in blue, full spectrum and numerical values are reported in Supplementary information). b Glycoprotein (GP) proportion and amino acid quantification in the cell wall extracts obtained from SDS-PAGE and HPLC, respectively. Source data are provided as a Source Data file.

hyperpolarization and low temperature enabled the detection of important glycan-protein contacts by MAS-DNP (Fig. 4c). As C_1 carbons have a relatively large chemical shift value and dispersion, they were used to identify glycans in the MAS-DNP spectrum. Since the spectral resolution is reduced by line broadening at cryogenic temperature, we used the assignment obtained at 283 K, assuming no major chemical shift differences[49,50]. These experiments, based on inter-spin dipolar coupling, only provides information on the spatial distribution, through-space contacts, but does not distinguish glycosylation via covalent bonds. We found contacts between Thr (Cγ at ~21 ppm) and terminal Man units 10 or 12 (C_1 ~ 95.3 ppm). We also observed contacts between all Hyp carbons (sidechain at ~35, 50, 59 and 73 ppm) and both Ara (C_1 ~ 110 ppm) and the terminal Man units 9 or 13 (C_1 at ~94.8 ppm). These connectivities might result from the specific geometry of the Man-Hyp contact or reflect a tighter binding with reduced mobility. Although the glycosylation of Ser is expected[13], Ser-glycan contacts could not be resolved due to the overlap of Ser Cα resonances with those of Hyp and Thr, and that of Ser Cβ resonances with glycans' C6. Other intense glycan C_1-amino-acid contacts could be detected for Glc or Rha (C_1 at 103.5 ppm), or Man/Gal (C_1 at 105.8 ppm), but the limited spectral resolution did not allow to identify the amino acid residues involved. Conversely, unidentified glycan C_1 atoms showed an intense contact with Asn's carbonyl by MAS-DNP PDSD with a long (1.5 s) mixing time (Fig. 4c, bottom).

The sensitivity enhancement provided by MAS-DNP also allowed us to record a ^{15}N-^{13}C ssNMR spectrum (Fig. 4d and Supplementary Fig. 13), and identify backbone nitrogen signals of amino acids, such as Hyp and Thr (~118 ppm) and Asn (~112 ppm). The one-bond NCα spectrum revealed a likely different unidentified glycan C_1 signal with an intense contact with Asn's amide (Fig. 4d) - a contact that was not detected at 283 K (Fig. 4d, purple spectrum). Using an additional ^{13}C-^{13}C mixing time in an NCaCx experiment, we allowed magnetization to transfer from Cα to surrounding carbons. Connections were thus revealed between O-glycosylated Hyp/Thr's amides (115 and 120 ppm) and several glycans' C_1 sites, including that of Ara (109 ppm) (Supplementary Fig. 13).

In summary, we detected unambiguous contacts between Hyp and Ara, Hyp and Man, Thr and Man, as well as Asn with unidentified glycan C_1s. While we could not quantify Ser or Asn glycosylations, the glycan-Hyp/Thr contacts and their relative intensities mostly identified using MAS-DNP DARR spectra, are summarized in Supplementary Fig. 10 and Supplementary Table 13.

https://doi.org/10.1038/s41467-024-45246-7

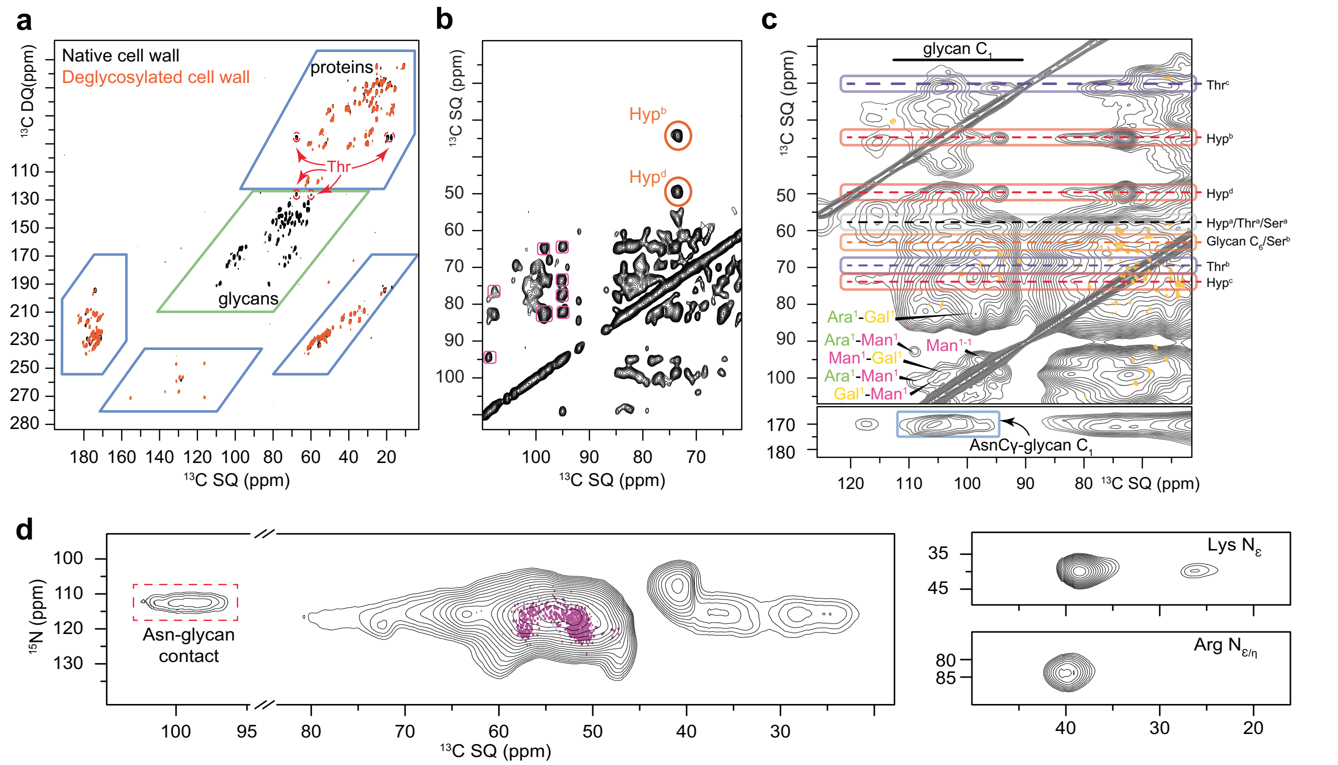

Fig. 4 | Glycan-glycan and glycan-protein contacts revealed by ssNMR. a The effect of deglycosylation on *C. reinhardtii* extracted cell-wall is probed by 2D through-bond ^{13}C experiments, by comparing native (black) and deglycosylated (orange) cell wall extracts. **b** Hyp detection, not possible via through bond experiment, is enabled using a 100 ms-long through-space PDSD, and inter-glycan contacts are highlighted in pink. **c** MAS-DNP experiments, which probe spatial proximities (DARR 50 ms) (gray), allow glycan-protein contact detection using the assignment obtained at 298 K (orange). Contacts between proteins and glycan C_1 are circled and color-coded (Ara (green), Gal (yellow), and Man (pink)). **d** Asn sidechain nitrogen (~113 ppm) covalently linked to GlcNAc C_1 (~100 ppm) involved in N-glycosylation are detected using a MAS-DNP enhanced N-Cα correlation (black spectrum). These contacts are not detected at 283 K (purple spectrum recorded at 800 MHz). Additional amino acids with N in their sidechains are also be detected (two top panels). Unique glycan-to-Thr/Hyp contacts are listed in Supplementary Fig. 10. **a**, **b** NMR spectra are recorded at a field of 600 MHz and 298 K under 13.5 kHz MAS while **c**, **d** data come from MAS-DNP experiments at 600 MHz/395 GHz and 100 K under 8 kHz MAS.

The high abundance of Man in *C. reinhardtii*'s cell wall suggests the presence of O-glycosylation to Thr. To verify this hypothesis, a cell-wall protein extract was digested with trypsin and enriched by Concanavalin A lectin weak affinity chromatography (ConA-LWAC)[51,52]. Our glycoproteomic analysis identified 9 unique glycopeptide sequences from 6 proteins (Supplementary Table 14) using higher-energy collisional activation (HCD) and electron-transfer dissociation (ETciD) MS. Although none of the identified proteins is annotated as a cell wall protein, it should be noted that the approach used favors abundant, small, soluble proteins with simple glycosylation patterns. Nevertheless, these glycoproteomic results suggest an O-linked glycosylation of Ser and Thr with hexose modifications, likely α-linked Man or Man2, thus demonstrating the presence of biosynthetic machineries in Chlamydomonas capable of catalyzing these modifications.

Large cell wall proteins with complex glycosylation patterns are notoriously difficult to detect by the approach described above, without using specific molecular separation techniques, enrichment and targeted detection and analysis[53,54]. They are however amenable to ssNMR methods as those used in this study. To further ascertain the high mannosylation of *C. reinhardtii*'s cell wall, our ssNMR approach could be applied on cell-wall extracts from which mannose residues would be removed by mannosidase and other enzymes[55]. Fluorescence imaging using mannose-specific antibodies followed by enzymatic treatment[56] could also be considered.

The presence of O-glycosylation in *C. reinhardtii*'s cell wall architecture, notably the O-glycosylation of Thr by Ara in HRGPs previously demonstrated, is confirmed by our MAS-DNP results[26,57,58]. In addition, our GC-MS analysis of partially methylated alditol acetates (Fig. 2b) shows that Man linkages (1,2 and 1,3) are consistent with Man oligosaccharides attached to proteins via N-linked glycosylation[27]. Since Asn residues are abundant in LWGPs (*ca.* 15%), and can only be N-glycosylated - a post-translational modification never reported in *C. reinhardtii's* cell wall - at least some of the LWGPs GP4 to GP7 should be N-glycosylated via their Asn residues, with GlcNAc linked to Man-rich oligosaccharides[59].

Our results suggest a model in which glycans are spatially isolated from the amino acid residues, and we postulate the presence of abundant but short Man-rich oligosaccharides. We confirmed the O-glycosylation of Hyp (and possibly Ser) to Ara in HRGP, and propose two glycosylation bonds in LWGPs: an N-glycosylation of Asn with GlcNAc and oligo-mannoside, and an O-glycosylation of Thr to Man. Finally, we also report new intermolecular contacts between Hyp and Man that would constitute the interface between HRGPs and LWGPs.

Glycans are more hydrated than proteins

Hydration heterogeneity in the cell wall is an essential feature for land plants[60]. This has been poorly investigated in microalgae and here we explored the water distribution in *C. reinhardtii*'s cell wall, using a water-edited 2D ^{13}C-^{13}C DARR experiment (Supplementary Fig. 14)[61]. The results shown in Fig. 5a and Supplementary Table 15 indicate that water is more tightly bound to glycans than to amino acid residues. Man and Gal with low C_1 chemical shifts, probably corresponding to terminal units, are more hydrated than other glycans. This superior hydration of glycans correlates with faster MAS-DNP hyperpolarization

https://doi.org/10.1038/s41467-024-45246-7

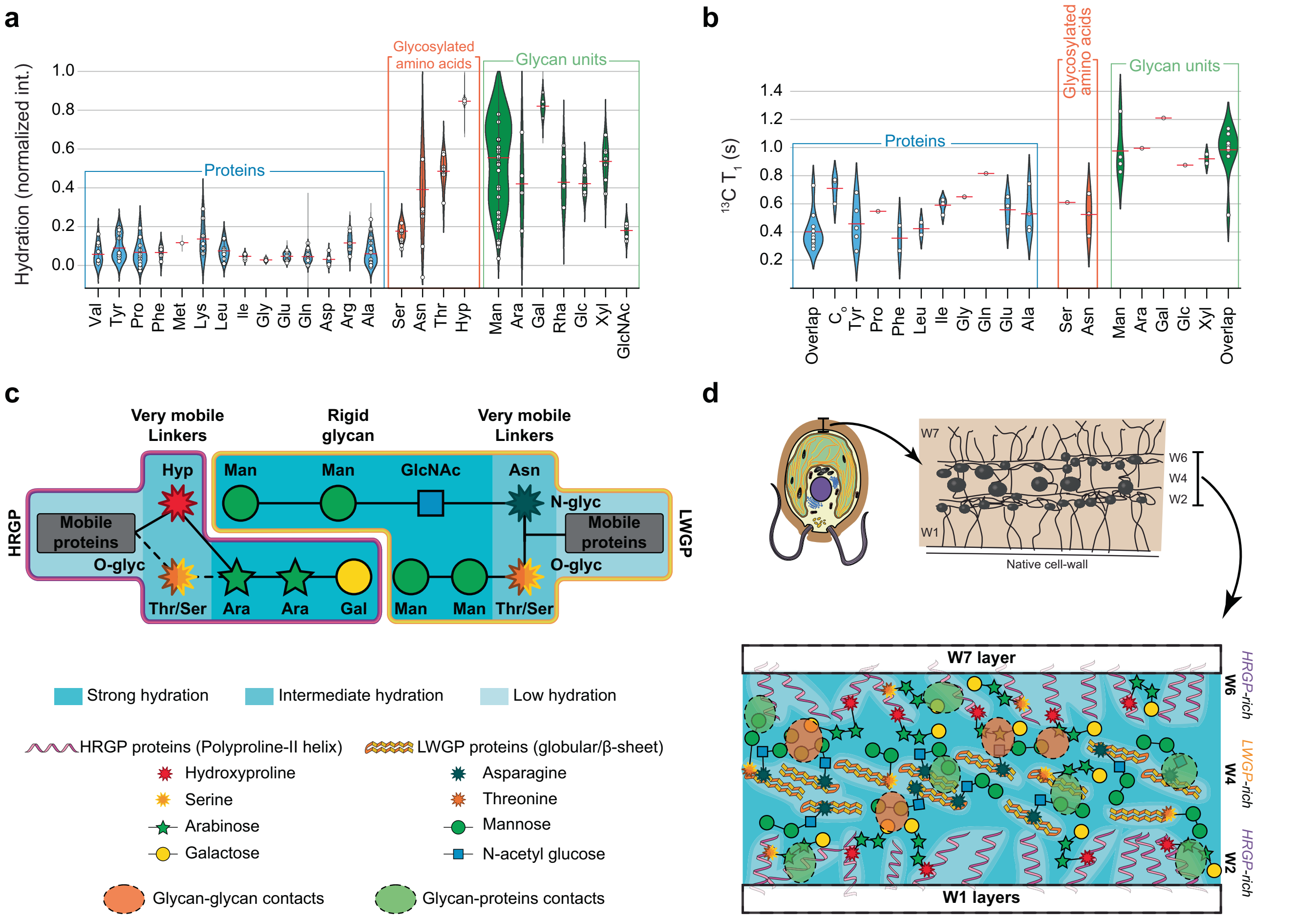

Fig. 5 | Hydration, dynamics and detailed model of *C. reinhardtii*'s cell wall. **a** Molecular hydration of amino acids and carbohydrates (see experimental section and Supplementary Table 15 for details). **b** Dynamics assessment by ^{13}C spin-lattice (T1) relaxation analysis of amino acids and glycans. **c** Representation of the cell wall components as suggested by ssNMR and GC-MS results. HRGPs rich in Hyp are O-glycosylated with Ara and Gal. LWGPs are most likely N-glycosylated on Asn with Man-rich oligosaccharides and O-glycosylated on Thr. Man-rich oligosaccharides are probably at the very hydrated interface between those two protein families. Glycosylated amino acids intermediate hydration and dynamics is also represented. **d** Schematic representation (top representation adapted from Goodenough et al.[19], used with permission of Rockefeller University Press, permission conveyed through Copyright Clearance Center, Inc.) of the molecular network determined from ssNMR and MAS-DNP results obtained on natively hydrated cell walls with proteins being overall more dynamic than glycans. Key carbohydrates and amino acids are identified using the symbols in the legend. Hydration is color coded, dark blue regions corresponding to the more hydrated regions. W1 (inner layer, not extracted), W2 (fibrous internal polyproline II helical HRGP-rich), W4 (likely beta-sheet LWGP-rich, abundant in our sample), W6 (fibrous external HRGP-rich) and W7 (outer layer, not extracted) are tentatively represented to locate the results of our study in the overall microalgal extracellular matrix. Source data are provided as a Source Data file.

build-up (Supplementary information), which may indicate proximity with the biradicals dispersed in the water phase. Moreover, the residues that can be glycosylated, i.e. Hyp, Thr and, to a lesser extent, Asn and Ser, have a much higher hydration level than other amino acids, in some cases almost reaching the hydration level of glycans. However, GlcNAc are less hydrated, suggesting that they are involved in structural domains where water is either absent or weakly bound. This is compatible with their implication in N-glycosylation of Asn residues, which are also less hydrated than other glycosylated amino acids.

Considering the LC-MS results and the resolution of our MAS-DNP spectra, glycosylation of at least a fraction of Ser residues is highly probable. We explain the fact that Ser and Asn overall appear less affected by deglycosylation, and that their spatial contacts to glycans are hard to detect, from their dilution by pools of non-glycosylated amino acids.

As mentioned before, the oligosaccharides bound to amino acids in the cell wall extract should include an average of three sugar units. Moreover, we determined a glycan/amino acid ratio of 1:2, which would correspond to 50% glycosylated amino acids with a single glycan or 16% with an average oligosaccharide length of three glycans. Therefore, Hyp and a significant part of Thr, Ser, and Asn residues must be glycosylated. As shown in Figs. 2c and 3a, our results are in good agreement with a model where all Hyp and approximately half of Ser are glycosylated in the form Hyp-O-Ara-Ara-Gal and Ser-O-Ara-Ara-Gal, as suggested in HRGPs[26], and potentially Thr-O-Ara-Ara-Gal. In addition, most remaining Thr and Ser residues as well as approximately half of Asn would be glycosylated in the forms Thr-O-Man-Man, Ser-O-Man-Man and Asn-N-GlcNAc-Man-Man in the LWGPs. There would be additional minor forms of glycosylated amino acids with Glc, Rha or Xyl glycans, but also possibly shorter, longer or branched oligosaccharides, as long as the ratio between glycans would remain similar[23,27].

Altogether, these results help refining the macromolecular organization of the cell wall, in which "dry" globular protein cores would be surrounded by hydrated layers containing glycans (Fig. 5a). Both regions would be linked through glycosylation, implying that the protein surfaces would contain glycosylated amino acids, mostly Hyp, Ser and maybe Thr in the HRGPs, Thr, Ser and Asn in the LWGP. The significant hydration of glycans is probably an integral part of the high plasticity of the cell wall, as observed in higher plants[62,63]. Moreover, water can provide the flexibility enabling the glycan interactions that are necessary for the bridging of structural proteins[64]. In higher plants, this is for example required to form nanostructures in secondary cell walls, or at the hemicellulose-cellulose interface[65].

Rigid glycans *and* mobile proteins

We then probed the dynamic properties of each chemical site by recording 1D ssNMR spectra with different ^{1}H-to-^{13}C polarization transfer schemes: Cross-Polarization (CP) - which enhances the sensitivity of the rigid molecular segments – and Insensitive Nuclei Enhancement by Polarization Transfer (INEPT)[32,66] for dynamic segments Despite the low resolution of the 1D spectra, especially in the carbohydrate region, 44 distinct carbon resonances could be identified, i.e., 20 from glycans and 24 from amino acids (Supplementary Fig. 16 and Supplementary Table 17). The CP build-up was faster for glycans, indicating a strong dipolar-coupling network, comparable to crystalline starch[35] (Supplementary Fig. 17). However, the CP decay was slower for glycans, indicating less motion on the millisecond regime. Glycans with low C_1 chemical shifts, i.e. involved in terminal groups, were particularly favored by INEPT. Terminal Man and Gal units are therefore both highly hydrated and very mobile as compared to other polysaccharides, suggesting their presence at the water-amino acid interface. Polarization transfer efficiency differences also explain why amino acids signals, including Hyp cross peaks, were preferentially detected by CP-DARR, or at low temperatures (100 K) (Supplementary Figs. 8 and 9). This is most likely due to their unfavorable dynamics or relaxation rates[67].

Motional differences were more quantitatively determined by measuring ^{1}H and ^{13}C longitudinal relaxation times in the laboratory (T_1) and the rotating frame ($T_{1\rho}$) (Supplementary Figs. 17 and 18). While T_1 probes motions with correlation times on the order of ns, $T_{1\rho}$ is sensitive to slower (ms) motions. Comparing relaxation times to published values measured in other contexts permits to refine our model. No differences were observed in the ^{1}H T_1 values, indicating that ^{1}H polarization is homogenized throughout the sample by spin diffusion. On the other hand, carbohydrate ^{13}C T_1 as well as ^{1}H and ^{13}C $T_{1\rho}$ values were slightly longer than those of amino acids, showing that glycans are less mobile than proteins, both on the nanosecond and millisecond scales. To illustrate these clear discrepancies between glycans and proteins, ^{13}C T_1s are shown in Fig. 5b as an example, while the other T_1 and $T_{1\rho}$ values are plotted in Supplementary Fig. 18. The response of carbohydrates and proteins to polarization transfer schemes indicates a higher mobility of glycans, in particular for those in terminal groups (see Supplementary Fig. 16 section for more details). Overall, ^{13}C and ^{1}H relaxation behaviors - both on the ns and ms timescales - are not indicative of large crystalline regions but more characteristic of a semi-mobile material akin to surface cellulose or hemicellulose.

In conclusion, proteins and glycans differ in both dynamics and hydration, with mobile protein domains, more rigid but hydrated glycan domains, and glycosylated proteins at the interface. These two families of molecules are spatially segregated, even if it is in small nanometer-scale regions that are chemically and dynamically heterogeneous, similarly to layered semi-crystalline polymers or plant cell walls[68].

Discussion

This work allowed refining the layered model of *C. reinhardtii*'s cell wall, which was primarily known from EM. The structural insights provided here by both ssNMR and MAS-DNP on a complex sample comprising proteins and glycans highlight the limitations of targeted analysis and data mining prediction. By studying a hydrated cell wall in a near native-environment in comparison with intact cells, we were able to obtain unique structural and dynamic information on the sugar and proteins that compose this complex biological scaffold. These molecular-level data improve the current model of the glycoprotein-rich cell wall of *C. reinhardtii*, and allow reconciling this organization with the cell wall function of microalgae, and higher plants to a certain extent. We determined the composition and relative abundance of glycans and proteins and the presence of previously underestimated lower molecular weight glycoproteins, LWGPs, as well as the high Man content of these samples. Our data support the presence of short length oligosaccharides, reveal the presence of β-sheets, the existence of both O- and N-linked glycosylations including mannosylation of Ser and Thr, show a spatial segregation of glycans and proteins in regions with differing dynamics and hydration, and uncover specific molecular interactions between them. The relevance of our findings was reinforced through comparisons with whole microalgal cells.

The surprising low abundance of Hyp residues and high abundance of Man are most likely explained by the preservation of LWGPs in our mild extraction process, which also contained the structurally important HRGPs previously identified. LWGPs are shown to contain short Man-rich oligosaccharides either O-glycosylated to Ser and Thr, or connected to GlcNAc that would be N-glycosylated to Asn. This provides an additional cross-linking strategy contributing to the structural integrity of the cell wall[69]. Considering that most of the Hyp detected in our sample are located in the HRGPs (Fig. 3b), which mostly contain oligosaccharides made of Ara residues and Man as a terminal group[23,24,26], the identified dipolar contacts of Hyp with Man would most certainly be not covalent, but due to spatial proximity, suggesting that Man is at the interface between the LWGPs and the Hyp/Ara-containing HRGPs.

These results, schematized in Fig. 5c, suggest that partially structured and highly mobile protein-rich domains are bound to less mobile and highly hydrated glycan-rich regions. The binding occurs by glycosylation to short (2–5 units long) oligosaccharides, thus contributing to the cohesion of the protein scaffold. Hyp, Ser and possibly Thr ensure O-glycosylation of HRGPs by Ara and Gal, while LWGPs are mostly O- and N-glycosylated by Man through Thr, Ser and Asn. At a larger scale, considering that we extracted the cell wall central triplet observed by TEM (between W2 and W7, Fig. 5d, top), the spatial segregation between protein- and glycan-rich regions by oligosaccharides suggests an alternating layered structure (Fig. 5d, bottom) in which hygroscopic glycans contribute to the cell-wall resiliency and flexibility. This model evokes the protective and hydrated surface of macroalgae enabling them to resist chemical and mechanical stresses[70].

Molecular-level details of the microalgal cell wall organization and rigidity is determinant to exploit this high-value renewable biomass[71]. The methodology employed here using in situ and in cell ssNMR and MAS-DNP paves the way to investigate the responses of microalgae to external contaminants or other stresses, or cellular processes during cell growth. This work is a step towards a better understanding of glycoprotein cell walls in intact cells.

Methods

Cell growth

The wild-type *wt* (CC-124), flagella deficient *bald2* (CC-4478 mt$^+$, also named *bld-2*)[72], cell-wall deficient *cw15* (CC-4349 mt$^+$), and starchless *sta 6-1* (CC-5374 mt$^+$) strains were obtained from the Chlamydomonas Culture Collection, University of Minnesota (Chlamydomonas Resource Center, http://chlamycollection.org). Whole *bald2* cells and cell wall extracts were used, unless specified. Cells were grown in a standard Tris bicarbonate-phosphate (TBP) medium buffered with HCl to pH 7.3[73]. The TBP medium was inoculated with microalgae

https://doi.org/10.1038/s41467-024-45246-7

previously kept on TAP-medium 1.6% agar plates. Autotrophic growth conditions were imposed using N_2 bubbling before sealing the flask. Then cells were grown asexually using continuous white light illumination (100 μmol photons·m^{-2}·s^{-1}) at 23 °C ± 1 °C with gentle orbital agitation (100 rpm). Typically, five days were required to reach the late exponential phase (5×10^6 cell·mL^{-1}) for 3 L of medium in a 6 L flask. Cells were harvested after a 1500 × *g* centrifugation for 10 min. For sexually differentiated cells, both mating types CC-124 ("mt+") and CC-125 ("mt−") were grown separately until the early exponential phase, which was followed by centrifugation, resuspension in N_2-depleted medium, and mixing. After flagella loss, differentiation and gametogenesis, mated cells undergo sexual reproduction and usually have a thicker cell wall.

^{13}C, ^{15}N isotope labeling

The growth medium was supplemented with either 1 g·L^{-1} of $NaH^{13}CO_3$ or 400 mg·L^{-1} of $^{15}NH_4Cl$ sterilized using 0.22 μm filters immediately prior to cell culture.

Cell viability

A fluorescence analysis was performed on a flow cytometer (BD Accuri™ C6) to test the cell viability after NMR experiments 1000 intact cells were acquired for each sample. This test measures the natural chlorophyll fluorescence and fluorescein diacetate (FDA)-derived fluorescence generation based on esterase activity level[74]. A total of 5 μL of a 1 mM FDA solution was added to 1 mL of cell solution at 2×10^6 cells·mL^{-1} for 20 min prior to measurement. Cell viability was shown to be ~90% before whole-cell NMR experiments, and above 60 % after 2 days of experiments at 298 K.

Cell wall extraction

To prevent cell wall extracts from contamination with flagella, we used the *bald2* strain, although similar results were obtained with the wild-type strain (Supplementary information). The cell wall was extracted using Goodenough and Heuser's protocol[14]. Briefly, cells were grown until the late exponential phase was reached (~5×10^6 cells·mL^{-1}), then harvested using a 15 min centrifugation at 1500 × *g* and 8 °C. The cell pellets were rinsed twice with a 1 mM phosphate buffer (pH 7.3) supplemented with 86 mM NaCl to mimic the ionic strength of the growth medium. The cell wall was extracted by diluting the pellets with a 2 M sodium perchlorate ($NaClO_4$) solution, to reach a final concentration of 6×10^8 cells·mL^{-1}. Cells were gently mixed by hand for 30 min before centrifugation at 2500 × *g* for 30 min at 8 °C. An additional extraction step was performed on the cell pellets to obtain cells totally devoid of a cell wall (called "uncovered cells"). The combined supernatants containing the cell walls were centrifuged at 30,000 × *g* for 40 min to remove any cellular material and debris from the solution. The solution (about 30 mL) was then dialyzed against 10 L of a 0.05% sodium azide solution in nanopure water under gentle agitation for 5 days. The dialysis solution was renewed twice a day. A precipitate progressively appeared in the dialysis tubing. The dialyzed solution was then lyophilized before being resuspended again in a minimal volume of $NaClO_4$. The cloudy solution was dialyzed again – an important step in the cell wall reconstruction. It can be noted that to obtain a cell wall extract that contains only HRGPs, several additional dialysis and freeze-drying steps are necessary[19], and lead to an insufficient amount of material for ssNMR analysis. In our case, after the second dialysis, the cell wall sample was lyophilized and rehydrated just before the ssNMR experiments.

For experiments on whole uncovered cells, the pellet obtained after $NaClO_4$ extractions was rinsed at least 5 times in a 1 mM phosphate buffer (pH 7.3) supplemented with a 86 mM NaCl solution. The cell pellet was used without further purification for ssNMR and GC-MS experiments.

Chemical deglycosylation

Chemical deglycosylation was performed as reported elsewhere[42]. Briefly, 100 mg of dry cell wall were cooled to 0 °C for at least 30 min. The dry powder was then added to 7.5 mL of a cold 2:1 v/v mixture of trifluoromethanesulfonic acid and anisole. After complete dissolution of the cell wall powder, the mixture was stirred at 0 °C under N_2 bubbling for 3 h. The solution was then cooled in a methanol-dry ice bath (−15 °C) for a few minutes, and 15 mL of diethyl ether were added, followed by a slow dropwise addition of 15 mL of 50% aqueous pyridine (v/v %) solution. The solution was gently mixed and the ether phase was removed. Ether extraction was performed a total of three times, and the aqueous phase was dialyzed against nanopure water with sodium azide. The protein extract was freeze-dried and hydrated prior to use.

Solid-state nuclear magnetic resonance

All 800 MHz (18.8 Tesla) experiments were conducted on a Bruker Avance III HD NMR spectrometer using a 3.2 mm triple resonance HCN probe at 10 °C, and at 13.5 kHz MAS to prevent rotational resonance and spinning sideband interferences. The typical radiofrequency field strength was 83 kHz for ^{1}H decoupling, using the two-pulse phase-modulated (TPPM) scheme, with 5.7 μs for each pulse. The radiofrequency field strengths were also 83 kHz for ^{1}H hard pulses and 50 kHz for ^{1}H ramped spin-lock, 63 kHz for ^{13}C hard pulses and spin-lock, 42 kHz for ^{15}N hard pulses, 34 kHz for ^{15}N spin-lock. The key acquisition parameters of all 1D and 2D experiments are summarized in Supplementary Table 20. See Supplementary Table 21 for details of the sample replicate compared by ssNMR. All assigned peaks will be deposited to the Complex Carbohydrate Magnetic Resonance Database (CCMRD)[34], and the Bruker Topspin dataset is freely available upon request.

We assess the protein/glycan ratio by using fully relaxed (30 s recycling delay) 1D direct polarization (DP) ^{13}C ssNMR spectra, and comparing the integrals of the carbohydrate C_1 (integral from 92.0 to 111.0 ppm, see the spectral regions highlighted in purple in Fig. 1e and Supplementary Fig. 16) and the amino acid carbonyl resonances (integral from 165.0 to 185.0 ppm, gray region in Supplementary Fig. 16). We measured a carbohydrate/protein molar ratio of 1:3 (adjusted to 1:2 considering the amount of Asp and Glu with their carboxyl end group). A significant part of the cell wall is thus composed of glycans, in agreement with the literature[27] and SDS-PAGE (Fig. 2a). Non-destructive qualitative assessment of the glycan/protein ratio is made available using simple 1D ^{13}C ssNMR, while it is challenging for colorimetric or MS approaches known to be destructive, especially for complex eukaryotic samples.

To probe polysaccharides with diverse mobility, four 1D ^{13}C spectra were recorded using different schemes to create initial magnetization. ^{13}C DP spectra were acquired using either a 30 s or a 2 s recycle delay for quantitative detection of all molecules or a selection of mobile molecules, respectively. Cross polarization (CP) was used with a 1 ms contact time for rigid molecules. Refocused Insensitive Nuclei Enhanced by Polarization Transfer (INEPT) experiments with two 1.72 ms delays followed by two 1.15 ms delays were used for mobile species. Interestingly and as shown on Fig. 1e, native cell spectra can be reconstructed by a weighted sum of those of the extracts and remainder after extraction (black spectra Fig. 1e) proving that the extraction protocol is lossless and that the cell wall accounts, here, for 38% of the overall intensity.

The spin-lattice (T_1) relaxation time was measured using inversion recovery for ^{13}C, and by inversion recovery followed by CP for ^{1}H. ^{13}C and ^{1}H rotating-frame spin-lattice relaxation ($T_{1\rho}$) were measured using both CP build-up and Lee-Goldberg cross polarization (LG-CP) at 298 K under 10 kHz MAS. The spin-lock field was 62.5 kHz for the ^{1}H-$T_{1\rho}$ measurement. Relaxation data were fit using a single exponential decay function.

To assign glycan and amino acid signals, a 2D ^{13}C DP refocused J-INADEQUATE spectrum was recorded using a 2 s recycle delay as reported in plant cell-wall[75]. ^{13}C CP refocused J-INADEQUATE was also employed to detect rigid molecules, using CP parameters described above for 1D experiments. INADEQUATE delays during the polarization transfer were set to 2.4 ms. The double quantum INADEQUATE spectra were sheared[76] using the "ptilt1" command available on Bruker TopSpin software to enable comparison with single quantum spectra. The resonance assignments of 37 sub-forms of carbohydrates are summarized and compared with literature values in Supplementary Tables 2 and 3.

We also assigned 339 peaks corresponding to 87 different spin systems in proteins, among 18 different amino acids. All of them were quantified using both HPLC and ssNMR with a method that accounts for overlapping peaks[32] (Fig. 3a and Supplementary Fig. 8, and Supplementary Tables 8–11). Chemical shift prediction according to secondary structure was provided by TALOS+[77] and CSI 3.0 (http://csi3.wishartlab.com/)[78]. Chemical shift differences between polyproline II (PPII) helices and random coils are still hard to detect using these tools, especially since PPII helices remain underexplored by NMR. In our sample for instance, Ile, Lys, Thr and Val would be located in β-strand environments, while Asx, Gly, Pro and Ser would either be in random coils or in PPII helices (Fig. 3a). The propensity of an amino acid to be included in a β-sheet has been shown to be more correlated to its neighboring residues than to its chemical nature[79] and, indeed, no correlation could be established between the hydrophobicity or charge of the residues and their β-sheet propensity here. In summary, while we can assert the presence of β-strands and exclude that of α-helices in our sample, we cannot rule out the presence of PPII helices previously reported in HRGPs[20,23,48]. Additional information is given in Supplementary Fig. 4 and Supplementary Table 1–5.

2D ^{13}C-^{15}N NCa and NCaCx spectra were acquired using a 1.7 s relaxation delay, 600 µs ^{1}H- ^{15}N CP, 5 ms ^{15}N-^{13}C CP, followed by 100 µs or 100 ms ^{13}C-^{13}C DARR correlation, respectively. DARR and PDSD experiments were recorded on a Bruker Avance III-HD spectrometer operating at a frequency of 599.95 MHz for ^{1}H and 150.87 MHz for ^{13}C. A 3.2 mm Varian triple resonance MAS probe was used, with a typical spinning frequency of 15 kHz, and the temperature was kept at 278 K with a dedicated cooling cabinet to prevent sample degradation. Dipolar based DARR and PDSD experiments were acquired with spin diffusion periods from 5 ms to 500 ms, and from10 ms to 1000 ms, respectively. Peak intensities were followed using CCPNMR software accordingly to peak assignment described in Supplementary information. 13C $T_{1\rho}$ filter is performed using a continuous 50 kHz Lee-Goldberg spin-lock on the ^{13}C channel before DARR mixing and detection.

Water-edited ^{13}C–^{13}C DARR spectra[80] were initiated with ^{1}H excitation followed by a ^{1}H-T_2 filter of 0.88 ms ×2 that eliminates 97% of overall signals but retains 80% of water magnetization. Then a 4-ms ^{1}H mixing period for water-to-glycan/amino acid transfer allows the best discrimination between hydrated and less hydrated regions. A 0.25 ms ^{1}H–^{13}C CP was used for ^{13}C detection. A 50-ms DARR mixing period was used for both the water-edited spectrum and the control 2D spectrum showing full intensity. Intensities were measured for all resolved and assigned correlations, and the intensity ratio between the water-edited spectrum and the control spectrum (S/S_0) was quantified. The error bar was calculated following the formula $(\frac{S}{S_0})^* \sqrt{\frac{1}{(sino)_S^2} + \frac{1}{(sino)_{S_0}^2}}$, with sino being the signal-to-noise ratio provided by TopSpin for a given peak on a slice of the 2D spectrum corresponding to the correlation of interest. See Supplementary Table 15 for details of the hydration intensities.

Magic angle spinning - dynamic nuclear polarization ssNMR

The sample is mixed with a biradical solution, which unpaired electrons have a 658-fold higher spin polarization than ^{1}H nucleus under the same experimental conditions. The electron spin polarization is transferred to the nuclei under microwave irradiation as the sample is maintained at a cryogenic temperature. The sample contains a cryoprotectant to avoid ice formation and preserve potentially fragile structures. A 10 mM biradical stock solution of AMUPol[81] was freshly prepared using d_8-glycerol/D_2O/H_2O (60/30/10 v%), referred to as the "DNP juice". Then 50 µL of the DNP juice were added to ~30 mg of the ^{13}C,^{15}N-labeled *C. reinhardtii* cell wall and mixed for 5–10 min. About 30 mg of well-hydrated sample was transferred into a 3.2-mm sapphire rotor. For whole-cell experiments, fully ^{13}C-labeled microalgae were centrifuged, then rinsed twice with a buffer containing 86 mM NaCl, before being resuspended in the DNP juice and pelleted after a few minutes in the solution.

All experiments were performed on a 600 MHz/395 GHz MAS-DNP spectrometer equipped with a gyrotron microwave (µw) source[82,83]. The cathode currents of the gyrotron were 160 mA. All MAS-DNP spectra were measured using a 3.2-mm triple resonance HCN probe at 8 kHz MAS frequency. The temperature was ~ 95–98 K with the µw off and ~100–110 K with the µw on. Typically, a 45-fold enhancement factor of NMR sensitivity with and without µw irradiation was achieved (Supplementary Fig. 1). We measured relatively short build-up time constants, T_B = 3–5 s, indicating a good mixing of the biradicals and biomolecules in these cellular samples. 2D correlation experiments were implemented with 50-ms DARR, 1.5-s PDSD, NCa, and 100-ms NCaCx experiments. The total acquisition time was 6 h for the DARR, 8 h for the PDSD and 2 h for the NC experiments. ^{13}C chemical shifts were externally referenced to TMS using adamantane's CH_2 signal set to 38.48 ppm[84]. The key acquisition parameters of all MAS-DNP experiments are summarized in Supplementary Table 20.

Cryogenic temperature ssNMR experiments

Low temperature experiments were performed at 98 K under the same conditions described for the MAS-DNP experiments.

Denaturing gel electrophoresis (SDS-PAGE)

SDS-PAGE was performed using 4–20% polyacrylamide (total concentration of both the acrylamide and bis-acrylamide crosslinker) gradient Mini-PROTEAN TGX Precast protein gels, with a Mini-PROTEAN II electrophoresis cell. Prior to any treatment, the dry cell wall was resuspended at 5 mg·mL^{-1} in nanopure water. Samples are then diluted 5 times with the proper amount of Laemmli buffer, reduced with β-mercaptoethanol (5 % final concentration), and treated for 25 min in an 85 °C bath. For electrophoresis, 10 µL corresponding to 10 µg of sample was injected per well, and Tris-glycine SDS running buffer (25 mM Tris, 192 mM glycine, 0.1% SDS, pH 8.3) was used at 10 mA for 15 min then 50 mA for approximately 1 h. The prestained protein ladder Precision Plus Protein Kaleidoscope for proteins in the molecular range 10–250 kDa was used as protein standards. After electrophoresis, total protein staining for relative protein proportion evaluation was performed using Coomassie Blue (0.05% w/v Coomassie Blue R-250) for 40 min, and destained with 30% v/v methanol/10% v/v glacial acetic acid for 5 h. Gels were acquired and visualized using ChemiDoc MP and ImageLab. Final image editing and protein quantification was performed with the same software. Error bars correspond to the standard deviation obtained after quantifying two cell wall extracts per strain. Uncropped pictures of the gels are found in the Supplementary Fig. 19.

High-performance liquid chromatography amino acid analysis

Samples were vacuum dried, suspended in 6N HCl containing 1% phenol, and hydrolyzed for 24 h at 110 °C under N_2 stream. Following hydrolysis, samples were vacuum dried to remove excess HCl, resuspended in a methanol:water:trimethylamine (2:2:1) redrying solution and dried under vacuum for 15 min. Samples were derivatized for 20 min at room temperature in methanol:water:trimethylamine:phenylisothiocyanate

(7:1:1:1) solution. This solution was then removed under vacuum, and the samples were washed with the redrying solution and vacuum dried for an additional 15 min. Chromatographic analysis was performed using a Waters Acquity Ultra-High Performance Liquid Chromatography (UPLC) System. Samples were dissolved and injected into an ethylene bridged hybrid C18 column, and a modified Pico-Tag gradient was used at 48 °C, with phenylthiohydantoin (PTH)-derivatized amino acid detection occurring at 254 nm. Cysteines were protected by performing acidic oxidation prior to hydrolysis. HPLC data correspond to the average of 4 replicates (Supplementary Table 11).

Glycosyl composition and linkage analysis by GC-MS

Glycosyl composition analysis of neutral sugars was achieved after an acetone extraction on dried cells removing most pigments in the sample. The dried sample was then dispersed in 0.5 mL of 2 M trifluoroacetic acid (TFA) in a sealed reaction tube. After 20 min of sonication in an ultra-sound water bath at room temperature, hydrolysis was performed at 121 °C for 2 h, followed by overnight reduction with $NaBD_4$, and 1 h acetylation with acetic anhydride and pyridine (1:1, v/v) at 80 °C. To obtain glycosyl linkage information, the cell wall is suspended in DMSO and, after permethylation, hydrolysis, reduction and acetylation, it is converted into partially methylated alditol acetates (PMMAs) that can be efficiently detected by GC-MS[85].

GC-MS analysis was performed on an HP-5890 GC interfaced to a mass selective detector 5970 MSD using a SupelcoSP2330 capillary column (30 × 0.25 mm ID) with the following temperature program: 60 °C for 1 min, then ramp to 170 °C at 27.5 °C·min^{-1}, and to 235 °C at 4 °C/min, with 2 min hold, and finally to 240 °C at 3 °C·min^{-1} with 12 min hold. Inositol was used as an internal standard. Glycosyl constituents were assigned, based on the GC-MS retention time of the derivatives of sugar standards, and on electron ionization MS (EI-MS) fragments of ^{13}C-labeled alditol acetate derivatives. Results of the quantitative GC-MS glycan composition is given in Supplementary Table 1 and identified glycan linkages are displayed in Supplementary Table 5. The relative EI detector response (percentage) obtained by GC-MS is a semi-quantitative reporter of linkage proportion, and is provided in Supplementary Table 1 for several samples, including whole cells.

O-glycoproteomic analysis by bottom-up mass spectrometry

Proteins from *C. reinhardtii's* cell wall were further extracted in 50 mM ammonium bicarbonate, 1% Rapigest before trypsin digestion, PNGase F digestion and Concanavalin A lectin weak affinity chromatography (ConA-LWAC) and mass spectrometry[51,86]. Our data mining strategy included variable hexose modifications of Ser or Thr residues for identification of Hex1, Hex2 or Hex3 modifications at each site, and we found evidence suggesting O-linked glycosylation of Ser and Thr with Hex1 and Hex2 modifications (Supplementary Fig. 20).

Scanning electron microscopy

Cells were first harvested by centrifugation, washed with deionized water, and fixed in 2.5% glutaraldehyde in 0.1 M cacodylate buffer (pH 7.2) for 2 h at 4 °C, and again in 1% buffered osmium tetroxide for 1 h at 4 °C. Samples were then washed three times with 0.1 M cacodylate buffer. Dehydration was carried out with a series of ethanol washes with concentrations from 10% to 100% on round glass slide. Specimens were coated (5 nm thickness) using a CCU-010 HV (turbo-pumped) Safematic Coating System. The SEM analysis was carried out with a high-resolution system capable of operating of up to 200 kV, equipped with an EDAX Genesis EDS on Philips CM200 and AMTXR-60BCCD camera.

Transmission electron microscopy

Microalgae were harvested by centrifugation, then washed several times with sterile isotonic buffer prior to cell fixation as describe above. Specimens were infiltrated with a resin, and thin sections of 70 nm were obtained using a diamond knife on a Reichert-Ultracut ultramicrotome. The sections were mounted on copper grids and coated with carbon for TEM observation. Images were recorded using a FEI Tecnai 12 BioTwin microscope operating at 120 kV and equipped with an AMT XR80C CCD camera system.

Supplementary Information

The online version contains supplementary material available at https://doi.org/xxxxxx. Cell-wall extract and control samples additional 1D/2D MAS-DNP and ssNMR spectra, complete glycan (by ssNMR and GC-MS) and protein (by ssNMR and HPLC) peak assignments and integrations, glycan linkages composition determined by GC-MS, mannosylated protein sequences identified by LC-MS, polarization build-ups (MAS-DNP, CP and PDSD), supplementary relaxation charts, detailed hydration calculation and a list of experiments with corresponding acquisition parameters can be found in the supplementary information.

Reporting summary

Further information on research design is available in the Nature Portfolio Reporting Summary linked to this article.

Data availability

Source data are provided with this paper. The NMR data generated in this study have been deposited in the Zenodo public database under accession code 10403721. The data generated in this study are provided in the Supplementary Information/Source Data file. Source data are provided with this paper. All relevant data that support the findings of this study are available within the article, as well as in the supplementary information and source data tables. The source data underlying Supplementary Tables ("Tables_Poulhazan_20231219" Excel file), Figs. 2d, 3a, b, and 5a, b and Supplementary Figs. 10, 15, 17, 18, and 12c ("SourceData_Poulhazan_20231219" Excel file) are provided as a Source Data file. The mass spectrometry proteomics data have been deposited to the ProteomeXchange Consortium via the PRIDE[87] partner repository with the dataset identifier PXD048024. Source data are provided with this paper.

References

1. Hwang, J.-H. et al. Photoautotrophic hydrogen production by eukaryotic microalgae under aerobic conditions. *Nat. Commun.* **5**, 3234 (2014).
2. Madadi, R., Maljaee, H., Serafim, L. S. & Ventura, S. P. M. Microalgae as Contributors to Produce Biopolymers. *Mar. Drugs* **19**, 466 (2021).
3. Rahman, A., Agrawal, S., Nawaz, T., Pan, S. & Selvaratnam, T. A review of algae-based produced water treatment for biomass and biofuel production. *Water* **12**, 2351 (2020).
4. Molina, A. et al. *Arabidopsis* cell wall composition determines disease resistance specificity and fitness. *Proc. Nat. Acad. Sci.* **118**, e2010243118 (2021).
5. Crozet, P. et al. Birth of a photosynthetic chassis: a MoClo toolkit enabling synthetic biology in the microalga *Chlamydomonas reinhardtii*. *ACS Synth. Biol.* **7**, 2074–2086 (2018).
6. Rasala, B. A. et al. Production of therapeutic proteins in algae, analysis of expression of seven human proteins in the chloroplast of *Chlamydomonas reinhardtii*. *Plant Biotechnol. J.* **8**, 719–733 (2010).
7. Zhang, B., Gao, Y., Zhang, L. & Zhou, Y. The plant cell wall: biosynthesis. *Constr. Funct. J. Integr. Plant Biol.* **63**, 251–272 (2021).
8. Harris, E. H. in *The Chlamydomonas Sourcebook (Second Edition)* 1 (eds Elizabeth H. H, David B. S, & George B. W) Ch. 2, 25–64 (Academic Press, 2009).
9. Salomé, P. A. & Merchant, S. S. A series of fortunate events: introducing *Chlamydomonas* as a reference organism. *Plant Cell* **31**, 1682–1707 (2019).

10. Merchant, S. S. et al. The *Chlamydomonas* genome reveals the evolution of key animal and plant functions. *Science* **318**, 245–250 (2007).
11. Miller, D. H., Lamport, D. T. & Miller, M. Hydroxyproline hetero-oligosaccharides in *Chlamydomonas*. *Science* **176**, 918–920 (1972).
12. Voigt, J., Frank, R. & Wöstemeyer, J. The chaotrope-soluble glycoprotein GP1 is a constituent of the insoluble glycoprotein framework of the *Chlamydomonas* cell wall. *FEMS Microbiol. Lett.* **291**, 209–215 (2009).
13. Saito, F. et al. Identification of novel peptidyl serine α-galactosyltransferase gene family in plants. *J. Biol. Chem.* **289**, 20405–20420 (2014).
14. Goodenough, U. W. & Heuser, J. E. The *Chlamydomonas* cell wall and its constituent glycoproteins analyzed by the quick-freeze, deep-etch technique. *J. Cell Biol.* **101**, 1550–1568 (1985).
15. Hwang, H. J., Kim, Y. T., Kang, N. S. & Han, J. W. A simple method for removal of the *Chlamydomonas reinhardtii* cell wall using a commercially available subtilisin (alcalase). *J. Mol. Microbiol. Biotechnol.* **28**, 169–178 (2018).
16. Imam, S. H. & Snell, W. J. The *Chlamydomonas* cell wall degrading enzyme, lysin, acts on two substrates within the framework of the wall. *J. Cell Biol.* **106**, 2211–2221 (1988).
17. Suzuki, L. et al. A zygote-specific protein with hydroxyproline-rich glycorpotein domains and lectin-like domains involved in the assembly of the cell wall of *Chlamydomonas reinhardtii* (Chlorophyta). *J. Phycol.* **36**, 571–583 (2000).
18. Adair, W. S. & Snell, W. J. in *Organization and Assembly of Plant and Animal Extracellular Matrix* (eds W. S. Adair & R. P. Mecham) 15–84 (Academic Press, 1990).
19. Goodenough, U. W., Gebhart, B., Mecham, R. P. & Heuser, J. E. Crystals of the *Chlamydomonas reinhardtii* cell wall: polymerization, depolymerization, and purification of glycoprotein monomers. *J. Cell Biol.* **103**, 405–417 (1986).
20. Voigt, J. & Frank, R. 14-3-3 proteins are constituents of the insoluble glycoprotein framework of the *Chlamydomonas* cell wall. *Plant Cell* **15**, 1399–1413 (2003).
21. Voigt, J., Liebich, I., Kieß, M. & Frank, R. Subcellular distribution of 14-3-3 proteins in the unicellular green alga *Chlamydomonas reinhardtii*. *Eur. J. Biochem.* **268**, 6449–6457 (2001).
22. Voigt, J. et al. A 14-3-3 protein of *Chlamydomonas reinhardtii* associated with the endoplasmic reticulum: nucleotide sequence of the cDNA and the corresponding gene and derived amino acid sequence. *Biochim. Biophys. Acta* **1679**, 180–194 (2004).
23. Ferris, P. J. et al. Glycosylated polyproline II rods with kinks as a structural motif in plant hydroxyproline-rich glycoproteins. *Biochemistry* **40**, 2978–2987 (2001).
24. Kilz, S., Waffenschmidt, S. & Budzikiewicz, H. Mass spectrometric analysis of hydroxyproline glycans. *J. Mass Spectrom.* **35**, 689–697 (2000).
25. Roberts, K., Gurney-Smith, M. & Hills, G. J. Structure, composition and morphogenesis of the cell wall of *Chlamydomonas reinhardi*. I. Ultrastructure and preliminary chemical analysis. *J. Ultrastruct. Res.* **40**, 599–613 (1972).
26. Bollig, K. et al. Structural analysis of linear hydroxyproline-bound O-glycans of *Chlamydomonas reinhardtii*—conservation of the inner core in *Chlamydomonas* and land plants. *Carbohydr. Res.* **342**, 2557–2566 (2007).
27. Mathieu-Rivet, E., Mati-Baouche, N., Walet-Balieu, M.-L., Lerouge, P. & Bardor, M. N- and O-glycosylation pathways in the microalgae polyphyletic group. *Front. Plant Sci.* **11**, 609993 (2020).
28. Gauto, D. et al. for biomolecular solid-state NMR. *Chem. Sci.* **12**, 6223–6237 (2021).
29. Hall, D. A. et al. Polarization-enhanced NMR spectroscopy of biomolecules in frozen solution. *Science* **276**, 930–932 (1997).
30. Monk, B. C., Adair, W. S., Cohen, R. A. & Goodenough, U. W. Topography of *Chlamydomonas*: fine structure and polypeptide components of the gametic flagellar membrane surface and the cell wall. *Planta* **158**, 517–533 (1983).
31. Voigt, J. Extraction by lithium chloride of hydroxyproline-rich glycoproteins from intact cells of *Chlamydomonas reinhardii*. *Planta* **164**, 379–389 (1985).
32. Poulhazan, A. et al. Identification and quantification of glycans in whole cells: architecture of microalgal polysaccharides described by solid-state nuclear magnetic resonance. *J. Am. Chem. Soc.* **143**, 19374–19388 (2021).
33. Mamedov, T. & Yusibov, V. Green algae *Chlamydomonas reinhardtii* possess endogenous sialylated N-glycans. *FEBS Open Bio* **1**, 15–22 (2011).
34. Kang, X. et al. CCMRD: a solid-state NMR database for complex carbohydrates. *J. Biomol. NMR* **74**, 239–245 (2020).
35. Poulhazan, A., Arnold, A. A., Warschawski, D. E. & Marcotte, I. Unambiguous ex situ and in cell 2D ^{13}C solid-state NMR characterization of starch and its constituents. *Int. J. Mol. Sci.* **19**, 3817 (2018).
36. Mathieu-Rivet, E. et al. Exploring the N-glycosylation pathway in *Chlamydomonas reinhardtii* unravels novel complex structures. *Mol. Cell Proteom.* **12**, 3160–3183 (2013).
37. Imam, S. H., Buchanan, M. J., Shin, H. C. & Snell, W. J. The *Chlamydomonas* cell wall: characterization of the wall framework. *J. Cell Biol.* **101**, 1599–1607 (1985).
38. Jiang, K.-s & Barber, G. A. Polysaccharide from cell walls of *Chlamydomonas reinhardtii*. *Phytochemistry* **14**, 2459–2461 (1975).
39. Barolo, L. et al. Perspectives for glyco-engineering of recombinant biopharmaceuticals from microalgae. *Cells* **9**, 633 (2020).
40. Voigt, J., Kiess, M., Getzlaff, R., Wöstemeyer, J. & Frank, R. Generation of the heterodimeric precursor GP3 of the *Chlamydomonas* cell wall. *Mol. Microbiol.* **77**, 1512–1526 (2010).
41. Voigt, J., Woestemeyer, J. & Frank, R. The chaotrope-soluble glycoprotein GP2 is a precursor of the insoluble glycoprotein framework of the *Chlamydomonas* cell wall. *J. Biol. Chem.* **282**, 30381–30392 (2007).
42. Edge, A. S. B. Deglycosylation of glycoproteins with trifluoromethanesulphonic acid: elucidation of molecular structure and function. *Biochem J.* **376**, 339–350 (2003).
43. San Clemente, H., Kolkas, H., Canut, H. & Jamet, E. Plant cell wall proteomes: the core of conserved protein families and the case of non-canonical proteins. *Int. J. Mol. Sci.* **23**, 4273 (2022).
44. Jamet, E. et al. Recent advances in plant cell wall proteomics. *Proteomics* **8**, 893–908 (2008).
45. Ding, Y.-H., Liu, N.-Y., Tang, Z.-S., Liu, J. & Yang, W.-C. *Arabidopsis* glutamine-rich $proteins_{23}$ is essential for early embryogenesis and encodes a novel nuclear PPR motif protein that interacts with RNA polymerase II subunit III. *Plant Cell* **18**, 815–830 (2006).
46. Takenaka, S. & Kawasaki, S. Characterization of alanine-rich, hydroxyproline-containing cell wall proteins and their application for identifying Pythium species. *Physiol. Mol. Plant Pathol.* **45**, 249–261 (1994).
47. Ringli, C., Keller, B. & Ryser, U. Glycine-rich proteins as structural components of plant cell walls. *Cell. Mol. Life Sci.* **58**, 1430–1441 (2001).
48. Homer, R. B. & Roberts, K. Glycoprotein conformation in plant cell walls: circular dichroism reveals a polyproline II structure. *Planta* **146**, 217–222 (1979).
49. Frederick, K. K. et al. Combining DNP NMR with segmental and specific labeling to study a yeast prion protein strain that is not parallel in-register. *Proc. Natl Acad. Sci.* **114**, 3642–3647 (2017).
50. Zhao, W. et al. Solid-state NMR of unlabeled plant cell walls: high-resolution structural analysis without isotopic enrichment. *Biotechnol. Biofuels* **14**, 14 (2021).

51. Vester-Christensen, M. B. et al. Mining the O-mannose glycoproteome reveals cadherins as major O-mannosylated glycoproteins. *Proc. Natl Acad. Sci. USA* **110**, 21018–21023 (2013).
52. Halim, A. et al. Discovery of a nucleocytoplasmic O-mannose glycoproteome in yeast. *Proc. Natl Acad. Sci. USA* **112**, 15648–15653 (2015).
53. Banazadeh, A., Veillon, L., Wooding, K. M., Zabet-Moghaddam, M. & Mechref, Y. Recent advances in mass spectrometric analysis of glycoproteins. *Electrophoresis* **38**, 162–189 (2017).
54. Tabang, D. N., Ford, M. & Li, L. Recent Advances in Mass Spectrometry-Based Glycomic and Glycoproteomic Studies of Pancreatic Diseases. *Front. Chem.* **9**, 707387 (2021).
55. Morales-Quintana, L. & Méndez-Yáñez, A. α-Mannosidase and β-d-N-acetylhexosaminidase outside the wall: partner exoglycosidases involved in fruit ripening process. *Plant Mol. Biol.* **112**, 107–117 (2023).
56. Marcus, S. E. et al. Restricted access of proteins to mannan polysaccharides in intact plant cell walls. *Plant J.* **64**, 191–203 (2010).
57. Nguema-Ona, E. et al. Cell wall O-glycoproteins and N-glycoproteins: aspects of biosynthesis and function. *Front. Plant Sci.* **5**, 499 (2014).
58. Velasquez, S., Salgado Salter, J., Petersen, B. L. & Estevez, J. Recent advances on the posttranslational modifications of EXTs and their roles in plant cell walls. *Front. Plant Sci.* **3**, 93 (2012).
59. Stanley, P., et al. Essentials of Glycobiology. *N-Glycans*. 9, (Cold Spring Harbor Laboratory Press, 2015).
60. Domozych, D. et al. The cell walls of green algae: a journey through evolution and diversity. *Front. Plant Sci*. **3** 82 (2012).
61. Takegoshi, K., Nakamura, S. & Terao, T. ^{13}C–^{1}H dipolar-assisted rotational resonance in magic-angle spinning NMR. *Chem. Phys. Lett.* **344**, 631–637 (2001).
62. Chen, P., Jung, N. U., Giarola, V. & Bartels, D. The dynamic responses of cell walls in resurrection plants during dehydration and rehydration. *Front. Plant Sci.* **10**, 1698 (2020).
63. MacDougall, A. J. & Ring, S. G. in *Advances in Pectin and Pectinase Research* (eds F. Voragen, H. Schols, & R. Visser) 123–135 (Springer Netherlands, 2003).
64. Thompson, D. S. & Islam, A. Plant cell wall hydration and plant physiology: an exploration of the consequences of direct effects of water deficit on the Plant cell wall. *Plants* **10**, 1263 (2021).
65. Cresswell, R. et al. Importance of water in maintaining softwood secondary cell wall nanostructure. *Biomacromolecules* **22**, 4669–4680 (2021).
66. Arnold, A. A. et al. Identification of lipid and saccharide constituents of whole microalgal cells by ^{13}C solid-state NMR. *Biochim. Biophys. Acta* **1848**, 369–377 (2015).
67. Lesage, A., Sakellariou, D., Steuernagel, S. & Emsley, L. Carbon –proton chemical shift correlation in solid-state NMR by through-bond multiple-quantum spectroscopy. *J. Am. Chem. Soc.* **120**, 13194–13201 (1998).
68. Ghassemi, N. et al. Solid-state NMR investigations of extracellular matrixes and cell walls of algae, bacteria, fungi, and plants. *Chem. Rev.* **122**, 10036–10086 (2021).
69. Perreault, F., Bogdan, N., Morin, M., Claverie, J. & Popovic, R. Interaction of gold nanoglycodendrimers with algal cells (*Chlamydomonas reinhardtii*) and their effect on physiological processes. *Nanotoxicology* **6**, 109–120 (2012).
70. Niklas, K. J., Cobb, E. D. & Matas, A. J. The evolution of hydrophobic cell wall biopolymers: from algae to angiosperms. *J. Exp. Bot.* **68**, 5261–5269 (2017).
71. Machado, L., Carvalho, G. & Pereira, R. N. Effects of innovative processing methods on microalgae cell wall: prospects towards digestibility of protein-rich biomass. *Biomass* **2**, 80–102 (2022).
72. Goodenough, U. W. & StClair, H. S. BALD-2: a mutation affecting the formation of doublet and triplet sets of microtubules in *Chlamydomonas reinhardtii*. *J. Cell Biol.* **66**, 480–491 (1975).
73. Surzycki, S. in *Methods in Enzymology*, vol. 23 Ch. 4, 67–73 (Academic Press, 1971).
74. Li, J., Ou, D., Zheng, L., Gan, N. & Song, L. Applicability of the fluorescein diacetate assay for metabolic activity measurement of Microcystis aeruginosa (Chroococcales, Cyanobacteria). *Phycological Res.* **59**, 200–207 (2011).
75. Terrett, O. M. et al. Molecular architecture of softwood revealed by solid-state NMR. *Nat. Commun.* **10**, 4978 (2019).
76. Webber, A. L. et al. Combination of DQ and ZQ coherences for sensitive through-bond NMR correlation experiments in biosolids under ultra-fast MAS. *ChemPhysChem* **13**, 2405–2411 (2012).
77. Shen, Y., Delaglio, F., Cornilescu, G. & Bax, A. TALOS+: a hybrid method for predicting protein backbone torsion angles from NMR chemical shifts. *J. Biomol. NMR* **44**, 213–223 (2009).
78. Hafsa, N. E., Arndt, D. & Wishart, D. S. CSI 3.0: a web server for identifying secondary and super-secondary structure in proteins using NMR chemical shifts. *Nucleic Acids Res.* **43**, W370–W377 (2015).
79. Fujiwara, K., Toda, H. & Ikeguchi, M. Dependence of α-helical and β-sheet amino acid propensities on the overall protein fold type. *BMC Struct. Biol.* **12**, 18 (2012).
80. White, P. B., Wang, T., Park, Y. B., Cosgrove, D. J. & Hong, M. Water–polysaccharide interactions in the primary cell wall of *Arabidopsis thaliana* from polarization transfer solid-state NMR. *J. Am. Chem. Soc.* **136**, 10399–10409 (2014).
81. Mentink-Vigier, F. et al. Computationally assisted design of polarizing agents for dynamic nuclear polarization enhanced NMR: The AsymPol family. *J. Am. Chem. Soc.* **140**, 11013–11019 (2018).
82. Dubroca, T. et al. A quasi-optical and corrugated waveguide microwave transmission system for simultaneous dynamic nuclear polarization NMR on two separate 14.1 T spectrometers. *J. Magn. Reson.* **289**, 35–44 (2018).
83. Rosay, M. et al. Solid-state dynamic nuclear polarization at 263 GHz: spectrometer design and experimental results. *Phys. Chem. Chem. Phys.* **12**, 5850–5860 (2010).
84. Morcombe, C. R. & Zilm, K. W. Chemical shift referencing in MAS solid state NMR. *J. Magn. Reson.* **162**, 479–486 (2003).
85. Ciucanu, I. & Kerek, F. A simple and rapid method for the permethylation of carbohydrates. *Carbohydr. Res.* **131**, 209–217 (1984).
86. Larsen, I. S. B. et al. The SHDRA syndrome-associated gene TMEM260 encodes a protein-specific O-mannosyltransferase. *Proc. Natl Acad. Sci. USA* **120**, e2302584120 (2023).
87. Perez-Riverol, Y. et al. The PRIDE database resources in 2022: a hub for mass spectrometry-based proteomics evidences. *Nucleic Acids Res.* **50**, D543–D552 (2021).

Acknowledgements

This research was funded by the Natural Sciences and Engineering Research Council (NSERC) of Canada (grant RGPIN-2018–06200 to I.M.), the Centre National de la Recherche Scientifique (UMR 7203 to D.E.W.), and the U.S. Department of Energy, Office of Science, Basic Energy Sciences (grant DE-SC0023702 to T.W.). A.P. would like to thank the *Fonds de recherche du Québec – Nature et technologies* (FRQNT), and the Quebec Network for Research on Protein Function, Engineering, and Applications (PROTEO) for the award of scholarships. The glycosyl composition and linkage analyses were supported in part by the Chemical Sciences, Geosciences and Biosciences Division, Office of Basic Energy Sciences, U.S. Department of Energy grant (DE-SC0015662) to P.A. at the Complex Carbohydrate Research Center. The National High Magnetic Field Laboratory is supported by National Science Foundation through NSF/DMR-1644779 and the State of Florida, the MAS-DNP instrument is supported by the NIH P41 GM122698 and NIH S10 OD018519. I.M. is a member of PROTEO and Resources Aquatiques Québec. A.H., S.Y.V., and H.J.J. wish to acknowledge funding from Danish National Research Foundation grant DNRF107, Novo Nordisk

Foundation grant NNF22OC0076899, Mizutani Foundation for Glycoscience and VILLUM FONDEN grant 00025438. We would like to thank S. Waffenschmidt (University of Cologne, Germany), U. Goodenough (Washington University in St. Louis, USA), O. Vallon and F. Zito (IBPC, Paris, France), B. Henrissat (AFMB, Marseille, France), and H. Wandall (University of Copenhagen, Denmark) for enlightening discussions.

Author contributions

A.P., A.A.A., T.W., D.E.W. and F.M.V. designed and conducted the NMR and MAS-DNP experiments. A.P. and F.M.V. prepared and optimized the DNP samples. A.M. and P.A. conducted the GC-MS experiments. A.H., S.Y.V. and H.J.J. conducted the LC-MS experiments. A.P., A.M. and F.M.V. analyzed the experimental data. A.P., A.A.A., T.W., D.E.W. and I.M. wrote the manuscript.

Competing interests

The authors declare no competing interests.

Additional information

Supplementary information The online version contains supplementary material available at https://doi.org/10.1038/s41467-024-45246-7.

Correspondence and requests for materials should be addressed to Tuo Wang, Dror E. Warschawski or Isabelle Marcotte.

Peer review information *Nature Communications* thanks Jae-Hyeok Lee and the other anonymous reviewer(s) for their contribution to the peer review of this work. A peer review file is available.

Supplementary Information

Molecular-Level Architecture of *Chlamydomonas reinhardtii's* Glycoprotein-Rich Cell Wall

Alexandre Poulhazan[1], Alexandre A. Arnold[1], Frederic Mentink-Vigier[2], Artur Muszyński[3], Parastoo Azadi[3], Adnan Halim[4], Sergey Y. Vakhrushev[4], Hiren Jitendra Joshi[4], Tuo Wang[5]*, Dror E. Warschawski[6]* and Isabelle Marcotte[1]*

[1] Department of Chemistry, University of Quebec at Montreal, Montreal, H2X 2J6, Canada

[2] National High Magnetic Field Laboratory, Florida State University, Tallahassee, FL 32310, USA

[3] Complex Carbohydrate Research Center, University of Georgia, Athens, GA 30602, USA

[4] Copenhagen Center for Glycomics, University of Copenhagen, Copenhagen, Denmark

[5] Department of Chemistry, Michigan State University, East Lansing, MI 48824, USA

[6] Laboratoire des Biomolécules, LBM, CNRS UMR 7203, Sorbonne Université, École Normale Supérieure, PSL University, 75005 Paris, France

* Corresponding authors:

marcotte.isabelle@uqam.ca, dror.warschawski@sorbonne-universite.fr, wangtuo1@msu.edu

Table of content

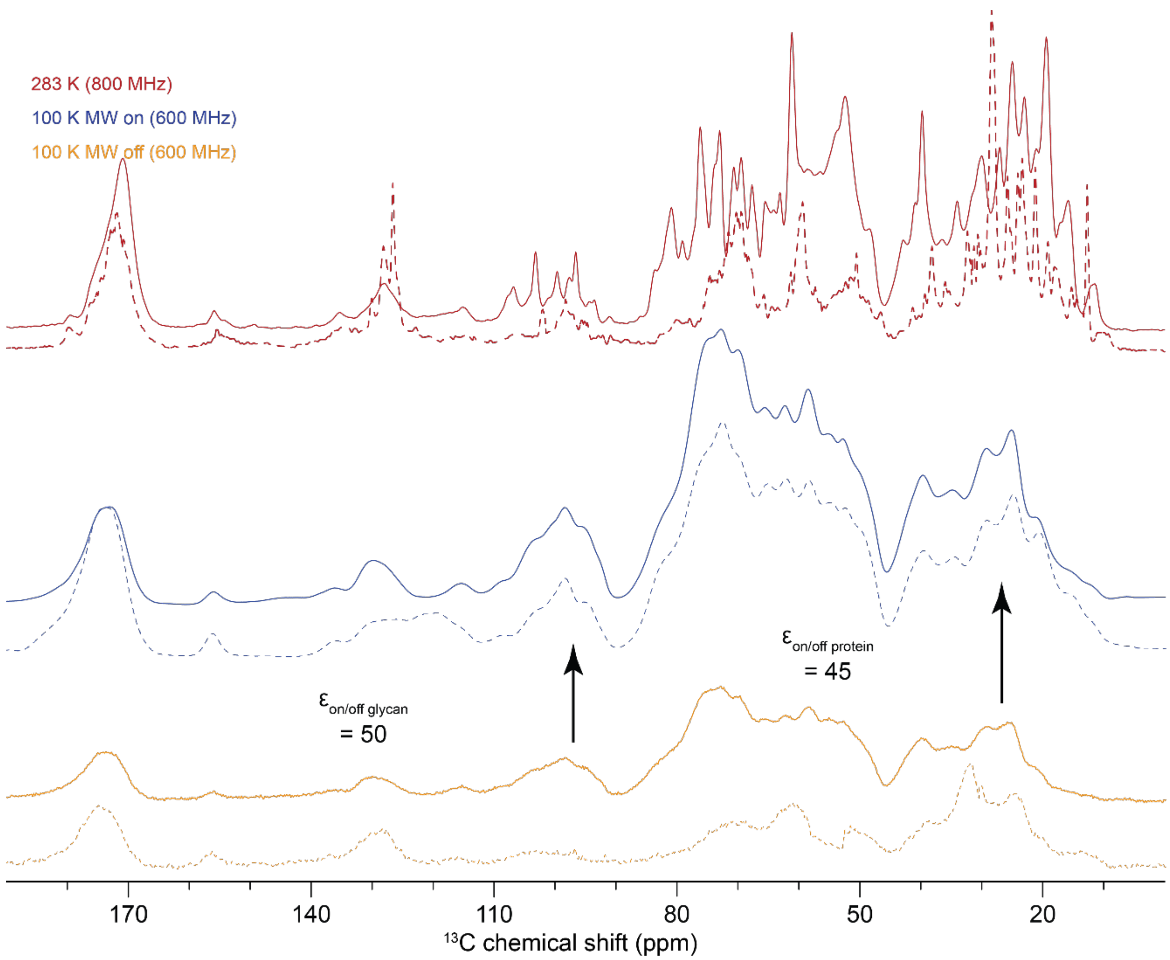

Supplementary Figure 1. MAS-DNP allows high sensitivity enhancement but loss in resolution. 1D ^{13}C CP spectra of *C. reinhardtii* cell-wall extract and whole cell (dashed line) at 600 MHz and 100 K with (microwaves signal enhancement ON, blue spectra) and without (microwave signal enhancement OFF, orange spectra) MAS-DNP enhancement (cryogenic temperature needed for MAS-DNP enhancement), and at 800 MHz and 283 K (red).

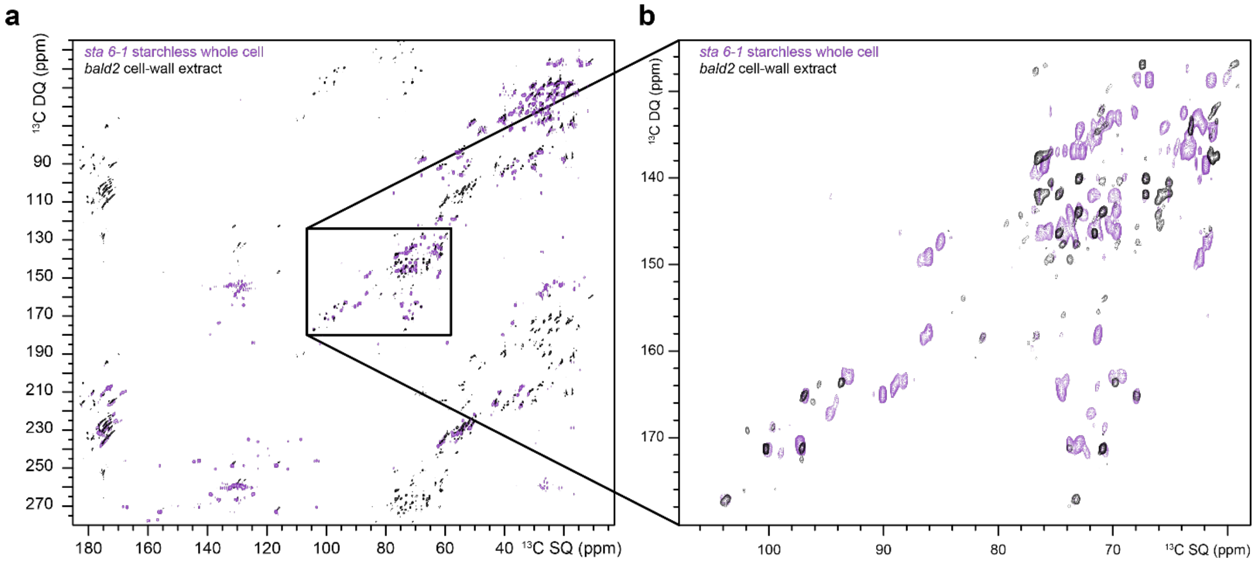

Supplementary Figure 2. Comparison of bald2 cell wall and stda 6-1 whole cell at 800 MHz. **a** Complete DP-INADEQUATE spectra of cell wall extracts (black) and whole cells (purple). **b** Zoom of the glycan region. At this temperature, 283 K, all glycans are detected quantitatively, and we know from GC-MS analysis that 40% of them are in the cell wall, but 60% are elsewhere in the cell (**Supplementary Table 8**). We therefore only expect at best a 40% overlap of the two spectra. Note that all peaks present in the cell wall spectra are indeed present in the whole cell spectra with the same chemical shifts.

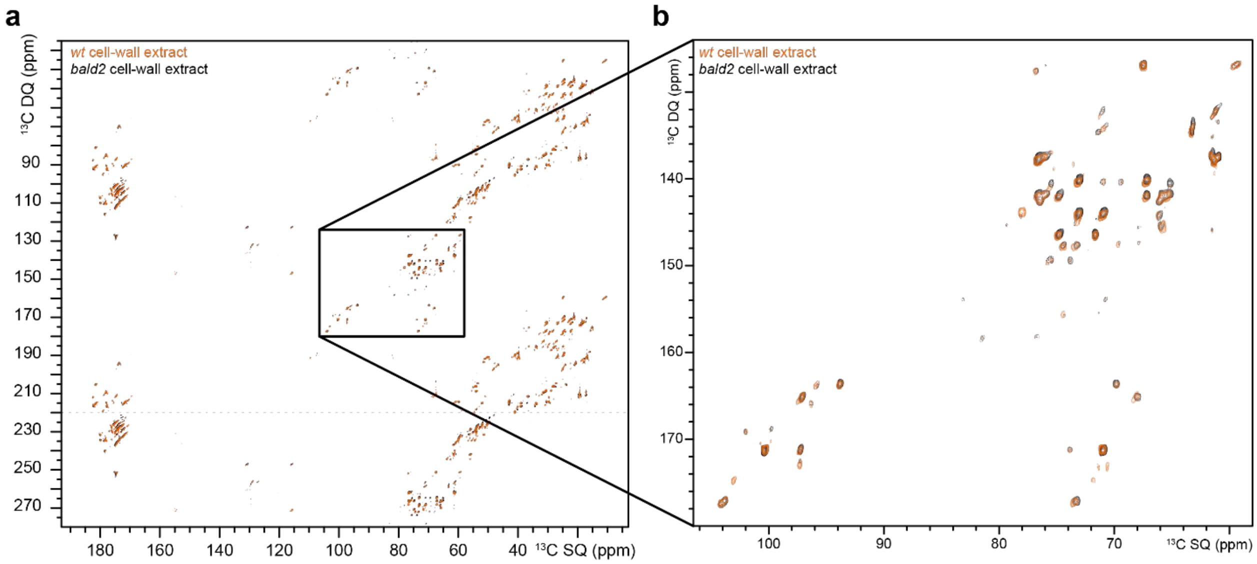

Supplementary Figure 3. Comparison of the cell wall spectra of *wt* and *bald2* strains. a Complete DP-INADEQUATE spectra of cell wall extracts from wild-type (orange) and flagella deficient (black) strains. **b** Zoom of the glycan region showing again very similar spectra. Spectra were recorded at fields of 18.8 T at 800 MHz, at 283 K.

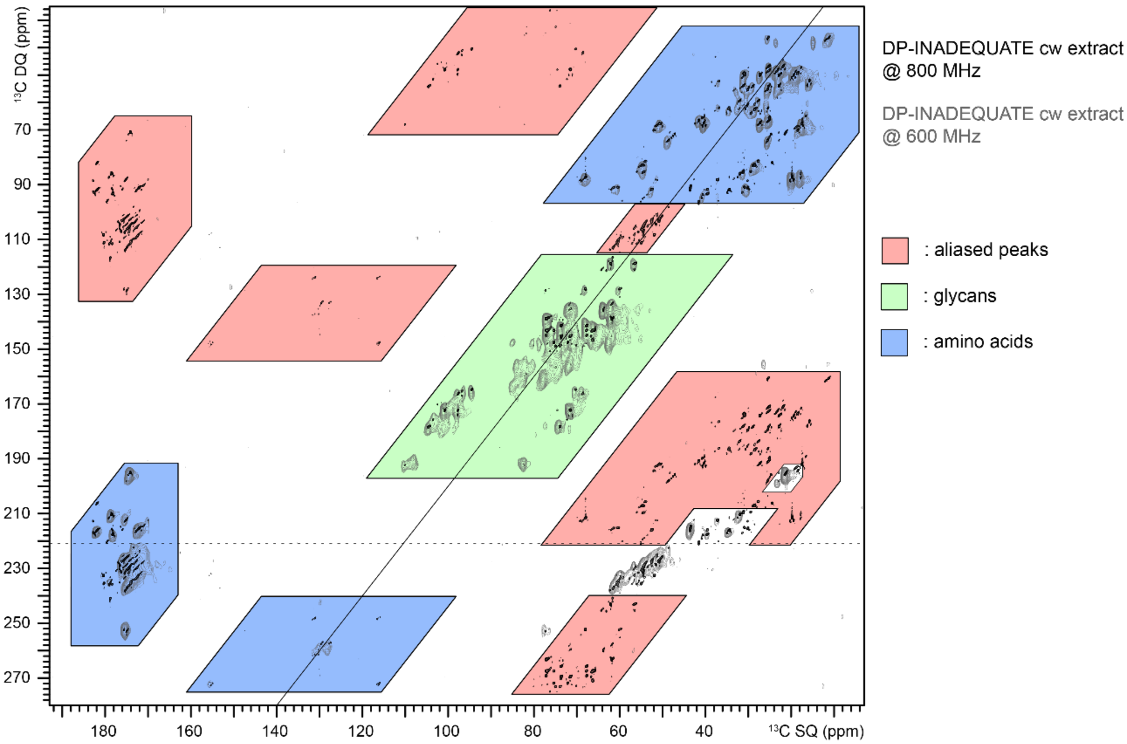

Supplementary Figure 4. Complete DP-INADEQUATE spectra of *C. reinhardtii's* cell wall. Comparison of spectra at two field strengths allow to assess resolution differences. Red regions are aliased peaks due to small indirect dimension used to save experimental time, but this artifact still allows assignment of glycans (green region used for assignment and quantification plotted on **Fig 2d**) and amino acids (blue region used for assignment and quantification reported in **Fig. 3a** and **Supplementary Fig. 5-7**).

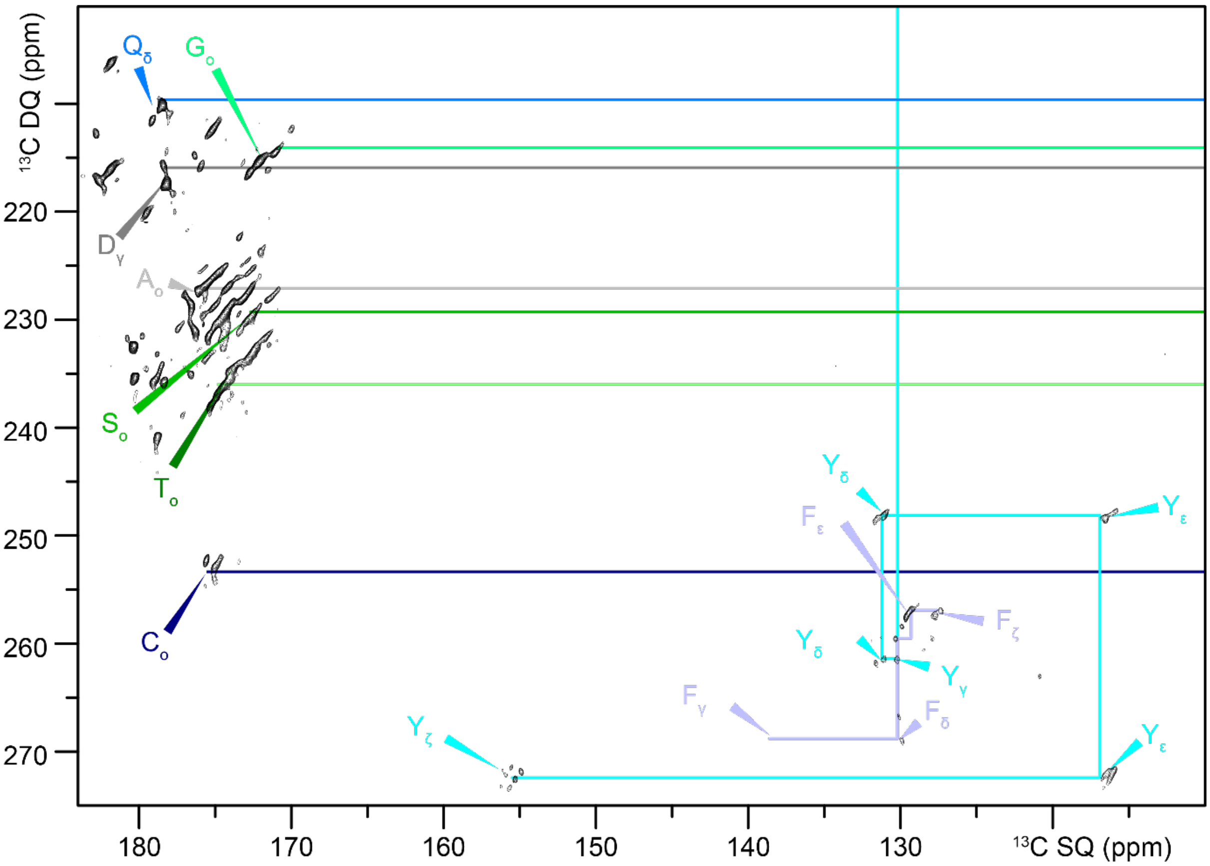

Supplementary Figure 5. Protein carbonyl assignment of *C. reinhardtii's* cell wall. Zoomed regions of the ^{13}C refocused DP-based *J*-INADEQUATE correlation spectrum with a short 3 s recycle delay. The zoom here shows the carbonyl and Tyr/Phe side chains correlations. This spectrum and the spectra plotted below on **Supplementary Figure 6** and **7** allow assessment of the overall resolution and provide examples of correlation paths for different amino acids (one-letter coded). For the overall ^{13}C-^{13}C *J*-INADEQUATE spectrum, see **Supplementary Fig. 4**.

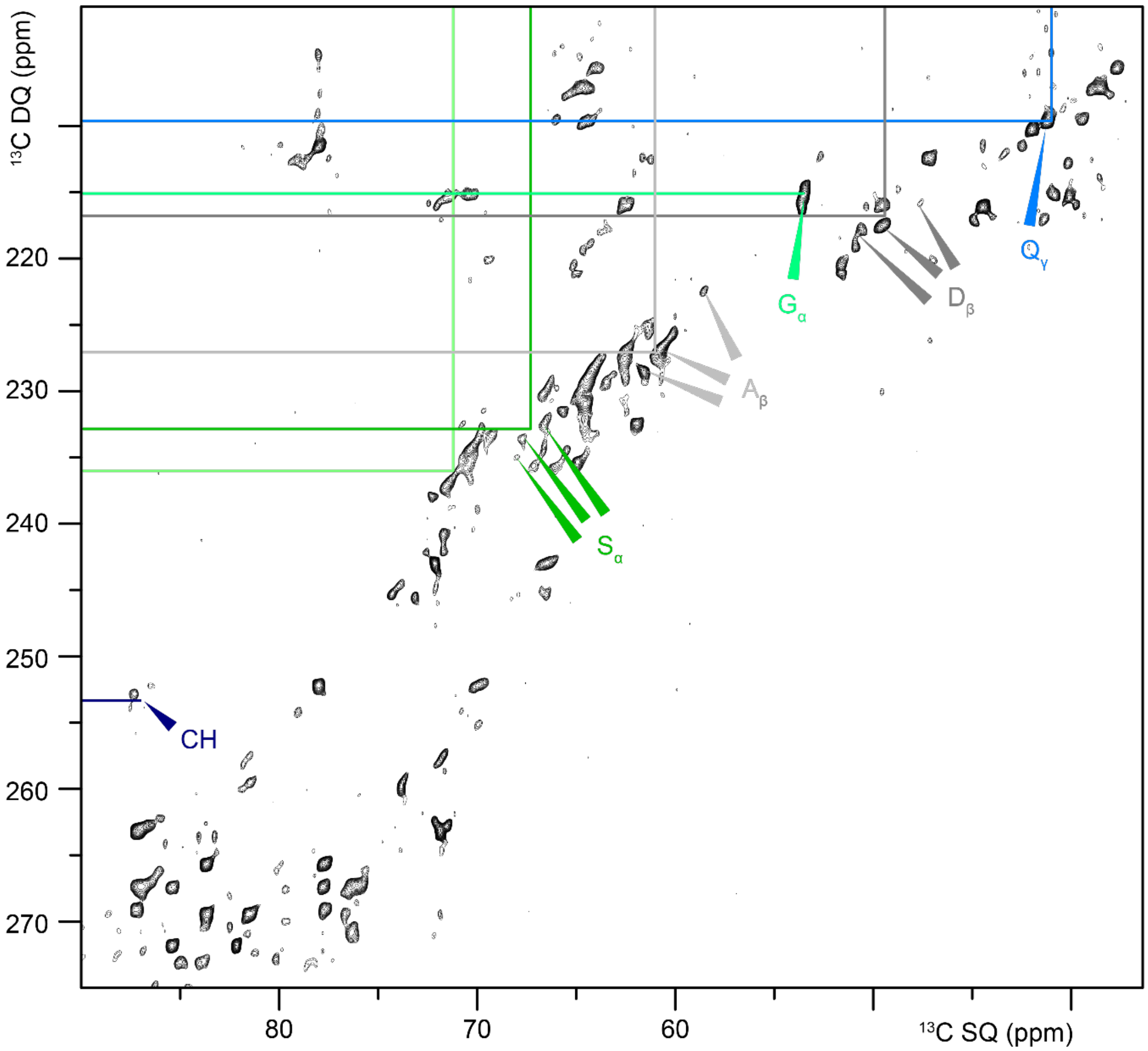

Supplementary Figure 6. Protein Cα assignment of *C. reinhardtii's* cell wall. Zoomed regions of the ^{13}C refocused DP-based *J*-INADEQUATE correlation spectrum with a short 3 s recycle delay. The zoom here shows the Cα of amino acid side chains. For the overall ^{13}C-^{13}C *J*-INADEQUATE spectrum, see **Supplementary Fig. 4**.

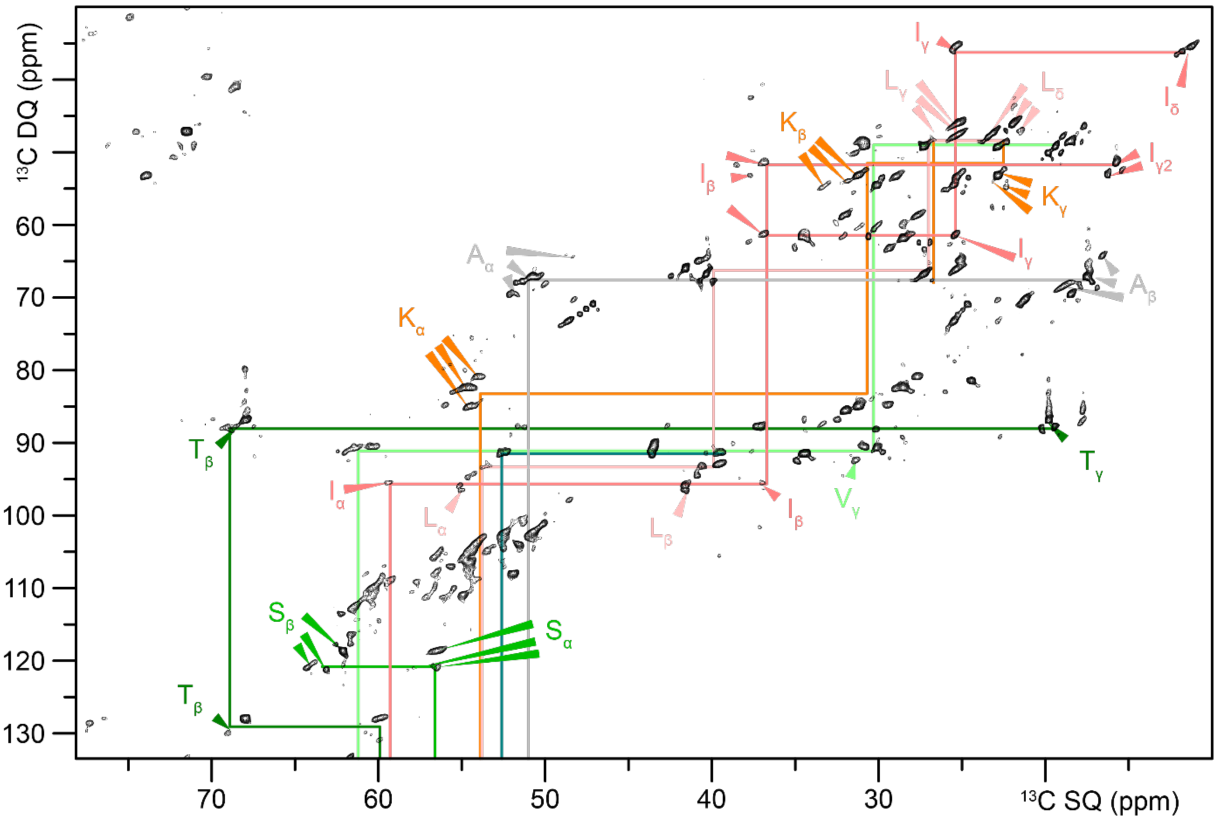

Supplementary Figure 7. Protein carbonyl assignment of *C. reinhardtii's* cell wall. Zoomed regions of the ^{13}C refocused DP-based *J*-INADEQUATE correlation spectrum with a short 3 s recycle delay. The zoom here shows the amino acid side chains correlations with one letter coding. For the overall ^{13}C-^{13}C *J*-INADEQUATE spectrum, see **Supplementary Fig. 4**.

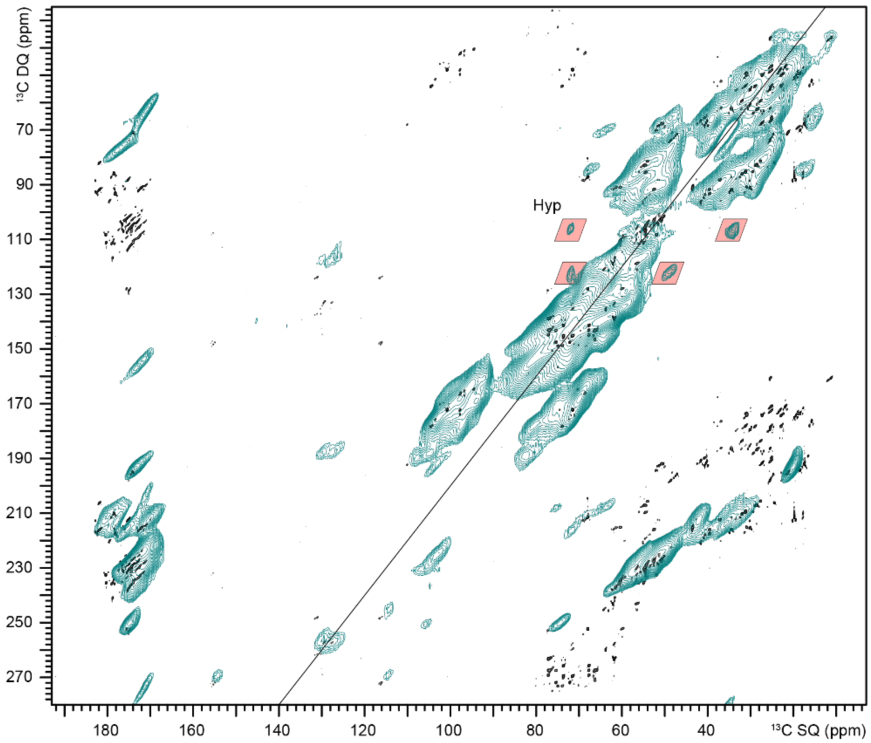

Supplementary Figure 8. ssNMR of *C. reinhardtii* cell wall at cryogenic and 283 K. Comparison of ^{13}C SQ-DQ *J*-INADEQUATE spectra recorded at 600 MHz using MAS-DNP and cryogenic temperature (100 K) (teal) and at 800 MHz using ssNMR at 283 K (black).

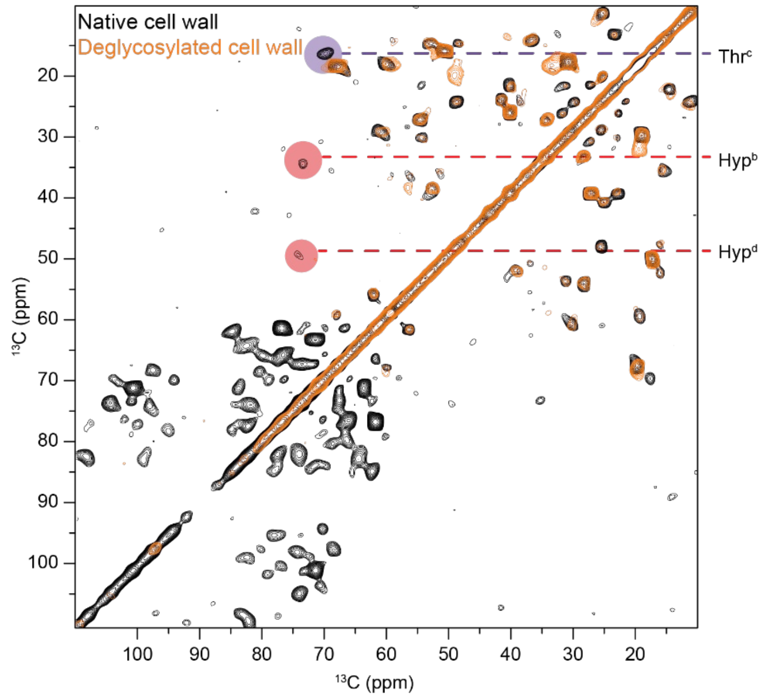

Supplementary Figure 9. Effect of deglycosylation on *C. reinhardtii* cell-wall extract. ^{13}C-^{13}C SQ-SQ DARR spectra with a mixing time of 50 ms of extracted cell wall (black) and deglycosylated extracted cell wall (orange). Resonances of O-glycosylated hydroxyproline and threonine are highlighted in red and purple, respectively.

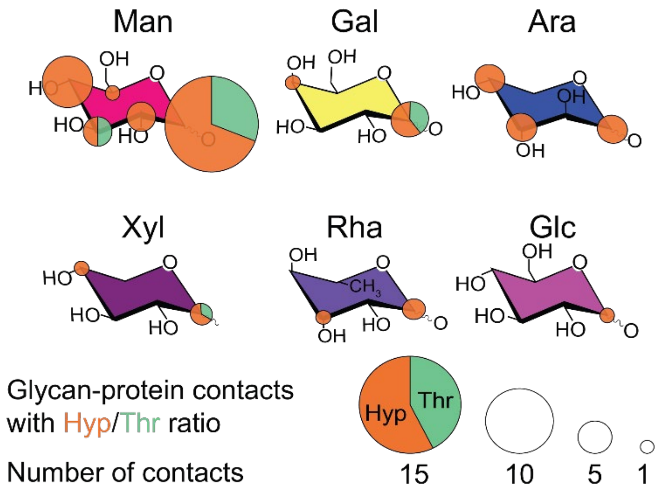

Supplementary Figure 10. Map of the resolved glycan-Hyp or -Thr spatial contacts. These contacts were detected by MAS-DNP. Pie chart diameters correspond to the number of contacts identified with a given glycan carbon. Sector area illustrates the propensity for this carbon to preferentially interact with Hyp (orange) or Thr (green).

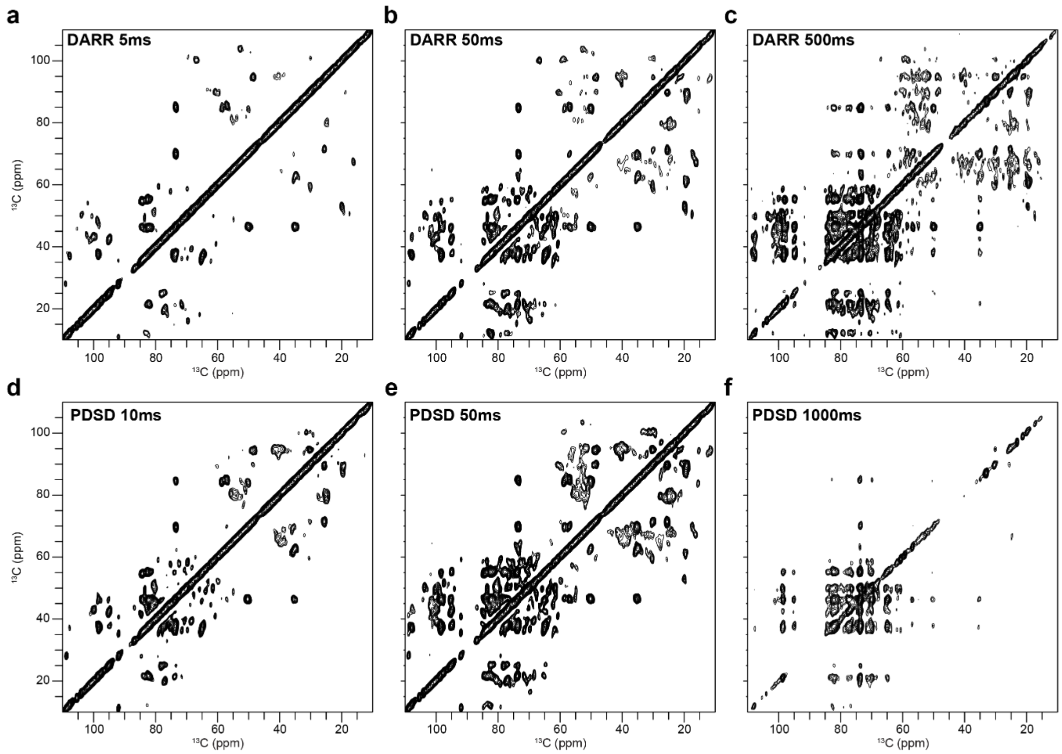

Supplementary Figure 11. DARR/PDSD build-up spectra. a-c DARR build-up with 5, 50 and 500 ms mixing times. **d-f** PDSD build-up with 10, 50 and 1000 ms mixing time.

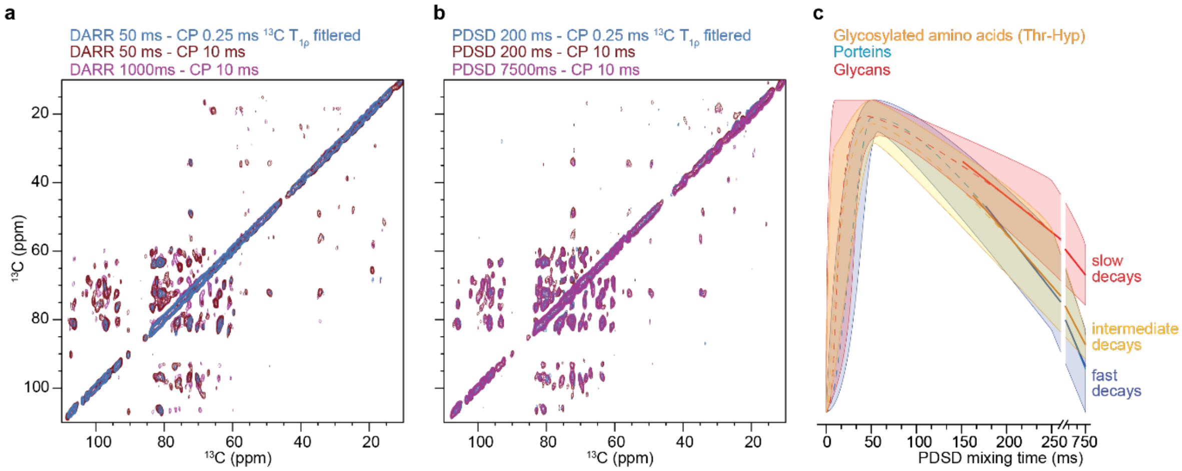

Supplementary Figure 12. DARR/PDSD 2D spectral editing. To understand the effect of different relaxations on spectral edition, we first applied long CP for both PDSD and DARR (**a** and **b** respectively, red spectra). Then by combining long CP and long DARR/PDSD mixing times (**a** and **b** respectively, purple spectra), we were able to further filter out the amino acid fraction. Finally, we show that the most efficient filter is a dedicated ^{13}C $T_{1\rho}$ filter (a and b respectively, blue spectra). All spectra were recorded with a 600 MHz spectrometer. **c** The PDSD cross peak normalized intensity build-ups show differences between glycans (red) and amino acids (blue), and the intermediate behavior of glycosylated amino acids (orange).

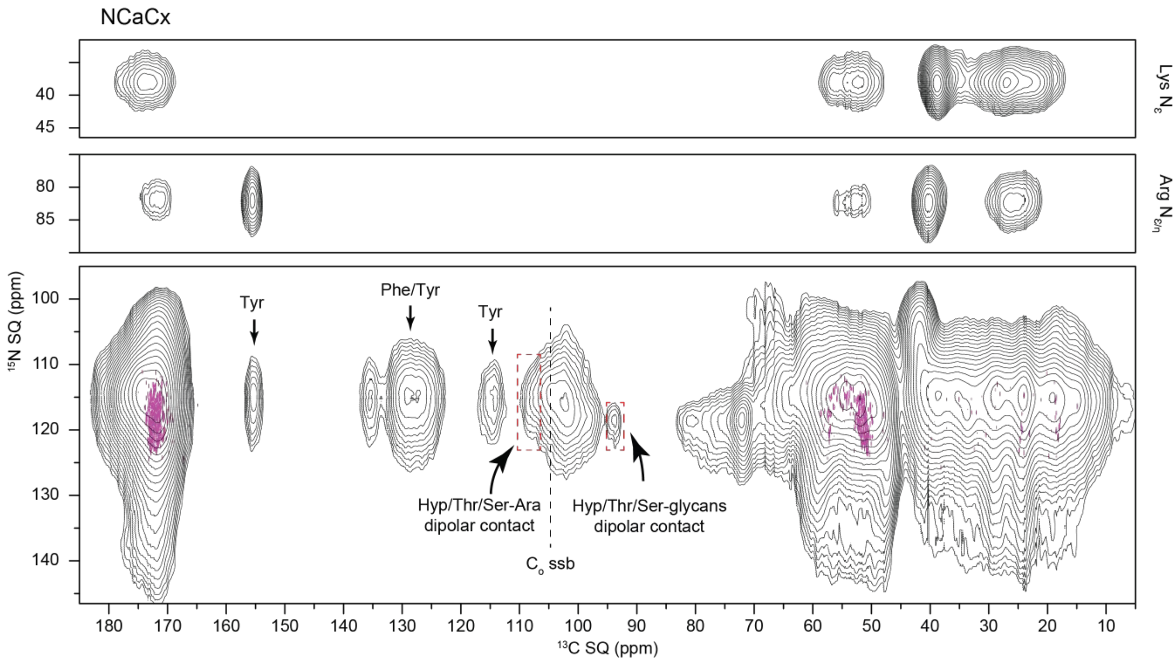

Supplementary Figure 13. NCaCx MAS-DNP and higher field spectra. NCaCx spectra of cell-wall extracts detected using MAS-DNP at 600 MHz, 100 K and 8kHz (black) and ssNMR at 800 MHz, 283 K and 13.5 kHz (purple). Allowing magnetisation to transfer from Cα to surrounding carbons, new peaks are detected. For example, O-glycosylated amino acids (hydroxyproline, threonine and serine) have their backbone nitrogen at ~115 and ~120 ppm correlating with anomeric carbons of glycans at ~110 ppm and ~95 ppm, respectively. Unfortunately, at 600 MHz and 8kHz spinning rate, previously NCa detected asparagine-glycan C_1 contacts (**Fig. 4d**) are now overlapping with the carbonyl spinning sideband (C_O ssb).

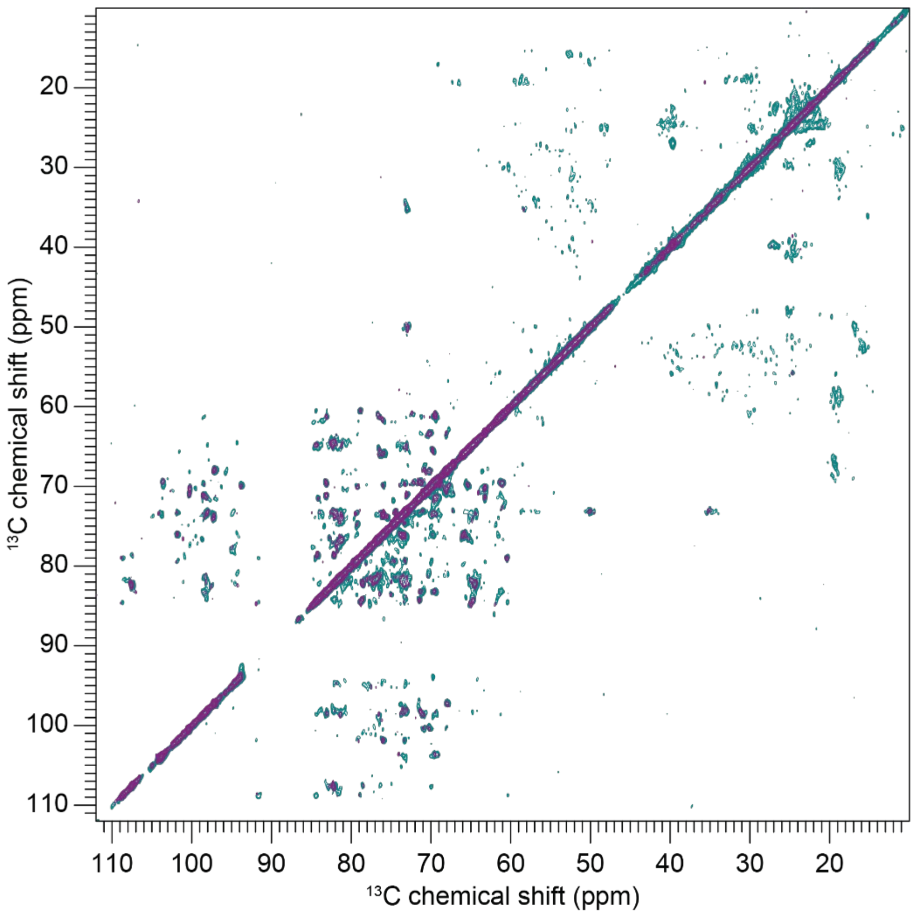

Supplementary Figure 14. 2D ^{13}C-^{13}C DARR water edition applied to *C. reinhardtii* cell wall. Control (teal) and water-edited (purple) 50 ms DARR spectra showing glycans and glycosylated amino acids to be more hydrated than other protein segments. Spectra were recorded on a 800 MHz spectrometer.

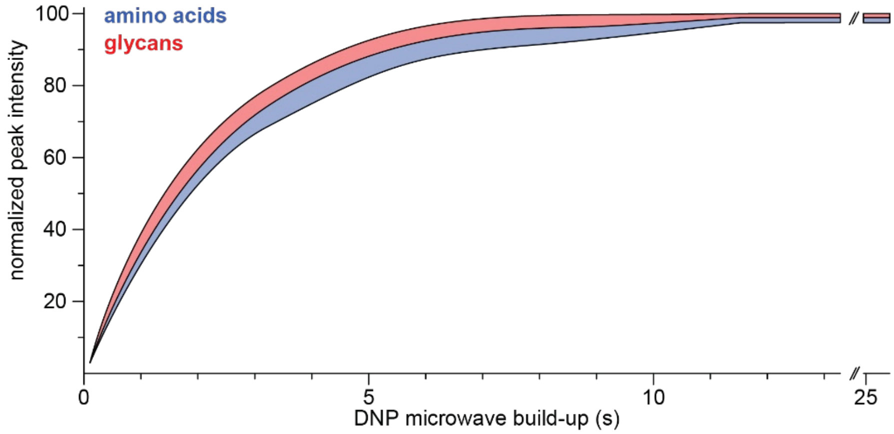

Supplementary Figure 15. DNP build-up of *C. reinhardtii's* cell wall extract. A slightly faster build-up is observed for glycans as compared to amino acids.

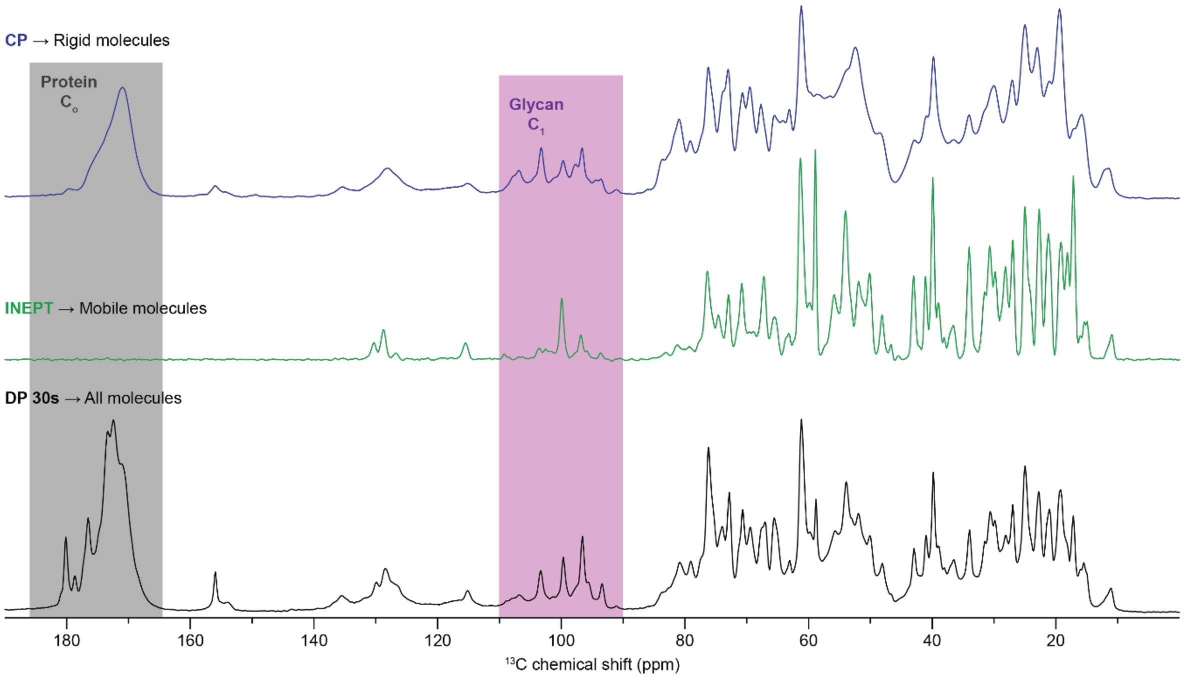

Supplementary Figure 16. 1D experiments revealing dynamics in *C. reinhardtii* cell wall. The CP spectrum (top, blue) selects rigid molecule segments, while the J-coupling-based refocused INEPT spectrum (middle, green) shows signals of highly mobile molecular segments when compared to the quantitative spectrum (bottom, black).

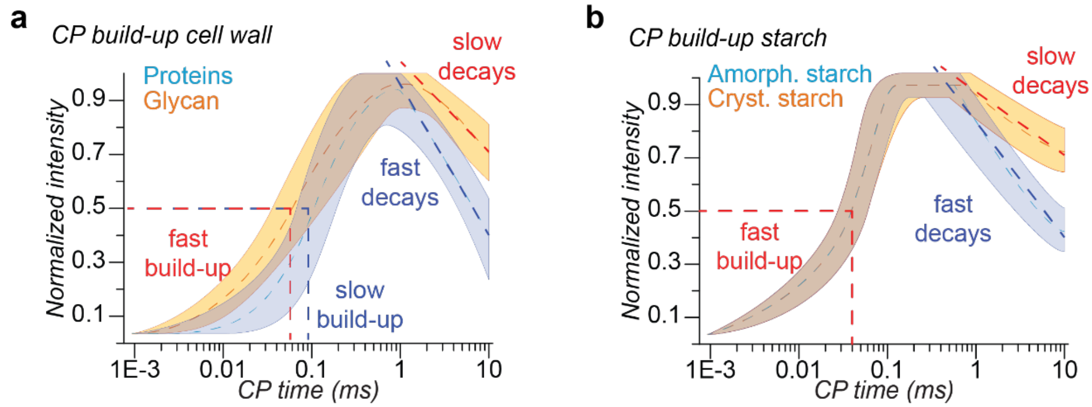

Supplementary Figure 17. CP build-up in *C. reinhardtii's* constituents. a CP build-up of amino acid and glycan carbons in the cell wall. **b** CP build-up of amorphous and crystalline starch carbons [15,16]. Details of the CP build-up for the cell wall and starch are given in **Supplementary Tables 17** and **18**, respectively. Fewer peaks were monitored compared to T_1 measurements, due to the lower resolution of the CP (**Supplementary Fig. 16**).

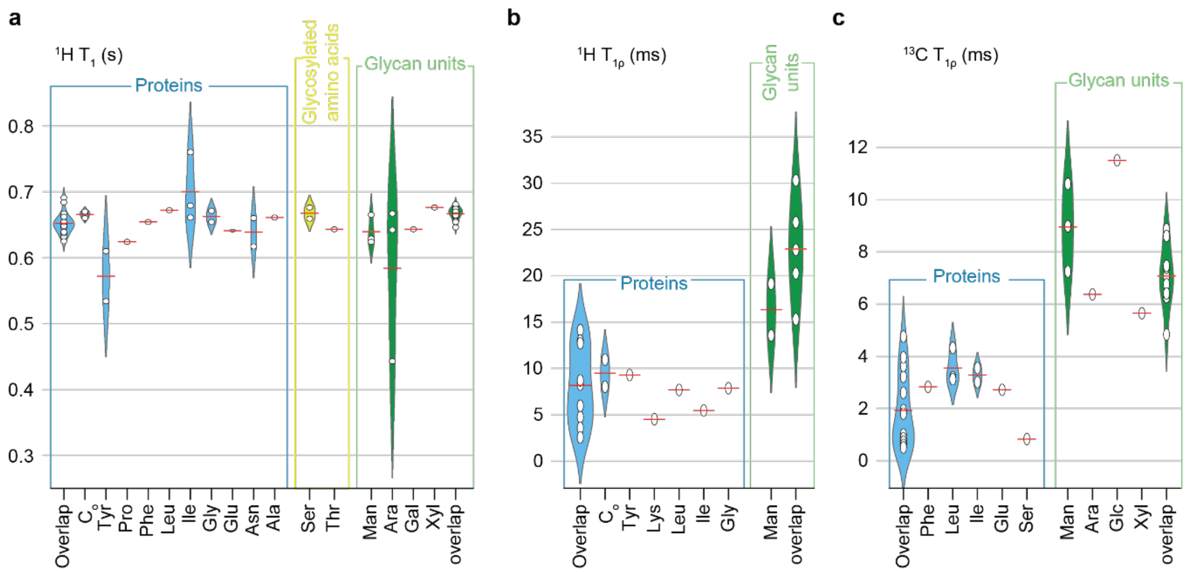

Supplementary Figure 18. Relaxation measurement of *C. reinhardtii's* cell wall. a ^{1}H spin-lattice (T_1) values of different amino acids and glycans. **b** ^{1}H and **c** ^{13}C $T_{1\rho}$ measurements of the same cell-wall extract. All fittings were performed on the most resolved peaks on the 1D spectra and separated based on the assignment obtained with the ^{13}C-^{13}C refocused *J*-INADEQUATE spectrum. Violin plots represent relaxation time dispersion within a single sample but corresponding to different protons/carbons from a specific residue or glycan unit.

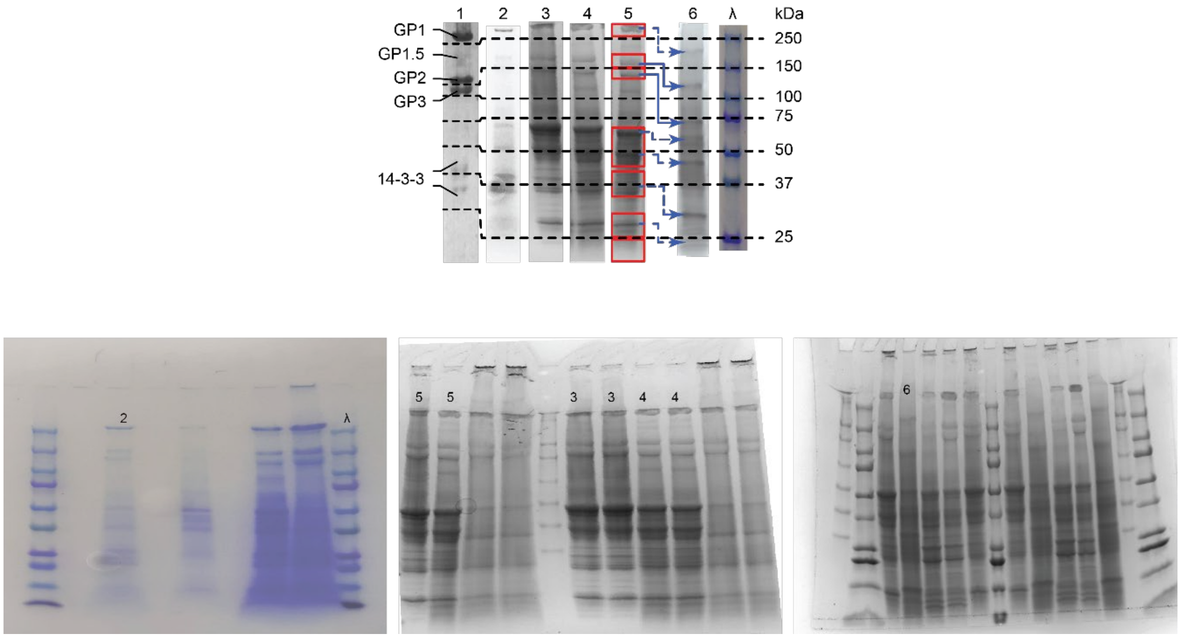

Supplementary Figure 19. Uncropped SD-PAGE gels. The uncropped gels were stained using Coomassie blue (0.05% w/v Coomassie Blue R-250) for 20-60 min, and destained with 30% v/v methanol/10% v/v glacial acetic acid for 5 h.

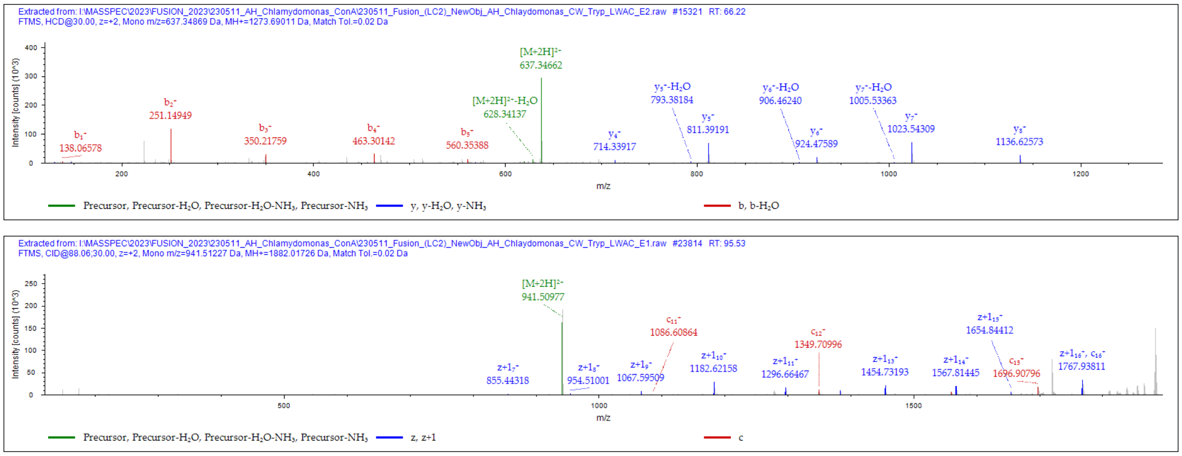

Supplementary Figure 20. Representative MS/MS spectra of glycopeptides. These hexose modified glycopeptides were identified in ConA-LWAC enriched fractions. Top spectrum is HCD fragmentation of HLVLPAATK (T8-Hex-Hex), z=+2, m/z=637.3487, derived from Protein kinase domain-containing protein. Bottom spectrum is ETciD fragmentation of VLSLASNDLVGTLPHAL (T12-Hex), z=+2, m/z=941.5123, derived from Guanylate cyclase domain-containing protein.

Supplementary Table 1. *wt* and *bald2* cell-wall glycan and amino acid composition. Glycan and amino acid composition of both strains are determined by GC/MS and HPLC, and compared with ssNMR, showing no significant differences. See **Supplementary Fig. 7** for details. Amino acids highlighted in orange are the amino acids that can be involved in O- or N-glycosylation.

	bald2		*wt*	
	MS	ssNMR	MS	ssNMR
Man	50.4	48.2	44.8	52.0
Ara	20.1	14.0	17.9	14.5
Gal	18.7	20.4	16.6	15.3
Rha	2.2	2.5	2.0	2.5
Glc	1.5	3.0	1.3	3.1
Xyl	1.5	2.2	1.3	2.5
GlcNAc	5.6	9.7	5.2	10.1

	bald2		*wt*	
	ssNMR	HPLC	ssNMR	HPLC
Gln	9.1	19.0 (0.3)	9.0	10.0
Glu	8.8		8.8	9.0
Asn	6.4	14.8 (0.3)	6.4	6.7
Asp	5.9		6.0	8.1
Ala	13.1	10.9 (0.3)	13.2	10.9
Gly	8.5	8.0 (0.3)	8.5	8.0
Leu	8.0	5.5 (0.3)	8.0	5.5
Lys	6.2	5.3 (0.1)	6.2	5.3
Ser	6.2	5.0 (0.2)	6.2	5.0
Pro	5.8	4.8 (0.2)	5.8	4.8
Val	5.7	5.6 (0.3)	5.6	5.6
Arg	5.1	3.5 (0.3)	5.1	3.5
Thr	4.3	4.7 (0.4)	4.3	4.6
Met	2.5	1.6 (0.2)	2.5	1.6
Ile	2.2	3.1 (0.3)	2.2	3.0
Tyr	1.5	2.4 (0.2)	1.5	2.4
Phe	0.7	2.8 (0.4)	0.7	2.8
His	*NA*	2.0 (0.1)	0.0	2.0
Hyp	*NA*	1.0 (0.1)	0.0	1.0

Supplementary Table 2. Glycosyl linkages determined by GC-MS in different samples.

Sample	*bald2* whole cell	*bald2* cw extracted	*bald2* cw extract	*wt* whole cell	*wt* cw extracted	*cw15* whole cell	*cw15* cw extracted	*Sta 6-1* whole cell	*Sta 6-1* cw extracted
t-Manp	2.8	2.6	7.2	2.0	1.3	2.6	21.1	11.5	10.8
2-Manp	**10.4**	**17.4**	**15.8**	**8.4**	**10.7**	6.0	1.5	**28.1**	**30.8**
3-Manp	0.0	0.0	0.0	0.0	2.0	2.1	3.4	1.5	0.0
2,3-Manp	3.2	3.1	5.4	3.9	1.6	2.3	**12.7**	8.1	8.5
2,4-Manp	0.0	0.0	0.9	2.2	1.3	0.0	0.0	0.0	0.0
t-Araf	1.4	1.4	1.7	1.0	1.1	**25.1**	7.7	4.0	2.5
t-Arap	0.8	1.5	1.4	0.0	1.0	0.0	3.8	3.7	2.1
2-Araf	2.6	4.0	6.4	1.9	2.3	4.3	**12.5**	8.6	8.5
2-Arap	0.0	0.0	0.0	0.0	0.0	0.0	1.7	1.5	2.5
2,4-Arap/2,5-Araf	0.0	0.0	0.0	0.0	0.0	0.0	2.0	4.1	3.1
t-Galp	3.8	8.5	5.0	3.5	4.6	2.8	3.4	7.6	7.2
t-Galf	1.5	2.4	3.1	2.5	1.6	1.5	5.7	4.9	4.5
4-Galp	0.0	0.0	0.0	0.0	0.0	0.0	2.3	1.1	1.5
3,4-Galp	0.0	0.0	0.0	0.0	0.0	2.9	5.3	0.0	0.0
t-Glcp	**17.6**	**12.2**	**15.3**	**19.8**	**14.0**	**18.7**	**13.6**	**8.9**	**13.2**
3-Glcp	0.9	0.2	2.5	0.7	0.6	1.7	1.5	1.6	1.7
4-Glcp	**42.7**	**33.9**	**20.2**	**42.0**	**42.0**	**18.1**	0.0	0.1	0.1
4,6-Glcp	3.3	2.9	2.0	4.5	4.6	1.9	0.5	1.0	1.4
3,4-Glcp	5.5	7.3	5.4	7.8	7.7	5.3	0.0	0.0	0.0
2,4-Rhap	0.0	0.0	2.9	0.0	0.0	0.0	1.3	1.0	1.6
3-Hexf	3.5	2.7	4.8	0.0	3.5	4.8	0.1	2.7	0.0

Supplementary Table 3. Full ^{13}C ssNMR glycan assignment of *C. reinhardtii bald2*'s cell wall.

Sugar Type	C1	C2	C3	C4	C5	C6	Ac	Met
Mannose units								
Man1	104.5	73.9	74.9	81.7	77.2	61.8		
Man2	97.7	74.6	76.2	65.7	77.2	61.4		
Man3	100.8	71.5	73.6	67.8	77.1	61.8		
Man4	103.6	72.2	75.4	67.9	77.2	61.9		
Man5	100.2	76.8	71.4	68.4	77.7	65.7		
Man6	102.4	67.8	77.2	65.7	76.0	62.1		
Man7	101.7	67.9	77.1	65.6	76.0	62.1		
Man8	103	71.1	77.1	67.8	75.3	63.1		
Man9	94.6	69.9	78.1	68.3	74.1	64.9		
Man10	96.7	70.4	76.8	65.8	76.0	62.2		
Man11	97.6	68.6	80	66.2	76.9	61.9		
Man12	96.8	68.6	80.8	66.3	76.9	61.5		
Man13	94.5	70.2	78.6	66.7	77	61.8		
Man14	99.2	73.6	78.5	65.9	70.5	66.2		
Arabinose units								
Ara1	110.3	82.4	77.6	81.8	61.8			
Ara2	110.1	82.2	77.7	81.7	61.8			
Ara3	109.8	81.9	77.2	81.4	66.1			
Ara4	109.8	81.8	75	81.3	67.2			
Galactose units								
Gal1	103.5	72.1	75.4	67.7	72.2	61.8		
Gal2	98.5	72.4	73.7	71.7	75.1	62.9		
Gal3	105.8	73.3	75	81.1	74.8	64.8		
Acetyl-methyl groups								
Ac1							23.4	175.5
Ac2							22.6	175.2
Ac3							23.8	173.4
Ac4							21.5	175.6
Rhamnose units								
Rha1	100.4	77.1	70.2	71.7	70.3	17.8		
Rha2	100.4	77.1	70.2	71.9	69.8	17.6		
Rha3	100.3	70.2	78.7	73.6	70.9	17.4		
Glucose units								
Glc1	100.4	69.6	74.1	72.5	70.9	63.6		
Glc2	100	76.8	71.3	63.8	71.8	61.9		
Xylose units								
Xyl1	97.7	76.1	77.2	67.7	60.2			
Xyl2	100.3	70.8	75.9	74.8	64.9			
Xyl3	100.9	77.4	75.1	79.5	67.8			

Supplementary Table 4. ^{13}C ssNMR glycan assignment and comparison with literature values.

Glycan units		SQ	SQ		Reference 1		Reference 2	
Man1					*Kang 2018*[14]		*Gorin 1975*[17]	
	C1	104.5	73.9	C2	101	69.4	94.6	72.3
	C3	73.9	74.9	C2	69.4	76.2	72.3	74.1
	C4	74.9	81.7	C3	76.2	83.4	74.1	67.8
	C4	81.7	77.2	C5	83.4	77.1	67.8	77.2
	C5	77.2	61.8	C6	77.1	61.6	77.2	62.1
Man2					*Bradbury 1984*[18]		*Gorin 1975*[17]	
	C1	97.7	74.6	C2	95.2	72.8	94.6	72.3
	C3	74.6	76.2	C2	72.8	74.8	72.3	74.1
	C3	76.2	65.7	C4	74.8	68.3	74.1	67.8
	C5	65.7	77.2	C4	68.3	77.6	67.8	77.2
	C5	77.2	61.4	C6	77.6	62.6	77.2	62.1
Man3					*Bradbury 1984*[18]		*Lundborg 2011*[19]	
	C1	100.8	71.5	C2	95.2	72.8	95	71.1
	C3	71.5	73.6	C2	72.8	74.8	71.1	79
	C3	73.6	67.8	C4	74.8	68.3	79	66.6
	C5	67.8	77.1	C4	68.3	77.6	66.6	71.8
	C5	77.1	61.8	C6	77.6	62.6	71.8	66.4
Man4					*Gorin 1975*[17]			
	C1	103.6	72.2	C2	94.6	72.3		
	C3	72.2	75.4	C2	72.3	74.1		
	C3	75.4	67.9	C4	74.1	67.8		
	C5	67.9	77.2	C4	67.8	77.2		
	C5	77.2	61.9	C6	77.2	62.1		
Man5					*Lundborg 2011*[19]		*Gorin 1975*[17]	
	C1	100.2	76.8	C2	97.8	77.9	94.6	72.3
	C2	76.8	71.4	C3	77.9	70.7	72.3	74.1
	C3	71.4	68.4	C4	70.7	68.3	74.1	67.8
	C5	68.4	77.7	C6	68.3	73.9	67.8	77.2
	C5	77.7	65.7	C4	73.9	62.4	77.2	62.1
Man6					*Gorin 1975*[17]		*Lundborg 2011*[19]	
	C1	102.4	67.8	C2	94.6	72.3	95	71.1
	C3	67.8	77.2	C2	72.3	74.1	71.1	79
	C3	77.2	65.7	C4	74.1	67.8	79	66.6
	C5	65.7	76.0	C4	67.8	77.2	66.6	71.8
	C5	76.0	62.1	C6	77.2	62.1	71.8	66.4
Man7					*Gorin 1975*[17]		*Lundborg 2011*[19]	
	C1	101.7	67.9	C2	94.6	72.3	95	71.1
	C3	67.9	77.1	C2	72.3	74.1	71.1	79
	C3	77.1	65.6	C4	74.1	67.8	79	66.6
	C5	65.6	76.0	C4	67.8	77.2	66.6	71.8
	C5	76.0	62.1	C6	77.2	62.1	71.8	66.4
Man8					*Gorin 1975*[17]		*Lundborg 2011*[19]	
	C1	103	71.1	C2	94.6	72.3	95	71.1
	C3	71.1	77.1	C2	72.3	74.1	71.1	79
	C3	77.1	67.8	C4	74.1	67.8	79	66.6
	C5	67.8	75.3	C4	67.8	77.2	66.6	71.8
	C5	75.3	63.1	C6	77.2	62.1	71.8	66.4
Man9					*Gorin 1975*[17]		*Lundborg 2011*[19]	
	C1	94.6	69.9	C2	94.6	72.3	95	71.1

	C3	69.9	78.1	C2	72.3	74.1	71.1	79
	C3	78.1	68.3	C4	74.1	67.8	79	66.6
	C5	68.3	74.1	C4	67.8	77.2	66.6	71.8
	C5	74.1	64.9	C6	77.2	62.1	71.8	66.4
Man10					*Gorin 1975*[17]		*Lundborg 2011*[19]	
	C1	96.7	70.4	C2	94.6	72.3	95	71.1
	C3	70.4	76.8	C2	72.3	74.1	71.1	79
	C3	76.8	65.8	C4	74.1	67.8	79	66.6
	C5	65.8	76.0	C4	67.8	77.2	66.6	71.8
	C5	76.0	62.2	C6	77.2	62.1	71.8	66.4
Man11					*Gorin 1975*[17]		*Lundborg 2011*[19]	
	C1	97.6	68.6	C2	94.6	72.3	95	71.1
	C3	68.6	80	C2	72.3	74.1	71.1	79
	C3	80	66.2	C4	74.1	67.8	79	66.6
	C5	66.2	76.9	C4	67.8	77.2	66.6	71.8
	C5	76.9	61.9	C6	77.2	62.1	71.8	66.4
Man12					*Gorin 1975*[17]		*Lundborg 2011*[19]	
	C1	96.8	68.6	C2	94.6	72.3	95	71.1
	C3	68.6	80.8	C2	72.3	74.1	71.1	79
	C3	80.8	66.3	C4	74.1	67.8	79	66.6
	C5	66.3	76.9	C4	67.8	77.2	66.6	71.8
	C5	76.9	61.5	C6	77.2	62.1	71.8	66.4
Man13					*Gorin 1975*[17]		*Lundborg 2011*[19]	
	C1	94.5	70.2	C2	94.6	72.3	95	71.1
	C3	70.2	78.6	C2	72.3	74.1	71.1	79
	C3	78.6	66.7	C4	74.1	67.8	79	66.6
	C5	66.7	77	C4	67.8	77.2	66.6	71.8
	C5	77	61.8	C6	77.2	62.1	71.8	66.4
Man14					*Lunborg 2011*[19]			
	C1	99.2	73.6	C2	94.9	71.2		
	C3	73.6	78.5	C2	71.2	79.3		
	C3	78.5	65.9	C4	79.3	66.9		
	C5	65.9	70.5	C6	66.9	71.9		
	C5	70.5	66.2	C4	71.9	66.8		
Ara1					*wang 2014*[20]			
	C1	110.3	82.4	C2	110	82.2		
	C2	82.4	77.6	C3	82.2	77.7		
	C4	77.6	81.8	C3	77.7	84.9		
	C4	81.8	61.8	C5	84.9	62.3		
Ara2					*wang 2014*[21]			
	C1	110.1	82.2	C2	110	82.2		
	C2	82.2	77.7	C3	82.2	77.7		
	C4	77.7	81.7	C3	77.7	84.9		
	C4	81.7	61.8	C5	84.9	62.3		
Ara3					*wang 2014*[20]		*Phyo 2017a*[22]	
	C1	109.8	81.9	C2	110	82.2	108.4	81.8
	C2	81.9	77.2	C3	82.2	77.7	81.8	77.8
	C4	77.2	81.4	C3	77.7	84.9	77.8	83.1
	C4	81.4	66.1	C5	84.9	62.3	83.1	67.8
Ara4					*wang 2014*[20]		*Phyo 2017a*[22]	
	C1	109.8	81.8	C2	110	82.2	108.4	81.8
	C2	81.8	75	C3	82.2	77.7	81.8	77.8
	C4	75	81.3	C3	77.7	84.9	77.8	83.1
	C4	81.3	67.2	C5	84.9	62.3	83.1	67.8

Gal1					*Wang 2014*[20]		
	C1	103.5	72.1	C2	103.4	74	
	C3	72.1	75.4	C2	74	76.4	
	C3	75.4	67.7	C4	76.4	73.8	
	C5	67.7	72.2	C4	73.8	74.8	
	C5	72.2	61.8	C6	74.8	61.7	
Gal2					*Arnold 2018*[15]		
	C1	98.5	72.4	C2	100.1	73.4	
	C3	72.4	73.7	C2	73.4	74.9	
	C3	73.7	71.7	C4	74.9	74.9	
	C5	71.7	75.1	C4	74.9	71.7	
	C5	75.1	62.9	C6	71.7	54.3	
Gal3					*Rondeau-Mouro 2008*[23]		
	C1	105.8	73.3	C2	105.5	72.9	
	C3	73.3	75	C2	72.9	74.4	
	C4	75	81.1	C3	74.4	78.8	
	C4	81.1	74.8	C5	78.8	75.7	
	C5	74.6	64.9	C6	75.7	61.6	
Ac1					Kang 2018[14]		King 2017[24]
	Ac	175.5	23.4	Met			
Ac2							
	Ac	175.2	22.6	Met			
Ac3							
	Ac	173.4	23.8	Met			
Ac4							
	Ac	175.6	21.5	Met			
Rha1					*Habibi 2004*[25]		
	C1	100.4	77.1	C2	99.2	77.5	
	C2	77.1	70.2	C3	77.5	70.2	
	C4	70.2	71.7	C3	70.2	71.3	
	C4	71.7	70.3	C5	71.3	69.8	
	C5	70.3	17.8	C6	69.8	17.5	
Rha2					*Habibi 2004*[25]		
	C1	100.4	77.1	C2	99.2	77.5	
	C2	77.1	70.2	C3	77.5	70.2	
	C4	70.2	71.9	C3	70.2	71.3	
	C4	71.9	69.8	C5	71.3	69.8	
	C5	69.8	17.6	C6	69.8	17.5	
Rha3					*Laguri 2018*[26]		
	C1	100.3	70.2	C2	101.2	71.2	
	C3	70.2	78.7	C2	71.2	81.2	
	C3	78.7	73.6	C4	81.2	73.8	
	C4	73.6	70.9	C5	73.8	70.2	
	C5	70.9	17.4	C6	70.2	18.1	
Glc1					*Pfeffer 1984*[27]		
	C1	100.4	69.6	C2	92.9	70.5	
	C3	69.6	74.1	C2	70.5	73	
	C3	74.1	72.5	C4	73	72.6	
	C4	72.5	70.9	C5	72.6	71.6	
	C5	70.9	63.6	C6	71.6	63.7	
Glc2					*Poulhazan 2018*[15]		
	C1	100	76.8	C2	100.5	72.3	
	C2	76.8	71.3	C3	72.3	73.7	

	C3	71.3	63.8	C4	73.7	70.4		
	C5	63.8	71.8	C4	70.4	73.7		
	C5	71.8	61.9	C6	73.7	61.1		
Xyl1					*Gorin 1975*[17]		*Gorin 1975*[17]	
	C1	97.7	76.1	C2	100.6	72.3	97.6	75.1
	C3	76.1	77.2	C2	72.3	74.3	75.1	76.9
	C3	77.2	67.7	C4	74.3	70.4	76.9	70.3
	C4	67.7	60.2	C5	70.4	62	70.3	66.3
Xyl2					*Wang 2014*[20]			
	C1	100.3	70.8	C2	102.4	73.9		
	C3	70.8	75.9	C4	73.9	76.7		
	C3	75.9	74.8	C2	76.7	74.6		
	C4	74.8	64.9	C5	74.6	63.6		
Xyl3					*Wang 2014*[20]			
	C1	100.9	77.4	C2	102.2	77.6		
	C2	77.4	75.1	C3	77.6	73.7		
	C4	75.1	79.5	C3	73.7	77.4		
	C4	79.5	67.8	C5	77.4	63.8		
Unk 1								
	C1	102.4	71.8	C2				
	C2	71.8	69.8	C3				
	C4	75.9	69.8	C3				
	C4	75.9	62.1	C5				
Unk 2								
	C1	100.2	76.9	C2				
	C2	76.9	71.4	C3				
	C4	83.7	71.4	C3				
	C4	83.7	61.7	C5				

Supplementary Table 5. Glycan integrals used for ssNMR quantification. Values in red correspond to peaks overlapping with other types of glycans, and therefore cannot be used for quantification. Nevertheless, as explained before[16], overlapping peaks among same glycan types, in orange, can be used for quantification.

Glycan unit	peak int.		SQ	SQ		peak int.	mono./poly.
Man 1	3.4E+07	C1	104.5	73.9	C2	1.9E+07	poly
	1.6E+07	C3	74.9	73.9	C2	1.5E+07	
	3.0E+06	C4	81.7	74.9	C3	**9.9E+06**	
	8.1E+06	C4	81.7	77.2	C5	**7.3E+06**	
	8.6E+07	C5	77.0	61.8	C6	**1.2E+07**	
Man 2	1.6E+07	C1	97.7	74.6	C2	6.6E+06	poly
	6.0E+06	C3	76.2	74.6	C2	**7.0E+06**	
	7.9E+06	C3	76.2	65.7	C4	**4.3E+06**	
	5.5E+07	C5	77.2	65.7	C4	**6.3E+07**	
	8.6E+07	C5	76.9	61.5	C6	**1.7E+07**	
Man 3	8.1E+07	C1	100.8	71.5	C2	6.3E+07	poly
	4.4E+07	C3	73.6	71.8	C2	**4.8E+07**	
	4.6E+07	C3	73.6	67.8	C4	**4.2E+07**	
	2.4E+07	C5	77.1	67.8	C4	**2.2E+07**	
	1.3E+06	C5	77.7	59.6	C6	1.4E+06	
Man 4	**1.0E+07**	C1	103.5	72.3	C2	**6.2E+06**	poly
	2.8E+07	C3	75.4	72.2	C2	**3.7E+07**	
	1.8E+07	C3	75.4	67.7	C4	**2.2E+07**	
	2.4E+07	C5	77.2	67.7	C4	**2.2E+07**	
	8.6E+07	C5	77.0	61.8	C6	**1.2E+07**	
Man 5	**2.8E+06**	C1	100.2	76.8	C2	**2.7E+06**	poly
	5.1E+06	C2	76.8	71.3	C3	**4.9E+06**	
	2.7E+06	C3	71.4	68.4	C4	**3.2E+06**	
	1.1E+06	C5	77.7	65.7	C6	1.8E+06	
	9.0E+05	C5	77.7	68.4	C4	**3.1E+06**	
Man 6	5.0E+06	C1	102.4	67.8	C2	2.2E+06	poly
	2.4E+07	C3	77.2	67.8	C2	**2.2E+07**	
	5.5E+07	C3	77.2	65.7	C4	**6.3E+07**	
	7.9E+06	C5	76.0	65.7	C4	**4.3E+06**	

	5.8E+06	C5	76.0	62.1	C6	**1.0E+07**	
Man 7	2.9E+06	C1	101.7	67.9	C2	3.0E+06	poly
	2.4E+07	C3	77.1	67.9	C2	**2.2E+07**	
	5.5E+07	C3	77.1	65.6	C4	**6.3E+07**	
	7.9E+06	C5	76.0	65.6	C4	**4.3E+06**	
	5.8E+06	C5	76.0	62.1	C6	**1.0E+07**	
Man 8	3.6E+06	C1	103.0	71.1	C2	7.0E+06	poly
	5.1E+06	C3	77.1	71.1	C2	**4.9E+06**	
	2.4E+07	C3	77.1	67.8	C4	**2.2E+07**	
	1.8E+07	C5	75.3	67.8	C4	**2.2E+07**	
	2.6E+06	C5	75.3	63.1	C6	2.3E+06	
Man 9	1.8E+07	C1	94.6	69.9	C2	**1.1E+07**	mono
	6.7E+06	C3	78.1	69.9	C2	**9.3E+06**	
	2.8E+06	C3	78.1	68.3	C4	**3.1E+06**	
	4.6E+07	C5	74.1	68.3	C4	**8.7E+05**	
	4.4E+06	C5	74.1	64.9	C6	**3.2E+06**	
Man 10	8.1E+06	C1	96.7	70.4	C2	4.3E+06	mono
	3.6E+06	C3	76.8	70.4	C2	3.6E+06	
	5.5E+07	C3	76.8	65.8	C4	**6.3E+07**	
	7.9E+06	C5	76.0	65.8	C4	**4.3E+06**	
	5.8E+06	C5	76.0	62.2	C6	**1.0E+07**	
Man 11	2.7E+07	C1	97.6	68.6	C2	**2.2E+07**	poly
	5.8E+06	C3	80.1	68.3	C2	6.2E+06	
	6.7E+06	C3	80.0	66.2	C4	2.4E+07	
	5.5E+07	C5	76.9	66.2	C4	**6.3E+07**	
	8.6E+07	C5	76.9	61.9	C6	**1.7E+07**	
Man 12	1.1E+07	C1	96.8	68.6	C2	**2.2E+07**	mono
	2.4E+06	C3	80.8	68.6	C2	3.2E+06	
	3.5E+06	C3	80.8	66.3	C4	4.9E+06	
	5.5E+07	C5	76.9	66.3	C4	**6.3E+07**	
	8.6E+07	C5	76.9	61.5	C6	**1.7E+07**	
Man 13	**1.8E+07**	C1	94.5	70.2	C2	**1.1E+07**	mono
	6.7E+06	C3	78.6	70.2	C2	**9.3E+06**	
	4.4E+06	C3	78.6	66.7	C4	8.2E+06	

	5.5E+07	C5	77.0	66.7	C4	**6.3E+07**	
	8.6E+07	C5	77.0	61.8	C6	**1.2E+07**	
Man 14	8.3E+05	C1	99.2	73.6	C2	4.2E+06	mono
	1.6E+06	C3	78.5	73.6	C2	1.8E+06	
	1.7E+06	C3	78.5	66.1	C4	3.5E+06	
	2.6E+06	C5	70.5	66.2	C6	**2.8E+06**	
	2.6E+06	C5	70.5	65.9	C4	**2.8E+06**	
Ara 1	**7.4E+06**	C1	110.3	82.4	C2	**4.4E+06**	poly
	7.1E+06	C2	82.4	77.6	C3	**1.4E+07**	
	8.1E+06	C4	81.8	77.6	C3	**7.3E+06**	
	1.5E+07	C4	81.8	61.8	C5	**1.4E+07**	
Ara 2	**7.4E+06**	C1	110.1	82.2	C2	**4.4E+06**	poly
	7.1E+06	C2	82.2	77.7	C3	1.4E+07	
	8.1E+06	C4	81.7	77.7	C3	**7.3E+06**	
	1.5E+07	C4	81.7	61.8	C5	**1.4E+07**	
Ara 3	2.6E+07	C1	109.8	81.9	C2	**2.2E+07**	poly
	8.1E+06	C2	81.9	77.2	C3	**7.3E+06**	
	8.1E+06	C4	81.4	77.2	C3	**7.3E+06**	
	1.5E+07	C4	80.7	66.2	C5	**4.9E+06**	
Ara 4	2.6E+07	C1	109.8	81.8	C2	**2.2E+07**	poly
	3.0E+06	C2	81.8	75.0	C3	**9.9E+06**	
	1.3E+06	C4	81.7	74.9	C3	**9.9E+06**	
	1.6E+07	C4	81.3	67.2	C5	2.4E+07	
Gal 1	**1.0E+07**	C1	103.5	72.1	C2	**6.2E+06**	poly
	2.8E+07	C3	75.4	72.1	C2	**3.7E+07**	
	1.8E+07	C3	75.4	67.7	C4	**2.2E+07**	
	9.5E+06	C5	72.2	67.7	C4	**3.2E+06**	
	7.4E+06	C5	72.2	61.8	C6	**1.8E+07**	
Gal 2	3.3E+07	C1	98.5	72.4	C2	2.3E+07	mono
	1.2E+07	C3	73.7	72.4	C2	**4.0E+06**	
	4.4E+07	C3	73.7	71.7	C4	**4.8E+07**	
	6.3E+06	C5	75.1	71.7	C4	3.3E+06	
	2.6E+06	C5	75.1	62.9	C6	2.2E+07	
Gal 3	1.9E+06	C1	105.8	73.3	C2	2.4E+06	poly

	1.0E+05	C3	75.0	73.3	C2	4.1E+05	
	1.3E+06	C4	81.1	75.0	C3	**9.9E+06**	
	1.3E+06	C4	81.1	74.8	C5	**9.9E+06**	
	7.2E+06	C5	74.8	64.8	C6	**3.2E+06**	
Ac-Met 1	3.0E+06	Met	175.5	79.4	Ac	1.1E+06	
Ac-Met 2	1.4E+07	Met	175.2	77.6	Ac	7.7E+06	
Ac-Met 3	4.0E+06	Met	173.4	78.8	Ac	1.5E+06	
Ac-Met 4	9.8E+06	Met	175.6	76.5	Ac	4.5E+06	
Rha 1	**2.8E+06**	C1	100.4	77.1	C2	**2.7E+06**	poly
	3.6E+06	C2	77.1	70.2	C3	**3.6E+06**	
	3.7E+06	C4	71.7	70.2	C3	**5.8E+06**	
	3.7E+06	C4	71.7	70.3	C5	**5.8E+06**	
	2.8E+06	C5	70.3	17.8	C6	1.0E+07	
Rha 2	**2.8E+06**	C1	100.4	77.1	C2	**2.7E+06**	poly
	3.6E+06	C2	77.1	70.2	C3	**3.6E+06**	
	3.7E+06	C4	71.9	70.2	C3	**5.8E+06**	
	3.7E+06	C4	71.9	69.8	C5	**5.8E+06**	
	2.8E+06	C5	69.8	17.6	C6	1.0E+07	
Rha 3	**2.6E+06**	C1	100.4	69.6	C2	1.2E+06	poly
	6.7E+06	C3	78.7	70.2	C2	**9.3E+06**	
	1.6E+06	C3	78.7	73.6	C4	**1.8E+06**	
	4.4E+07	C4	73.6	70.9	C5	**4.8E+07**	
	3.0E+06	C5	70.9	17.4	C6	3.1E+06	
Glc 1	2.6E+06	C1	100.4	69.6	C2	2.6E+06	poly
	1.6E+06	C3	74.1	69.6	C2	4.5E+06	
	1.2E+07	C3	74.2	72.5	C4	**4.0E+06**	
	2.6E+06	C4	72.5	70.9	C5	1.3E+06	
	1.3E+07	C5	70.9	63.6	C6	**1.5E+07**	
Glc 2	2.9E+06	C1	100.0	76.8	C2	2.5E+06	poly
	5.1E+06	C2	76.8	71.3	C3	**4.9E+06**	
	1.3E+07	C3	71.3	63.8	C4	**1.5E+07**	
	1.3E+07	C5	71.8	63.8	C4	**1.5E+07**	
	7.4E+06	C5	71.8	61.9	C6	**8.8E+06**	
Xyl 1	1.0E+06	C1	97.7	76.1	C2	5.4E+06	mono

	2.0E+06	C3	77.2	76.1	C2	4.7E+06	
	2.4E+07	C3	77.2	67.7	C4	**2.2E+07**	
	3.2E+07	C4	67.7	60.2	C5	**2.2E+07**	
Xyl 2	1.0E+06	C1	100.3	70.8	C2	1.6E+06	poly
	6.0E+06	C3	75.9	74.8	C4	**7.0E+06**	
	1.4E+06	C3	75.9	70.8	C2	1.3E+06	
	7.2E+06	C4	74.8	64.9	C5	**3.2E+06**	
Xyl 3	1.3E+06	C1	100.9	77.4	C2	**1.3E+06**	poly
	2.0E+06	C2	77.4	75.1	C3	1.2E+06	
	1.5E+06	C4	79.5	75.1	C3	1.3E+06	
	1.3E+06	C4	79.5	67.8	C5	1.2E+06	

Unk 1	2.7E+06	C1	102.4	71.8	C2	4.6E+06	poly
	3.7E+06	C2	71.8	69.8	C3	5.8E+06	
	4.4E+06	C4	75.9	69.8	C3	4.5E+06	
	5.8E+06	C4	75.9	62.1	C5	**1.0E+07**	
Unk 2	**2.8E+06**	C1	100.2	76.9	C2	**2.7E+06**	poly
	5.1E+06	C2	76.9	71.4	C3	**4.9E+06**	
	2.0E+07	C4	83.7	71.4	C3	5.5E+07	
	3.2E+07	C4	83.7	61.7	C5	3.8E+07	

Supplementary Table 6. Results of the ssNMR-based glycan quantification. SsNMR can quantify the total amount of each glycan but also its relative abundance as mono- or polysaccharides, according to their C_1 chemical shifts. Glycan quantification has been performed as described before[16]. Briefly, quantification takes into account all the carbon peak integrals corresponding to one glycan type (values in black and orange in **Supplementary Table 5**). Then integrals are normalized using the number of carbon integrated (*tot nC*) and, for comparison with other glycans, we take into account the number of spin system assigned (*n spin syst.*). Results of the GC/MS-based quantification are shown for comparison in the last column.

		sum int.	nC	nC overlap	tot nC	int/nC_{total}	n spin syst.	$(int/nC)*n_{spin\ system}$	% norm.	GC/MS
Man	TOTAL	8.9E+08	63	47	110	8.1E+06	14	1.1E+08	48.2	
	poly.	5.8E+08	47	38	85	6.8E+06	10	6.8E+07	29.0	45
	mono.	3.1E+08	16	9	25	1.2E+07	4	5.0E+07	21.3	
Ara	TOTAL	1.6E+08	10	9	19	8.2E+06	4	3.3E+07	14.0	
	poly.	1.6E+08	10	9	19	8.2E+06	4	3.3E+07	14.0	16
	mono.	0.0E+00	0	0	0	0.0E+00	0	0.0E+00	0.0	
GlcNAc	TOTAL	4.6E+07	8	0	8	5.7E+06	4	2.3E+07	9.7	
	poly.	4.6E+07	8	0	8	5.7E+06	4	2.3E+07	9.7	5.6
	mono.	0.0E+00	0	0	0	0.0E+00	0	0.0E+00	0.0	
Gal	TOTAL	1.6E+08	10	0	10	1.6E+07	3	4.8E+07	20.4	
	poly.	1.4E+07	5	0	5	2.9E+06	2	5.7E+06	2.4	17
	mono.	1.5E+08	5	0	5	2.9E+07	1	2.9E+07	12.4	
Rha	TOTAL	2.0E+07	5	2	7	2.9E+06	2	5.8E+06	2.5	
	poly.	2.0E+07	5	2	7	2.9E+06	2	5.8E+06	2.5	2
	mono.	0.0E+00	0	0	0	0.0E+00	0	0.0E+00	0.0	
Glc	TOTAL	4.9E+07	10	4	14	3.5E+06	2	6.9E+06	3.0	
	poly.	4.9E+07	10	4	14	3.5E+06	2	6.9E+06	3.0	1.3
	mono.	0.0E+00	0	0	0	0.0E+00	0	0.0E+00	0.0	
Xyl	TOTAL	2.6E+07	14	1	15	1.7E+06	3	5.2E+06	2.2	
	poly.	1.3E+07	10	1	11	1.2E+06	2	2.4E+06	1.0	1.3
	mono.	1.3E+07	4	0	4	3.3E+06	1	3.3E+06	1.4	

Supplementary Table 7. ^{13}C glycan composition of different intact *C. reinhardtii* strains. Highlighted column (*bald2* cell-wall extract) corresponds to the cell-wall extract reported in the main text. The strains reported are the wild-type (*wt*) strain, strain without flagella (*bald2*), cell-wall deprived (*cw15*) and starchless mutants. The reported ^{13}C alditol values show relative mole percentages (%).

Strain / ^{13}C alditol	*bald2* whole cell	*bald2* cw extracted	*bald2* cw extract	*wt* whole cell	*wt* cw extracted	*wt* cw extract	*cw15* whole cell	*cw15* cw extracted	sta6-1 whole cell	sta6-1 cw extracted
Man	27.2	12.8	50.4	12.9	4.9	48.4	2.4	10.5	28.6	12.8
Ara	22.9	24.8	20.1	13.3	11.8	19.6	9.5	10.2	24.9	30.6
Gal	15.9	14.2	18.7	11.6	9.8	20.0	1.7	7.7	29.8	34.0
Rha	4.9	6.5	2.2	0.9	0.6	2.6	0.0	0.7	3.2	5.1
Glc	22.7	35.9	1.5	54.4	66.2	2.0	85.1	66.0	3.8	5.6
Xyl	1.7	1.9	1.5	1.6	1.7	1.5	1.0	1.6	2.2	4.7
GlcNAc	4.7	4.0	5.6	5.2	5.0	5.9	0.2	3.3	7.5	7.1

Supplementary Table 8. Glycan content determined by GC-MS.

	Whole cell	Whole cell after wall extraction	Cell wall extract	Proportionality factor
Man	27.2	12.8	50.4	38
Ara	22.9	24.8	20.1	40
Gal	15.9	14.2	18.7	38
Rha	4.9	6.5	2.2	37
Glc	22.7	35.9	1.5	38
Xyl	1.7	1.9	1.5	50
GlcNAc	4.7	4.0	5.6	44

Glycan contents (in molar %) of cells before and after wall extraction, and in the extracted cell wall. The proportionality factor corresponds to the cell wall contribution (molar %) in the whole cell glycans. See **Supplementary Table 7** for glycan quantification in other samples.

We calculated the contribution of glycans in the whole cells that originate from the cell wall, and found a similar proportionality factor for each glycan, confirming that almost no sugar units were lost or altered during the extraction and reconstitution, with an uncertainty for xylose, which proportion is close to ssNMR and MS detection limits. This proportionality factor indicates that about 40% of the whole cell glycans are contained in the cell wall.

Supplementary Table 9. ^{13}C ssNMR amino acid assignment of *C. reinhardtii bald2* cell wall. Amino acid assignment is performed using 800 MHz DP-based *J*-INADEQUATE and DARR spectra. ^{13}C chemical shifts are referenced using TMS (by setting adamantane CH_2 chemical shift to 38.48 ppm), therefore TALOS+ calculation have been made shifting all the chemical shifts by 2.0 ppm to match DSS referencing. "b" and "c" correspond to beta-sheet and random-coil/polyproline helix prediction given by TALOS+ calculation, respectively.

Amino acids residues	secondary structure	Co	Cα	Cβ	Cγ	Cδ	Cε	Cζ
Lys1	b	174.0	53.9	30.7	22.5	26.7	41.9	
Lys2	b	174.3	54.0	31.9	23.1	27.7	40.6	
Lys3	b	174.8	54.3	31.2	22.9	27.2	40.4	
Lys4	b	174.3	54.1	33.3	22.3	26.9	40.1	
Asp1	b	174.0	54.0	40.9	178.9			
Asp2	c	174.0	54.0	40.3	177.8			
Asp3	c	175.6	53.6	39.3	178.2			
Asp4	c	175.2	54.1	37.6	178.3			
Asn1	c	174.2	52.6	39.3	176.0			
Asn2	c	174.3	52.3	38.6	176.4			
Asn3	c	174.4	51.1	37.2	175.2			
Glu1	b	173.9	55.8	29.4	33.8	182.9		
Glu2	c	179.1	54.0	25.4	30.1	182.7		
Glu3	b	174.4	54.1	29.2	34.9	182.6		
Glu4	c	175.2	55.1	28.3	34.4	181.8		
Gln1	c	175.2	54.6	28.4	32.5	179.0		
Gln2	b	174.3	53.7	30.2	31.0	178.6		
Gln3	b	174.1	53.9	27.6	32.0	178.4		
Gln4	c	175.5	55.7	29.9	33.3	178.1		
Gln5	b	174.5	54.4	30.5	32.0	178.4		
Hyp1	u	171.9	58.8	34.8	73.1	50.2		
Pro1	c	175.3	60.6	30.5	25.7	49.0		
Pro2	c	175.4	61.3	30.1	25.4	48.5		
Pro3	c	174.0	59.2	29.0	25.2	47.9		
Pro4	c	175.8	61.7	28.5	25.0	47.4		
Pro5	c	175.9	62.0	29.8	24.6	47.1		
Arg1	b	174.4	54.2	31.5	24.9	40.6		
Arg2	b	175.6	53.5	30.4	25.8	37.7		
Arg3	b	173.9	53.9	30.7	24.9	40.6		
Arg4	b	175.6	53.7	30.1	25.2	41.6		
Arg5	c	173.9	55.8	29.8	24.6	41.6		
Arg6	b	174.4	54.2	28.9	25.4	41.6		
Arg7	c	176.5	54.6	28.5	25.0	40.4		
Se1	b	172.7	56.6	64.4				
Ser2	c	175.6	57.6	64.1				
Ser3	b	172.7	56.6	63.9				
Ser4	c	176.9	58.1	63.2				
Ser5	c	176.1	56.6	62.1				
Thr1	b	174.1	60.4	68.0	19.6			
Thr2	b	173.9	61.1	68.9	19.4			
Thr3	b	173.9	59.9	70.8	17.5			

Gly1	b	169.9	42.6					
Gly2	c	171.1	43.4					
Gly3	c	172.0	43.3					
Gly4	c	172.8	43.6					
Gly5	c	173.2	42.6					
Ala1	b	173.7	49.0	25.7				
Ala2	b	173.6	48.5	25.4				
Ala3	b	/	47.9	25.2				
Ala4	b	/	47.4	25.0				
Ala5	b	/	47.1	24.6				
Ala6	b	173.6	48.3	22.8				
Ala7	c	176.6	51.8	18.4				
Ala8	b	177.0	50.6	19.2				
Ala9	b	175.1	50.0	18.9				
Ala10	c	176.7	51.5	17.2				
Ala11	c	176.1	51.0	17.2				
Ala12	c	177.2	50.4	17.5				
Ala13	b	175.2	50.1	17.3				
Ala14	c	173.6	48.4	16.6				
Tyr1	c	174.6	51.1	37.4	130.2	131.6	116.7	156.4
Tyr2	c	174.6	51.1	37.4	130.2	131.2	116.9	155.5
Tyr3	c	174.6	51.1	37.4	130.2	131.6	116.0	156.0
Tyr4	c	174.6	51.1	37.4	130.2	131.6	116.5	155.1
Tyr5	c	174.6	51.1	37.4	130.2	131.6	115.9	155.5
Leu1	c	175.8	54.9	41.8	26.6	21.5		
Leu2	c	175.2	55.0	41.5	25.4	21.9		
Leu3	b	174.0	54.2	40.8	25.1	23.2		
Leu4	c	176.2	53.8	39.9	27.0	22.2		
Leu5	c	176.6	53.3	40.5	27.2	22.9		
Leu6	b	175.9	53.3	40.6	27.8	23.3		
Leu7	c	176.6	52.4	39.7	28.8	23.0		
Met1	c	175.6	54.7	30.6	32.0	19.0		
Met2	c	176.4	53.6	30.2	31.0	18.5		
Met3	c	176.2	53.8	30.7	29.7	19.0		
Met4	c	174.7	54.4	30.9	29.8	17.6		
Val1	c	175.8	62.1	29.8	17.7			
Val2	c	175.6	62.3	29.7	19.0			
Val3	b	174.8	61.5	31.4	19.7			
Val4	b	174.8	61.2	30.3	19.5			
Val5	b	172.1	60.7	30.1	18.4			
Val6	b	172.4	60.1	30.9	18.5			
Ile1	b	173.9	59.3	36.7	25.2	11.1		
					15.8			
Ile2	b	174.2	59.3	36.7	25.4	11.8		
					15.8			
Ile3	b	173.7	59.2	36.9	25.5	12.0		
					15.7			
Ile4	b	/	/	37.7	/	/		
					16.3			
Phe1	u	/	/	138.6	130.2	129.3	127.6	
Phe2	u	/	/	138.6	130.1	129.4	128.1	

Supplementary Table 10. Integrals of the amino acid used for their quantification. Values in red correspond to amino-acid peaks overlapping with other types of amino acids, and therefore cannot be used for quantification, while overlapping peaks among same kinds of residues, in orange, can be used for quantification. This table also allows to see the TALOS+ secondary structure prediction.

	peak int.		SQ	SQ		peak int.	TALOS second. Struct.
Ala 1	1.3E+07	Ca	49.0	25.7	Cb	1.1E+07	Beta-sheet
	5.7E+06	Co	173.7	49.0	Ca	**5.5E+06**	
Ala 2	1.3E+07	Ca	48.5	25.4	Cb	1.6E+07	Beta-sheet
	5.7E+06	Co	173.6	48.5	Ca	**5.5E+06**	
Ala 3	5.5E+06	*Ca*	47.9	25.2	*Cb*	9.5E+06	Beta-sheet
Ala 4	1.4E+07	*Ca*	47.4	25.0	*Cb*	4.7E+06	Beta-sheet
Ala 5	1.6E+07	*Ca*	47.1	24.6	*Cb*	1.2E+07	Beta-sheet
Ala 6	5.9E+06	Ca	48.3	22.8	Cb	5.2E+06	Beta-sheet
	5.7E+06	Ca	173.6	48.3	Ca	**5.5E+06**	
Ala 7	1.4E+07	Ca	51.8	18.4	Cb	3.9E+07	Random coil
	1.1E+07	Co	176.6	51.8	Ca	1.9E+06	
Ala 8	9.8E+05	Ca	50.6	19.2	Cb	1.1E+07	Beta-sheet
	7.6E+06	Co	177.0	50.6	Ca	**4.2E+06**	
Ala 9	7.6E+06	Ca	50.0	18.9	Cb	2.3E+07	Beta-sheet
	3.6E+07	Co	175.1	50.0	Ca	**3.0E+06**	
Ala 10	1.0E+07	Ca	51.5	17.2	Cb	1.6E+07	Random coil
	2.7E+07	Co	176.7	51.5	Ca	**1.9E+07**	
Ala 11	1.6E+06	Ca	51.0	17.2	Cb	3.2E+07	Random coil
	2.7E+07	Co	176.1	51.0	Ca	**1.9E+07**	
Ala 12	**5.8E+06**	Ca	50.4	17.5	Cb	**1.1E+07**	Random coil
	7.6E+06	Co	177.2	50.4	Ca	**4.2E+06**	
Ala 13	**5.8E+06**	Ca	50.1	17.3	Cb	**1.1E+07**	Beta-sheet
	3.6E+07	Co	175.2	50.1	Ca	**3.0E+06**	
Ala 14	5.5E+06	Ca	48.4	16.6	Cb	1.2E+07	Random coil
	5.7E+06	Co	173.6	48.4	Ca	**5.5E+06**	
Arg 1	**2.6E+07**	Ca	54.2	31.5	Cb	**4.4E+07**	Beta-sheet
	3.1E+06	Cb	31.5	24.9	Cc	3.2E+06	
	2.7E+07	Cd	40.6	24.9	Cc	**2.4E+07**	
	9.0E+07	Co	174.4	54.2	Ca	**9.9E+07**	
Arg 2	**3.1E+06**	Ca	53.5	30.4	Cb	**3.6E+06**	Beta-sheet
	2.4E+06	Cb	30.4	25.8	Cc	**1.3E+07**	
	5.6E+06	Cd	37.7	25.8	Cc	5.6E+06	
	6.2E+06	Co	175.6	53.5	Ca	**1.2E+07**	
Arg 3	**2.6E+07**	Ca	53.9	30.7	Cb	**4.4E+06**	Beta-sheet
	1.8E+06	Cb	30.7	24.9	Cc	1.6E+06	
	2.7E+07	Cd	40.6	24.9	Cc	**2.4E+07**	
	9.0E+07	Co	173.9	53.9	Ca	**9.9E+07**	
Arg 4	**3.1E+06**	Ca	53.7	30.1	Cb	**3.6E+06**	Beta-sheet
	2.8E+07	Cb	30.1	25.2	Cc	**3.1E+07**	
	8.5E+07	Cd	41.6	25.2	Cc	**6.9E+07**	
	6.2E+06	Co	175.6	53.7	Ca	**1.2E+07**	

Arg 5	**7.4E+06**	Ca	55.8	29.8	Cb	**1.6E+07**	Random coil
	7.0E+06	Cb	29.8	24.6	C	5.3E+06	
	8.5E+07	Cd	41.6	24.6	Cc	**6.9E+07**	
	2.4E+06	Co	173.9	55.8	Ca	**3.2E+06**	
Arg 6	**4.5E+06**	Ca	54.2	28.9	Cb	**7.5E+06**	Beta-sheet
	1.3E+07	Cb	28.9	25.4	Cc	1.5E+07	
	8.5E+07	Cd	41.6	25.4	Cc	**6.9E+07**	
	9.0E+07	Co	174.4	54.2	Ca	**9.9E+07**	
Arg 7	**3.3E+07**	Ca	54.6	28.5	Cb	**5.5E+07**	Random coil
	3.2E+06	Cb	28.5	25.0	Cc	**7.6E+06**	
	2.7E+07	Cd	40.4	25.0	Cc	**2.4E+07**	
	1.5E+07	Co	176.5	54.6	Ca	**3.6E+07**	
Asn 1	**2.6E+07**	Ca	52.6	39.3	Cb	**1.9E+07**	Random coil
	9.4E+06	Cc	176.0	39.3	Cb	4.0E+06	
	2.6E+07	Co	174.2	52.6	Ca	4.3E+07	
Asn 2	2.2E+06	Ca	52.3	38.6	Cb	4.6E+06	Random coil
	5.7E+06	Cc	176.4	38.6	Cb	4.6E+06	
	2.6E+07	Co	174.3	52.3	Ca	4.3E+07	
Asn 3	**9.1E+06**	Ca	51.1	37.2	Cb	**2.9E+07**	Random coil
	4.6E+07	Cc	175.2	37.2	Cb	2.9E+07	
	3.6E+07	Co	174.4	51.1	Ca	**1.3E+07**	
Asp 1	6.7E+06	Ca	54.0	40.9	Cb	9.5E+06	Beta-sheet
	1.4E+07	Cc	178.9	40.9	Cb	**1.3E+07**	
	9.0E+07	Co	174.0	54.0	Ca	**9.9E+07**	
Asp 2	7.9E+06	Ca	53.1	40.3	Cb	**1.2E+07**	Random coil
	6.7E+06	Cc	177.8	40.3	Cb	**1.2E+07**	
	9.0E+07	Co	174.0	54.0	Ca	**9.9E+07**	
Asp 3	2.0E+06	Ca	53.6	39.3	Cb	**3.1E+07**	Random coil
	5.8E+07	Cc	178.2	39.3	Cb	**3.1E+07**	
	6.2E+06	Co	175.6	53.6	Ca	**1.2E+07**	
Asp 4	2.0E+06	Ca	54.1	37.6	Cb	**3.1E+07**	Random coil
	1.5E+07	Cc	178.3	37.6	Cb	**3.5E+06**	
	9.0E+07	Co	175.2	54.1	Ca	**9.9E+07**	
Gln 1	**3.3E+07**	Ca	54.6	28.4	Cb	**5.5E+07**	Random coil
	9.1E+06	Cc	32.5	28.4	Cb	1.2E+07	
	1.1E+07	Cd	179.0	32.5	Cc	**8.2E+06**	
	9.0E+07	Co	175.2	54.2	Ca	**9.9E+07**	
Gln 2	**3.1E+06**	Ca	53.7	30.2	Cb	**3.6E+06**	Beta-sheet
	7.3E+06	Cc	31.0	30.2	Cb	**1.2E+07**	
	5.6E+07	Cd	178.6	31.0	Cc	4.0E+07	
	9.0E+07	Co	174.3	54.2	Ca	**9.9E+07**	
Gln 3	1.4E+07	Ca	53.9	27.6	Cb	1.9E+07	Beta-sheet
	2.7E+07	Cc	32.0	27.6	Cb	2.7E+07	
	5.6E+07	Cd	178.4	32.0	Cc	4.0E+07	
	9.0E+07	Co	174.1	54.0	Ca	**9.9E+07**	
Gln 4	**7.4E+06**	Ca	55.7	29.9	Cb	**1.6E+07**	Random coil
	1.4E+06	Cc	33.3	29.9	Cb	1.8E+06	
	1.1E+07	Cd	178.1	33.3	Cc	5.9E+06	
	2.7E+07	Co	175.5	55.7	Ca	1.0E+07	
Gln 5	**2.6E+07**	Ca	54.4	30.5	Cb	**4.4E+06**	Beta-sheet

	6.5E+06	Cc	32.0	30.5	Cb	**1.0E+07**	
	5.6E+07	Cd	178.4	32.0	Cc	4.0E+07	
	9.0E+07	Co	174.5	54.4	Ca	**9.9E+07**	
Glu 1	7.4E+06	Ca	55.8	29.4	Cb	1.6E+07	Beta-sheet
	5.7E+06	Cc	33.8	29.4	Cb	**1.7E+07**	
	2.3E+07	Cd	182.9	33.8	Cc	4.2E+06	
	2.4E+06	Co	173.9	55.8	Ca	**3.2E+06**	
Glu 2	2.0E+06	Ca	54.0	25.4	Cb	2.2E+06	Random coil
	2.8E+07	Cc	30.1	25.4	Cb	**3.1E+07**	
	9.0E+06	Cd	182.7	30.1	Cc	8.0E+06	
	2.6E+06	Co	179.1	54.0	Ca	7.3E+06	
Glu 3	**4.5E+06**	CA	54.1	29.1	Cb	**7.5E+06**	Beta-sheet
	6.0E+06	Cc	34.9	29.2	Cb	**1.7E+07**	
	2.4E+07	Cd	182.6	34.9	Cc	1.5E+07	
	9.0E+07	Co	174.4	54.1	Ca	**9.9E+07**	
Glu 4	7.6E+06	Ca	55.1	28.3	Cb	8.7E+06	Random coil
	3.3E+07	Cc	34.4	28.3	Cb	4.6E+07	
	1.5E+08	Cd	181.8	34.4	Cc	7.6E+07	
	3.5E+07	Co	175.2	55.1	Ca	**1.4E+07**	
Gly 1	5.3E+06	Co	169.9	42.6	Ca	6.9E+06	Beta-sheet
Gly 2	1.9E+07	Co	171.1	43.4	Ca	9.7E+06	Random coil
Gly 3	3.5E+07	Co	172.0	43.3	Ca	1.9E+07	Random coil
Gly 4	3.5E+07	Co	172.8	43.6	Ca	2.9E+07	Random coil
Gly 5	2.8E+06	Co	173.2	42.6	Ca	1.2E+06	Random coil
Ile 1	**6.9E+06**	Ca	59.3	36.7	Cb	**4.3E+06**	Beta-sheet
	1.3E+07	Cb	36.7	25.2	Cc1	**1.7E+07**	
	6.6E+06	Cb	36.7	15.8	Cc2	**1.5E+07**	
	1.4E+07	Cc1	25.2	11.1	Cd	2.7E+07	
	1.4E+06	Co	173.9	59.3	Ca	**1.3E+07**	
Ile 2	**6.9E+06**	Ca	59.3	36.7	Cb	**4.3E+06**	Beta-sheet
	1.3E+07	Cb	36.7	25.4	Cc1	**1.7E+07**	
	6.6E+06	Cb	36.7	15.8	Cc2	**1.5E+07**	
	1.4E+07	Cc1	25.4	11.8	Cd	**8.5E+06**	
	1.4E+06	Co	174.2	59.3	Ca	**1.3E+07**	
Ile 3	**6.9E+06**	Ca	59.2	36.9	Cb	**4.3E+06**	Beta-sheet
	1.3E+07	Cb	36.9	25.5	Cc1	**1.7E+07**	
	6.6E+06	Cb	36.9	15.7	Cc2	**1.5E+07**	
	1.4E+07	Cc1	25.5	12.0	Cd	**8.5E+06**	
	1.4E+06	Co	173.7	59.2	Ca	**1.3E+07**	
Ile 4	4.8E+06	Cb	37.7	16.3	Cb	1.6E+07	Beta-sheet
Leu 1	6.0E+06	Ca	54.9	41.8	Cb	8.9E+06	Random coil
	5.3E+06	Cb	41.8	26.6	Cc	1.6E+06	
	1.6E+06	Cc	26.6	21.5	Cd	1.1E+07	
	3.0E+07	Co	175.8	54.9	Ca	**3.6E+07**	
Leu 2	**4.8E+06**	Ca	55.0	41.5	Cb	**1.3E+07**	Random coil
	8.5E+07	Cb	41.5	25.4	Cc	**6.9E+07**	
	5.9E+06	Cc	25.4	21.9	Cd	1.2E+07	
	3.5E+07	Co	175.2	55.0	Ca	**1.4E+07**	
Leu 3	6.7E+06	Ca	54.2	40.8	Cb	3.5E+06	Beta-sheet
	2.7E+07	Cb	40.8	25.1	Cc	**2.4E+07**	

	7.0E+07	Cc	25.1	23.2	Cd	1.6E+07	
	9.0E+07	Co	174.0	54.2	Ca	**9.9E+07**	
Leu 4	7.9E+06	Ca	53.8	39.9	Cb	**1.2E+07**	Random coil
	1.7E+08	Cb	39.9	27.0	Cc	**1.1E+08**	
	5.9E+06	Cc	27.0	22.2	Cd	**2.1E+07**	
	6.2E+06	Co	176.2	53.8	Ca	**1.2E+07**	
Leu 5	2.7E+06	Ca	53.3	40.5	Cb	3.1E+07	Random coil
	1.7E+08	Cb	40.5	27.2	Cc	**1.1E+08**	
	7.0E+07	Cc	27.2	22.9	Cd	**6.0E+07**	
	6.2E+06	Co	176.6	53.3	Ca	**1.2E+07**	
Leu 6	2.7E+06	Ca	53.3	40.6	Cb	3.1E+07	Beta-sheet
	1.9E+07	Cb	40.6	27.8	Cc	1.0E+07	
	3.5E+06	Cc	27.8	23.3	Cd	**1.5E+06**	
	1.8E+07	Co	175.9	53.3	Ca	3.0E+06	
Leu 7	**2.6E+07**	Ca	52.4	39.7	Cb	**1.9E+07**	Random coil
	1.2E+07	Cb	39.7	28.8	Cc	2.0E+06	
	4.7E+06	Cc	28.8	23.0	Cd	9.9E+05	
	1.3E+07	Co	176.6	52.4	Ca	1.1E+07	
Lys 1	**2.6E+07**	Ca	53.9	30.7	Cb	**4.4E+06**	Beta-sheet
	5.4E+06	Cb	30.7	22.5	Cc	5.7E+06	
	5.9E+06	Cd	26.7	22.5	Cc	**2.1E+07**	
	5.5E+06	Ce	41.9	26.7	Cd	2.9E+06	
	9.0E+07	Co	174.0	53.9	Ca	**9.9E+07**	
Lys 2	**2.6E+07**	Ca	54.0	31.9	Cb	4.0E+07	Beta-sheet
	9.4E+06	Cb	31.9	23.1	Cc	3.8E+06	
	3.5E+06	Cd	27.7	23.1	Cc	**1.5E+06**	
	1.9E+07	Ce	40.6	27.7	Cd	1.0E+07	
	9.0E+07	Co	174.3	54.0	Ca	**9.9E+07**	
Lys 3	**2.6E+07**	Ca	54.3	31.2	Cb	**4.4E+07**	Beta-sheet
	4.2E+07	Cb	31.2	22.9	Cc	5.1E+07	
	7.0E+07	Cd	27.2	22.9	Cc	**6.0E+07**	
	1.7E+08	Ce	40.4	27.2	Cd	**1.1E+08**	
	9.0E+07	Co	174.8	54.3	Ca	**9.9E+07**	
Lys 4	4.7E+04	Ca	54.1	33.3	Cb	**5.9E+06**	Beta-sheet
	6.5E+06	Cb	33.3	22.3	Cc	4.6E+06	
	5.9E+06	Cd	26.9	22.3	Cc	**2.1E+07**	
	1.7E+08	Ce	40.1	26.9	Cd	**1.1E+08**	
	9.0E+07	Co	174.3	54.1	Ca	**9.9E+07**	
Met 1	**2.6E+07**	Ca	54.7	30.6	Cb	**4.4E+06**	Random coil
	6.5E+06	Cc	32.0	30.6	Cb	**1.0E+07**	
	3.4E+06	Cc	32.0	19.0	Cd	1.3E+07	
	1.9E+06	Co	175.6	54.7	Ca	**3.6E+07**	
Met 2	**3.1E+06**	Ca	53.6	30.2	Cb	**3.6E+06**	Random coil
	7.3E+06	Cc	31.0	30.2	Cb	**1.2E+07**	
	6.1E+07	Cc	31.0	18.5	Cd	**6.3E+07**	
	6.2E+06	Co	176.4	53.6	Ca	**1.2E+07**	
Met 3	**2.6E+07**	Ca	53.8	30.7	Cb	**4.4E+06**	Random coil
	7.3E+06	Cb	30.7	29.7	Cc	**1.2E+07**	
	2.6E+06	Cc	29.7	19.0	Cd	**1.3E+07**	
	6.2E+06	Co	176.2	53.8	Ca	**1.2E+07**	

Met 4	**2.6E+07**	Ca	54.4	30.9	Cb	**4.4E+07**	Random coil
	7.3E+06	Cb	30.9	29.8	Cc	**1.2E+07**	
	4.4E+06	Cc	29.8	17.6	Cd	**9.7E+06**	
	9.0E+07	Co	174.7	54.4	Ca	**9.9E+07**	
Phe 1-u	2.0E+06	Cc	138.6	130.2	Cd	6.3E+06	Unknown
	3.1E+06	Cd	130.2	129.3	Ce	**1.7E+06**	
	7.1E+06	Ce	129.3	127.6	Cf	4.2E+06	
Phe 2-u	2.0E+06	Cc	138.6	130.1	Cd	6.3E+06	Unknown
	1.7E+06	Cd	130.1	129.4	Ce	**1.7E+06**	
	5.9E+06	Ce	129.4	128.1	Cf	5.0E+06	
Pro 1	**1.8E+07**	Ca	60.6	30.5	Cb	**1.9E+07**	Random coil
	2.4E+06	Cb	30.5	25.7	Cc	**1.3E+07**	
	1.3E+07	Cd	49.0	25.7	Cc	1.1E+07	
	4.5E+06	Co	175.3	60.6	Ca	2.3E+07	
Pro 2	**1.8E+07**	Ca	61.3	30.1	Cb	**2.2E+07**	Random coil
	2.8E+07	Cb	30.1	25.4	Cc	3.1E+07	
	2.6E+07	Cd	48.5	25.4	Cc	3.1E+07	
	3.1E+06	Co	175.4	61.3	Ca	**2.1E+07**	
Pro 3	2.2E+06	Ca	59.2	29.0	Cb	2.1E+06	Random coil
	2.6E+07	Cb	29.0	25.3	Cc	3.0E+07	
	5.5E+06	Cd	47.9	25.2	Cc	9.5E+06	
	1.4E+06	Co	174.0	59.2	Ca	**1.3E+07**	
Pro 4	1.5E+06	Ca	61.7	28.5	Cb	2.8E+06	Random coil
	3.2E+06	Cb	28.5	25.0	Cc	7.6E+06	
	1.4E+07	Cd	47.4	25.0	Cc	4.7E+06	
	3.1E+06	Co	175.8	61.7	Ca	**2.1E+07**	
Pro 5	5.3E+06	Ca	62.0	29.8	Cb	8.4E+06	Random coil
	7.0E+06	Cb	29.8	24.6	Cc	5.3E+06	
	1.6E+07	Cd	47.1	24.6	Cc	1.2E+07	
	2.7E+07	Co	175.9	62.0	Ca	7.8E+06	
Ser 1	1.1E+07	Cb	64.4	56.5	Ca	1.0E+07	Beta-sheet
	3.3E+07	Co	172.7	56.6	Ca	**1.9E+07**	
Ser 2	1.5E+06	Cb	64.1	57.6	Ca	8.3E+05	Random coil
	1.1E+07	Co	175.6	57.6	Ca	7.2E+06	
Ser 3	6.5E+06	Cb	63.9	56.2	Ca	3.1E+06	Beta-sheet
	3.3E+07	Co	172.7	56.6	Ca	**1.9E+07**	
Ser 4	8.5E+06	Cb	63.2	58.1	Ca	4.4E+06	Random coil
	7.6E+06	Co	176.9	58.1	Ca	3.5E+06	
Ser 5	6.3E+07	Cb	62.1	56.6	Ca	3.1E+07	Random coil
	3.5E+06	Co	176.1	56.6	Ca	1.1E+07	
Thr 1	**3.2E+07**	Cb	68.0	60.4	Ca	**2.2E+07**	Beta-sheet
	4.4E+07	Cb	68.0	19.6	Cc	1.9E+07	
	1.6E+07	Co	174.1	60.4	Ca	**2.4E+07**	
Thr 2	7.6E+06	Cb	68.9	61.1	Ca	3.1E+06	Beta-sheet
	1.4E+07	Cb	68.9	19.4	Cc	2.9E+07	
	2.7E+07	Co	173.9	61.1	Ca	2.8E+06	
Thr 3	1.9E+06	Cb	70.8	59.9	Ca	7.9E+06	Beta-sheet
	5.8E+06	Cb	70.8	17.5	Cc	1.3E+07	
	1.6E+07	Co	173.9	59.9	Ca	**2.4E+07**	
Tyr 1	**9.1E+06**	C1	51.1	37.4	Cb	**2.9E+07**	Random coil

	4.0E+06	Cc	130.2	37.4	Cb	**6.5E+06**	
	3.4E+06	Cd	131.6	130.2	Cc	**4.7E+06**	
	1.4E+07	Cd	131.6	116.7	Ce	**7.9E+06**	
	8.4E+06	Cf	156.4	116.7	Ce	2.9E+06	
	3.6E+07	Co	174.6	51.1	Ca	**1.3E+07**	
Tyr 2	**9.1E+06**	Ca	51.1	37.4	Cb	**2.9E+07**	Random coil
	4.0E+06	Cc	130.2	37.4	Cb	**6.5E+06**	
	4.4E+06	Cd	131.2	130.2	Cc	**4.7E+06**	
	1.4E+07	Cd	131.2	116.9	Ce	**7.9E+06**	
	3.8E+06	Cf	155.5	116.9	Ce	6.8E+06	
	3.6E+07	Co	174.6	51.1	Ca	**1.3E+07**	
Tyr 3	9.1E+06	Ca	51.1	37.4	Cb	**2.9E+07**	Random coil
	4.0E+06	Cc	130.2	37.4	Cb	**6.5E+06**	
	3.4E+06	Cd	131.6	130.2	Cc	**4.7E+06**	
	1.4E+07	Cd	131.6	116.0	Ce	**7.9E+06**	
	8.1E+06	Cf	156.0	116.0	Ce	6.0E+06	
	3.6E+07	Co	174.6	51.1	Ca	**1.3E+07**	
Tyr 4	**9.1E+06**	Ca	51.1	37.4	Cb	**2.9E+07**	Random coil
	4.0E+06	Cc	130.2	37.4	Cb	**6.5E+06**	
	3.4E+06	Cd	131.6	130.2	Cc	**4.7E+06**	
	1.4E+07	Cd	131.6	116.5	Ce	**7.9E+06**	
	8.3E+06	Cf	155.1	116.5	Ce	8.6E+06	
	3.6E+07	Co	174.6	51.1	Ca	**1.3E+07**	
Tyr 5	**9.1E+06**	Ca	51.1	37.4	Cb	**2.9E+07**	Random coil
	4.0E+06	Cc	130.2	37.4	Cb	**6.5E+06**	
	3.4E+06	Cd	131.6	130.2	Cc	**4.7E+06**	
	1.4E+07	Cd	131.6	115.9	Ce	**7.9E+06**	
	8.7E+06	Cf	155.5	115.9	Ce	8.5E+06	
	3.6E+07	Co	174.6	51.1	Ca	**1.3E+07**	
Val 1	2.0E+06	Ca	61.6	31.4	Cb	9.5E+06	Random coil
	1.1E+06	Cb	31.4	19.7	Cc	3.9E+06	
	2.7E+07	Co	175.8	62.1	Ca	**7.8E+06**	
Val 2	**5.3E+06**	Ca	62.1	29.8	Cb	**8.4E+06**	Random coil
	4.4E+06	Cb	29.8	17.7	Cc	**9.7E+06**	
	2.7E+07	Co	175.6	62.3	Ca	**7.8E+06**	
Val 3	**5.3E+06**	Ca	62.3	29.7	Cb	**8.4E+06**	Beta-sheet
	2.6E+06	Cb	29.7	19.0	Cc	**1.3E+07**	
	5.0E+07	Co	174.8	61.5	Ca	**1.0E+06**	
Val 4	1.5E+07	Ca	61.2	30.3	Cb	3.9E+06	Beta-sheet
	6.1E+06	Cb	30.3	19.5	Cc	6.8E+06	
	5.0E+07	Co	174.8	61.2	Ca	**1.0E+06**	
Val 5	**1.8E+07**	Ca	60.7	30.1	Cb	**2.2E+07**	Beta-sheet
	2.6E+06	Cb	30.1	18.4	Cc	1.8E+06	
	3.9E+07	Co	172.1	60.7	Ca	**3.1E+06**	
Val 7	**1.8E+07**	Ca	60.1	30.9	Cb	**1.9E+07**	Beta-sheet
	6.1E+07	Cb	30.9	18.5	Cc	**6.3E+07**	
	9.6E+06	Co	172.4	60.1	Ca	2.1E+06	

Supplementary Table 11. Results of the amino acid quantification. SSNMR can quantify the total amount of each amino acid, but also its relative abundance according to their predicted secondary structure. Note that TALOS+ predicts β-sheet or random coil environments, but that we cannot exclude the occurrence of PPII environment within the predicted random coils. Amino-acid quantification can take into account overlapping peaks only if they involve the same kind of residue, while two different residue overlapping peaks cannot be used using our quantification methodology (**Supplementary Table 10**). By analogy with glycan quantification, integrals are normalized using the number of carbon integrated (*tot nC*) and, for comparison with other residues, we take into account the number of spin system assigned (*n spin syst.*). Results of the HPLC-based quantification are shown for comparison in the last column.

		sum int.	nC	nC overlap	tot nC	int/nC_{total}	n spin syst.	$(int/nC)*n_{spin\ system}$	% norm.	HPLC
Ala	TOTAL	3.4E+08	30	8	38	8.9E+06	14	1.2E+08	13.03	
	c random	1.6E+08	12	6	18	8.8E+06	5	4.4E+07	4.64	5.30
	b beta	1.8E+08	18	2	20	9.0E+06	9	8.1E+07	8.52	
Gln	TOTAL	3.6E+08	18	4	22	1.6E+07	5	8.2E+07	8.59	
	c random	9.8E+07	10	0	10	9.8E+06	2	2.0E+07	2.06	8.10
	b beta	2.6E+08	8	4	12	2.2E+07	3	6.6E+07	6.95	
Glu	TOTAL	4.5E+08	20	0	20	2.3E+07	4	9.0E+07	9.40	
	c random	3.5E+08	12	0	12	2.9E+07	2	5.8E+07	6.12	6.70
	b beta	1.0E+08	8	0	8	1.3E+07	2	2.5E+07	2.66	
Asp	TOTAL	1.8E+08	13	0	13	1.4E+07	4	5.6E+07	5.82	
	c random	1.4E+08	9	0	9	1.5E+07	3	4.6E+07	4.83	9.00
	b beta	4.3E+07	4	0	4	1.1E+07	1	1.1E+07	1.14	
Gly	TOTAL	1.6E+08	10	0	10	1.6E+07	5	8.1E+07	8.46	
	c random	1.5E+08	8	0	8	1.9E+07	4	7.5E+07	7.88	8.00
	b beta	1.2E+07	2	0	2	6.1E+06	1	6.1E+06	0.64	
Asn	TOTAL	2.4E+08	12	0	12	2.0E+07	3	6.1E+07	6.36	
	c random	2.4E+08	12	0	12	2.0E+07	3	6.1E+07	6.41	1.00
	b beta	0.0E+00	0	0	0	0.0E+00	0	0.0E+00	0.00	
Val	TOTAL	2.3E+08	19	5	24	9.4E+06	6	5.6E+07	5.88	
	c random	3.0E+07	6	0	6	5.0E+06	2	1.0E+07	1.06	4.80
	b beta	2.0E+08	13	5	18	1.1E+07	4	4.3E+07	4.56	
Leu	TOTAL	3.2E+08	26	2	28	1.1E+07	7	7.9E+07	8.22	
	c random	1.7E+08	18	0	18	9.3E+06	5	4.7E+07	4.91	3.50
	b beta	1.5E+08	8	2	10	1.5E+07	2	2.9E+07	3.09	
Lys	TOTAL	2.1E+08	14	0	14	1.5E+07	4	5.9E+07	6.15	5.00
	c random	0.0E+00	0	0	0	0.0E+00	0	0.0E+00	0.00	

	b beta	2.1E+08	14	0	14	1.5E+07	4	5.9E+07	6.19	
Ser	TOTAL	2.4E+08	18	2	20	1.2E+07	5	5.9E+07	6.18	4.60
	c random	1.5E+08	12	0	12	1.3E+07	3	3.8E+07	4.03	
	b beta	8.4E+07	6	2	8	1.0E+07	2	2.1E+07	2.20	
Pro	TOTAL	3.9E+08	29	6	35	1.1E+07	5	5.6E+07	5.80	8.00
	c random	3.9E+08	29	6	35	1.1E+07	5	5.6E+07	5.84	
	b beta	0.0E+00	0	0	0	0.0E+00	0	0.0E+00	0.00	
Thr	TOTAL	2.2E+08	14	2	16	1.4E+07	3	4.1E+07	4.23	4.60
	c random	0.0E+00	0	0	0	0.0E+00	0	0.0E+00	0.00	
	b beta	2.2E+08	14	2	16	1.4E+07	3	4.1E+07	4.26	
Arg	TOTAL	7.6E+07	11	0	11	6.9E+06	7	4.8E+07	5.05	2.40
	c random	2.7E+07	3	0	3	9.1E+06	2	1.8E+07	1.91	
	b beta	4.9E+07	8	0	8	6.1E+06	5	3.1E+07	3.21	
Ile	TOTAL	1.0E+08	9	11	20	5.1E+06	4	2.0E+07	2.13	2.00
	c random	0.0E+00	0	0	0	0.0E+00	0	0.0E+00	0.00	
	b beta	1.0E+08	9	11	20	5.1E+06	4	2.0E+07	2.15	
Phe	TOTAL	4.5E+07	11	2	13	3.5E+06	2	7.0E+06	0.73	5.50
	c random	4.5E+07	11	2	13	3.5E+06	2	7.0E+06	0.73	
	b beta	0.0E+00	0	0	0	0.0E+00	0	0.0E+00	0.00	
Tyr	TOTAL	1.1E+08	17	23	40	2.9E+06	5	1.4E+07	1.49	1.60
	c random	1.1E+08	17	23	40	2.9E+06	5	1.4E+07	1.51	
	b beta	0.0E+00	0	0	0	0.0E+00	0	0.0E+00	0.00	
His	TOTAL	0.0E+00	0	0	0	0.0E+00	0	0.0E+00	0.00	5.60
	c random	0.0E+00	0	0	0	0.0E+00	0	0.0E+00	0.00	
	b beta	0.0E+00	0	0	0	0.0E+00	0	0.0E+00	0.00	
Met	TOTAL	1.8E+07	3	0	3	5.9E+06	4	2.4E+07	2.48	3.00
	c random	1.8E+07	3	0	3	5.9E+06	4	2.4E+07	2.50	
	b beta	0.0E+00	0	0	0	0.0E+00	0	0.0E+00	0.00	
Hyp	TOTAL	0.0E+00	0	0	0	0.0E+00	0	0.0E+00	0.00	2.80
	c random	0.0E+00	0	0	0	0.0E+00	0	0.0E+00	0.00	
	b beta	0.0E+00	0	0	0	0.0E+00	0	0.0E+00	0.00	
Cys	TOTAL	0.0E+00	0	0	0	0.0E+00	0	0.0E+00	0.00	0.20
	c random	0.0E+00	0	0	0	0.0E+00	0	0.0E+00	0.00	
	b beta	0.0E+00	0	0	0	0.0E+00	0	0.0E+00	0.00	

Supplementary Table 12. Amino acid composition of *wt* and *bald2 C. reinhardtii* strains. These quantities are obtained by HPLC from cell-wall extracts. Amino acids highlighted in orange are the amino acids that can be involved in O- or N-glycosylation. Therefore, standard deviation given in the last column represent a statistical analysis over 4 different samples.

Amino acid	wt-1 Relative mol (%)	wt-2 Relative mol (%)	bald2-1 Relative mol (%)	bald2-2 Relative mol (%)	Relative mole (%) avg	 **stdDev**
Asx (Asn+Asp)	15.0	15.2	14.6	14.5	14.8	**0.3**
Glx(Glu+Gln)	18.9	18.6	19.4	19.2	19.0	**0.3**
Hydroxyproline	1.0	1.2	0.8	1.1	1.0	**0.1**
Serine	5.2	5.2	4.9	4.8	5.0	**0.2**
Glycine	8.5	7.8	7.7	8.1	8.0	**0.3**
Histidine	1.9	2.2	1.8	2.0	2.0	**0.1**
Arginine	3.6	3.7	3.0	3.5	3.5	**0.3**
Threonine	4.8	4.2	5.3	4.6	4.7	**0.4**
Alanine	10.5	11.0	10.8	11.2	10.9	**0.3**
Proline	5.0	4.7	4.5	5.0	4.8	**0.2**
Tyrosine	2.0	2.6	2.5	2.3	2.4	**0.2**
Valine	6.0	5.2	5.7	5.6	5.6	**0.3**
Methionine	1.7	1.4	2.0	1.4	1.6	**0.2**
Isoleucine	2.6	2.9	3.5	3.2	3.1	**0.3**
Leucine	5.1	5.8	5.4	5.8	5.5	**0.3**
Phenylalanine	2.9	3.2	2.7	2.2	2.8	**0.4**
Lysine	5.3	5.1	5.4	5.5	5.3	**0.1**

Supplementary Table 13. Protein-glycan contacts detected by MAS-DNP in the cell wall. MAS-DNP ^{13}C-^{13}C DARR spectra allows identification of contacts between hydroxyproline/threonine (red and green values, respectively, on the left table) and surrounding glycans. Despite low MAS-DNP resolution, specific glycan to amino acid contacts could be detected with Hyp or Thr (red and green values, respectively, on the right table) or both (bold underlined values).

Amino acid	δ_1 (ppm)	AA
Hyp	58.8	**Hypa**
	34.8	**Hypb**
	73.1	**Hypc**
	50.2	**Hypd**
Thr	19.6	**Thrc**
	19.4	**Thrc**
	17.5	**Thrc**

Sugar unit	C_1	C_2	C_3	C_4	C_5	C_6
Man1	**104.5**	73.9	74.9	**81.7**	77.2	61.8
Man2	**97.7**	74.6	76.2	65.7	77.2	61.4
Man3	100.8	71.5	73.6	67.8	77.1	61.8
Man4	**103.6**	72.2	75.4	67.9	77.2	61.9
Man5	**100.2**	76.8	71.4	68.4	77.7	65.7
Man6	**102.4**	67.8	77.2	65.7	76.0	62.1
Man7	**101.7**	67.9	77.1	65.6	76.0	62.1
Man8	**103**	71.1	77.1	67.8	75.3	63.1
Man9	**94.6**	69.9	78.1	68.3	74.1	64.9
Man10	**96.7**	70.4	**76.8**	65.8	**76.0**	62.2
Man11	97.6	68.6	80	66.2	76.9	61.9
Man12	**96.8**	68.6	**80.8**	66.3	76.9	61.5
Man13	**94.5**	70.2	78.6	66.7	77	61.8
Man14	**99.2**	73.6	78.5	65.9	70.5	66.2
Ara1	**110.3**	**82.4**	77.6	**81.8**	61.8	
Ara2	**110.1**	**82.2**	77.7	**81.7**	61.8	
Ara3	**109.8**	**81.9**	77.2	**81.4**	66.1	
Ara4	**109.8**	**81.8**	75	**81.3**	67.2	
Gal1	**103.5**	72.1	75.4	67.7	72.2	61.8
Gal2	**98.5**	72.4	73.7	71.7	75.1	62.9
Gal3	**105.8**	73.3	75	**81.1**	74.8	64.8
Rha1	**100.4**	77.1	70.2	71.7	70.3	17.8
Rha2	**100.4**	77.1	70.2	71.9	69.8	17.6
Rha3	**100.3**	70.2	**78.7**	73.6	70.9	17.4
Glc1	**100.4**	69.6	74.1	72.5	70.9	63.6
Glc2	**100**	76.8	71.3	63.8	71.8	61.9
Xyl1	97.7	76.1	77.2	67.7	60.2	
Xyl2	**100.3**	70.8	75.9	74.8	64.9	
Xyl3	**100.9**	77.4	75.1	**79.5**	67.8	

Supplementary Table 14. Glycoproteomics and identification of hexose modified proteins/peptides. These proteins/peptides were identified using ConA-LWAC enrichment. The accession number is based on taxonomy ID 3A3052_29 downloaded from Uniprot (May 13, 2023), and the table includes identifications for *Chlamydomonas reinhardtii* only. The "Modification" column indicates number of hexoses identified on each peptide; the specific site is indicated for specific entries based on the reliability of MS/MS data. Mass accuracy of precursor ions and deviation (ppm) from theoretical glycopeptide mass is indicated in the last column.

Protein	Peptide	Accession (Uniprot)	Modification	Activation	Charge	m/z	Δ ppm
Guanylate cyclase domain-containing protein	VLSLASNDLVGTLPHALSR	A0A2K3DIV2	T12(Hex)	ETciD	3	709.05511	0.37
Guanylate cyclase domain-containing protein	VLSLASNDLVGTLPHALSR	A0A2K3DIV2	T12(Hex)	ETciD	3	709.05505	0.28
Guanylate cyclase domain-containing protein	VLSLASNDLVGTLPH	A0A2K3DIV2	T12(Hex)	ETciD	2	849.45160	0.15
Guanylate cyclase domain-containing protein	VLSLASNDLVGTLPHAL	A0A2K3DIV2	T12(Hex)	ETciD	2	941.51227	0.21
Guanylate cyclase domain-containing protein	VLSLASNDLVGTLPH	A0A2K3DIV2	T12(Hex)	ETciD	2	849.45227	0.94
Guanylate cyclase domain-containing protein	VLSLASNDLVGTLPHALS	A0A2K3DIV2	T12(Hex)	ETciD	2	985.02826	0.18
Guanylate cyclase domain-containing protein	VLSLASNDLVGTLPHALSR	A0A2K3DIV2	(Hex)	HCD	3	709.05511	0.37
Guanylate cyclase domain-containing protein	VLSLASNDLVGTLPHALSR	A0A2K3DIV2	(Hex)	HCD	3	709.05505	0.28
Guanylate cyclase domain-containing protein	VLSLASNDLVGTLPH	A0A2K3DIV2	(Hex)	HCD	2	849.45160	0.15
Guanylate cyclase domain-containing protein	VLSLASNDLVGTLPHALS	A0A2K3DIV2	(Hex)	HCD	2	985.02856	0.49
Guanylate cyclase domain-containing protein	VLSLASNDLVGTLPHAL	A0A2K3DIV2	(Hex)	HCD	2	941.51227	0.21
Guanylate cyclase domain-containing protein	VLSLASNDLVGTLPH	A0A2K3DIV2	(Hex)	HCD	2	849.45227	0.94
Guanylate cyclase domain-containing protein	VLSLASNDLVGTLPHALS	A0A2K3DIV2	(Hex)	HCD	2	985.02826	0.18
Guanylate cyclase domain-containing protein	VLSLASNDLVGTLPHAL	A0A2K3DIV2	(Hex)	HCD	2	941.51245	0.40
Leucine-rich repeat-containing N-terminal plant-type domain-containing protein	ISGTLPPSWQSWQSVR	A0A2K3D0L8	(Hex)	HCD	2	995.99768	0.57
Leucine-rich repeat-containing N-terminal plant-type domain-containing protein	DNSFSGTLPDSWQLLR	A0A2K3DTP7	(Hex)	HCD	2	999.47589	-0.33
Leucine-rich repeat-containing N-terminal plant-type domain-containing protein	NPNIAGSLPPEWAAGL	A0A2K3DTP7	S7(Hex)	HCD	2	884.94159	0.34
Leucine-rich repeat-containing N-terminal plant-type domain-containing protein	DNSFSGTLPDSWQLLR	A0A2K3DTP7	(Hex)	HCD	2	999.47614	-0.08
Leucine-rich repeat-containing N-terminal plant-type domain-containing protein	LVGTVPEVLGSLPYLSR	A0A2K3DN96	(Hex)	HCD	2	981.54352	0.15
Oxygen-evolving enhancer protein 2, chloroplastic	VTNKSGFVPYAGDGFALLLPAK	P11471	S5(Hex-Hex)	ETciD	3	863.78308	0.46
Oxygen-evolving enhancer protein 2, chloroplastic	HQLIGATVGSDNKLYIIK	P11471	S10(Hex-Hex)	ETciD	3	765.40918	0.16
Protein kinase domain-containing protein	HLVLPAATK	A0A835SF10	T8(Hex-Hex)	HCD	2	637.34888	1.50

Uncharacterized protein	SGTLPALPTSLQVLR	A0A2K3DV32	(Hex)	HCD	3	572.32440	0.02
Uncharacterized protein	SSNSFSGTLPALPTSLQVLR	A0A2K3DV32	(Hex)	HCD	2	1119.08630	-0.32
Uncharacterized protein	SNSFSGTLPALPTSLQVLR	A0A2K3DV32	(Hex)	HCD	2	1075.57080	0.14
Uncharacterized protein	NSLSGTLPR	A0A2K3DV32;A0A835TDM1	(Hex)	HCD	2	553.78815	0.16

Supplementary Table 15. ^{13}C DARR cross-peak intensities and calculated hydration level. Resonance-specific control and water-edited spectra (**Supplementary Fig. 12**) were used for this hydration level calculation.

Spin system	Resolved peaks	S/S0	error bar	average/unit
Lys	Lys-c-1-b/c	0.23	0.12	
	Lys-c-1-e/d	0.14	0.05	
	Lys-c-2-a/b	0.28	0.12	
	Lys-c-2-b/c	0.07	0.03	
	Lys-c-2-e/d	0.05	0.02	
	Lys-c-3-b/c	0.08	0.03	
	Lys-c-4-b/c	0.10	0.05	0.14
Asp	Asp-b-1-c/b	0.02	0.01	
	Asp-b-2-c/b	0.01	0.01	
	Asp-c-3-c/b	0.07	0.02	
	Asp-a-4-a/b	0.02	0.01	
	Asp-a-4-c/b	0.04	0.01	0.03
Asn	Asn-b-1-c/b	0.20	0.09	
	Asn-b-1-o/a	0.22	0.07	
	Asn-b-2-a/b	0.13	0.05	
	Asn-b-2-c/b	0.34	0.14	
	Asn-b-2-o/a	0.22	0.07	
	Asn-c-3-c/b	0.06	0.02	0.20
Glu	Glu-c-1-a/b	0.03	0.01	
	Glu-c-1-d/c	0.04	0.01	
	Glu-c-1-o/a	0.06	0.03	
	Glu-a-2-a/b	0.06	0.03	
	Glu-a-2-d/c	0.05	0.01	
	Glu-c-3-d/c	0.03	0.01	
	Glu-c-4-a/b	0.02	0.01	
	Glu-c-4-c/b	0.06	0.02	
	Glu-c-4-d/c	0.07	0.02	0.05
Gln	Gln-b-1-c/b	0.01	0.02	
	Gln-b-1-d/c	0.09	0.17	
	Gln-b-2-d/c	0.05	0.02	
	Gln-c-3-d/c	0.04	0.07	
	Gln-b-4-a/b	0.07	0.02	
	Gln-b-4-c/b	0.02	0.01	
	Gln-b-4-d/c	0.03	0.01	
	Gln-b-5-c/b	0.07	0.02	
	Gln-b-5-d/c	0.04	0.01	
	Gln-b-5-o/a	0.03	0.01	0.05

Pro	Pro-c-1-b/c	0.07	0.03	
	Pro-c-1-d/c	0.06	0.02	
	Pro-c-1-o/a	0.11	0.04	
	Pro-c-2-a/b	0.01	0.03	
	Pro-c-2-b/c	0.02	0.01	
	Pro-c-2-d/c	0.03	0.06	
	Pro-b-3-b/c	0.08	0.03	
	Pro-b-3-d/c	0.09	0.04	
	Pro-b-3-o/a	0.22	0.00	
	Pro-c-4-a/b	0.05	0.02	
	Pro-c-4-b/c	0.00	0.00	
	Pro-c-4-d/c	0.02	0.01	
	Pro-c-5-a/b	0.02	0.01	
	Pro-c-5-b/c	0.03	0.01	
	Pro-c-5-d/c	0.13	0.05	
	Pro-c-5-o/a	0.18	0.09	0.07
Arg	Arg-b-1-b/c	0.17	0.05	
	Arg-b-2-d/c	0.11	0.04	
	Arg-b-3-b/c	0.09	0.03	
	Arg-c-5-b/c	0.07	0.03	
	Arg-c-6-b/c	0.16	0.06	0.12
Gly	Gly-b-1-o/a	0.04	0.01	
	Gly-c-2-o/a	0.02	0.01	
	Gly-c-3-o/a	0.03	0.01	
	Gly-c-4-o/a	0.02	0.01	
	Gly-a-5-o/a	0.03	0.01	0.03
Ala	Ala-b-1-a/b	0.06	0.02	
	Ala-b-2-a/b	0.03	0.01	
	Ala-b-3-a/b	0.09	0.03	
	Ala-b-4-a/b	0.02	0.01	
	Ala-b-5-a/b	0.13	0.06	
	Ala-b-6-a/b	0.05	0.02	
	Ala-c-7-a/b	0.01	0.00	
	Ala-c-9-a/b	0.02	0.01	
	Ala-c-10-a/b	0.00	0.00	
	Ala-c-10-o/a	0.01	0.00	
	Ala-c-11-a/b	0.01	0.00	
	Ala-c-11-o/a	0.10	0.04	
	Ala-c-12-a/b	0.07	0.02	
	Ala-c-13-a/b	0.14	0.05	
	Ala-c-14-a/b	0.17	0.05	0.06
Tyr	Tyr-b-1-c/b	0.05	0.02	

	Tyr-b-1-d/c	0.06	0.03	
	Tyr-b-1-d/e	0.04	0.01	
	Tyr-b-1-f/e	0.14	0.04	
	Tyr-b-2-f/e	0.19	0.08	
	Tyr-b-3-c/b	0.05	0.02	
	Tyr-b-3-d/c	0.06	0.02	
	Tyr-b-3-d/e	0.18	0.07	
	Tyr-b-3-f/e	0.16	0.05	
	Tyr-b-4-c/b	0.05	0.02	
	Tyr-b-4-d/c	0.06	0.03	
	Tyr-b-4-d/e	0.04	0.02	
	Tyr-b-4-f/e	0.19	0.07	
	Tyr-b-5-c/b	0.05	0.01	
	Tyr-b-5-d/c	0.06	0.02	
	Tyr-b-5-d/e	0.18	0.08	
	Tyr-b-5-f/e	0.02	0.01	0.09
Leu	Leu-a-1-a/b	0.10	0.04	
	Leu-a-1-b/c	0.07	0.02	
	Leu-a-1-c/d	0.15	0.05	
	Leu-a-2-c/d	0.07	0.04	
	Leu-a-3-a/b	0.09	0.03	
	Leu-a-3-c/d	0.08	0.03	
	Leu-c-5-a/b	0.05	0.02	
	Leu-c-6-b/c	0.02	0.01	
	Leu-c-6-o/a	0.02	0.01	
	Leu-c-7-b/c	0.15	0.04	
	Leu-c-7-c/d	0.07	0.03	
	Leu-c-7-o/a	0.02	0.01	0.08
Met	Met-c-1-c/d	0.12	0.04	0.12
Val	Val-c-1-o/a	0.16	0.06	
	Val-a-2-a/b	0.01	0.01	
	Val-a-2-b/c	0.10	0.03	
	Val-a-3-a/b	0.11	0.04	
	Val-c-4-a/b	0.01	0.00	
	Val-c-4-b/c	0.07	0.02	
	Val-c-5-a/b	0.02	0.01	
	Val-c-5-b/c	0.07	0.03	
	Val-c-6-a/b	0.02	0.01	
	Val-c-6-o/a	0.02	0.01	0.06
Ile	Ile-c-1-a/b	0.05	0.02	
	Ile-c-1-c1/d	0.03	0.01	
	Ile-c-2-b/c2	0.06	0.02	
	Ile-c-3-c1/d	0.04	0.01	

	Ile-u-4-b/c	0.06	0.03	0.05
Phe	Phe-u-1-c/d	0.10	0.05	
	Phe-u-1-e/f	0.05	0.02	
	Phe-u-2-c/d	0.10	0.03	
	Phe-u-2-d/e	0.08	0.04	
	Phe-u-2-e/f	0.02	0.01	0.07
Hyp	Hyp-u-a/b	0.86	0.16	
	Hyp-u-c/b	0.84	0.17	
	Hyp-u-c/d	0.85	0.16	0.85
Ser	Ser-b-1-b/a	0.40	0.08	
	Ser-b-1-o/a	0.41	0.09	
	Ser-b-2-b/a	0.23	0.05	
	Ser-b-2-o/a	0.31	0.07	
	Ser-b-3-b/a	0.31	0.07	
	Ser-c-4-b/a	0.33	0.08	
	Ser-c-4-o/a	0.27	0.06	
	Ser-c-5-b/a	0.42	0.10	
	Ser-c-5-o/a	0.50	0.11	0.35
Thr	Thr-b-1-b/c	0.32	0.07	
	Thr-b-2-b/a	0.47	0.10	
	Thr-b-2-b/c	0.50	0.10	
	Thr-b-2-o/a	0.49	0.09	
	Thr-b-3-b/a	0.58	0.11	
	Thr-b-3-b/c	0.46	0.08	
	Thr-b-3-o/a	0.57	0.13	0.49
GlcNAc	Ac-1	0.21	0.05	
	Ac-2	0.13	0.03	
	Ac-3	0.16	0.04	
	Ac-4	0.22	0.05	0.18
Ara	Ara-1-2/3	0.37	0.09	
	Ara-2-4/5	0.46	0.09	
	Ara-3-1/2	0.66	0.14	
	Ara-4-4/5	0.19	0.04	0.42
Gal	Gal-2-1/2	0.90	0.21	
	Gal-2-3/2	0.81	0.18	
	Gal-3-1/2	0.74	0.15	
	Gal-3-4/5	0.81	0.18	
	Gal-3-5/6	0.84	0.19	0.82

Glc	Glc-1-1/2	0.46	0.11	
	Glc-1-3/4	0.36	0.08	
	Glc-1-4/5	0.51	0.11	
	Glce-2-1/2	0.41	0.08	
	Glce-2-3/4	0.37	0.08	0.42
Man	Man-1-1/2	0.25	0.06	
	Man-1-4/5	0.72	0.16	
	Man-1-5/6	0.54	0.11	
	Man-2-1/2	0.53	0.13	
	Man-3-1/2	0.73	0.17	
	Man-3-5/6	0.91	0.20	
	Man-4-1/2	0.78	0.18	
	Man-4-3/2	0.87	0.19	
	Man-4-5/4	0.79	0.16	
	Man-5-1/2	0.34	0.08	
	Man-5-2/3	0.32	0.07	
	Man-6-3/2	0.79	0.17	
	Man-6-3/4	0.69	0.15	
	Man-6-5/6	0.18	0.04	
	Man-7-1/2	0.67	0.14	
	Man-7-3/2	0.74	0.15	
	Man-8-3/4	0.79	0.19	
	Man-8-5/6	0.49	0.11	
	Man-9-1/2	0.41	0.09	
	Man-9-3/2	0.24	0.05	
	Man-9-3/4	0.27	0.06	
	Man-9-5/4	0.26	0.06	
	Man-10-1/2	0.35	0.08	
	Man-10-3/2	0.75	0.18	
	Man-11-3/2	0.39	0.08	
	Man-11-3/4	0.70	0.16	
	Man-11-5/6	0.66	0.14	
	Man-12-3/2	0.41	0.10	
	Man-12-5/4	0.66	0.16	
	Man-13-3/2	0.31	0.07	
	Man-14-3/2	0.36	0.08	0.55
Rha	Rha-1-5/6	0.26	0.05	
	Rha-2-1/2	0.59	0.14	
	Rha-2-5/6	0.37	0.09	
	Rha-3-1/2	0.54	0.13	
	Rha-3-5/6	0.38	0.09	0.43
Xyl	Xyl-1-1/2	0.52	0.11	
	Xyl-1-3/2	0.60	0.14	

	Xyl-2-1/2	0.56	0.12	
	Xyl-2-3/4	0.37	0.08	
	Xyl-3-2/3	0.59	0.13	
	Xyl-3-4/3	0.45	0.10	
	Xyl-3-4/5	0.68	0.16	0.54

Supplementary Table 16. Resonance-specific ^{13}C intensity DNP build-up. Intensities are measured on 1D 13C MAS-DNP spectra at 600 MHz/395 GHz, using AMUPol as polarizing agent and 8 kHz MAS frequency. Intensities are indicated as a function of DNP microwave (MW) time and plotted on **Supplementary Fig. 13**. Tentative assignment is given but the resolution is not as good as on 2D spectra.

	Assignment	^{13}C δ(ppm) \ MW time	0.1	0.2	0.4	0.8	1.6	3.2	6.4	12.8	25.6
Amino acids	Ile C_γ	15.6	3.4	6.8	14.6	26.2	45.3	67.8	88.0	98.4	100.0
	Leu C_δ	21.7	3.2	7.3	14.9	28.1	48.5	72.9	91.8	98.9	100.0
	Ile C_γ/Pro C_γ/Ala C_β/Arg C_γ	25.2	2.8	6.4	13.6	26.3	46.1	71.2	90.9	98.5	100.0
	Gln C_β	29.9	2.8	7.0	13.8	26.6	46.4	71.5	91.7	99.5	100.0
	Glu C_γ/Hyp C_β/Glu C_γ	34.7	3.0	6.8	14.2	26.5	46.9	71.9	92.2	99.3	100.0
	Leu C_β	39.8	2.7	6.8	13.4	26.1	46.2	71.4	91.8	99.3	100.0
	Ala C_α	49.6	2.8	6.9	14.3	26.4	45.8	70.6	90.5	99.3	100.0
	Asn C_α	52.9	3.0	6.6	13.8	26.1	46.3	71.0	91.2	99.0	100.0
	Ala C_o	173.5	3.1	7.0	14.2	27.0	47.7	73.5	92.9	99.6	100.0
	Hyp C_α	58.7	3.3	7.3	14.9	**28.1**	**48.7**	73.5	92.3	99.4	100.0
	glycan C_6/ Val Cα	62.5	3.4	7.6	15.4	**29.1**	**50.0**	74.7	93.1	99.2	100.0
glycans	Man $C_{4/6}$	65.8	3.6	7.9	15.8	**29.6**	**50.4**	75.1	93.1	99.1	100.0
	Man C_2/Rha C_5/Glc C_2	69.8	3.6	8.0	15.8	**29.8**	**50.5**	75.3	93.2	99.2	100.0
	Gal C_2	73.0	3.6	7.9	15.8	**30.0**	**51.1**	75.7	93.6	99.3	100.0
	Ara C_2	82.3	4.4	8.2	16.6	**30.7**	**53.1**	78.3	97.0	99.9	100.0
	Gal C_1	98.5	3.7	8.4	16.1	**30.4**	**51.3**	75.9	94.5	98.9	100.0

Supplementary Table 17. Assignment of 1D INEPT and CP ^{13}C ssNMR peaks.

Amino acids

^{13}C δ (ppm)	Assignment	INEPT	CP
54.1	Asp4Cα	x	
179.1	Glu2Co		x
30.1	Glu2Cγ		x
28.3	Glu4Cβ	x	
179.0	Gln1Cδ		x
30.5	Gln5Cβ		x
58.8	Hyp1Cα	x	
50.2	Hyp1Cδ	x	
59.2	Pro3Cα	x	
31.5	Arg1Cβ	x	
30.4	Arg2Cβ		x
55.8	Arg5Cα	x	
173.9	Thr2Co		x
43.6	Gly4Cα		x
17.3	Ala13Cβ	x	
51.1	Tyr4Cα		x
130.2	Tyr5Cγ	x	
23.0	Leu7Cδ	x	
53.8	Met3Cα	x	
172.4	Val6Co		x
11.1	Ile1Cδ	x	
173.7	Ile3Co		x
16.3	Ile4Cγ2		x
128.1	Phe2Cε	x	

Glycans

^{13}C δ (ppm)	Assignment	INEPT	CP
81.7	Man1C4	x	
77.2	Man1C5	x	
61.4	Man2C6	x	
103	Man8C1		x
67.8	Man8C4		x
69.9	Man9C2		x
96.7	Man10C1	x	
97.6	Man11C1		x
80.8	Man12C3		x
94.5	Man13C1		x
67.7	Gal1C4	x	
105.8	Gal3C1		x
81.1	Gal3C4		x
69.8	Rha2C5		x
73.6	Rha3C4		x
69.6	Glc1C2		x
74.1	Glc1C3		x
67.7	Xyl1C4	x	
100.3	Xyl2C1	x	
74.8	Xyl2C4	x	

Supplementary Table 18. ^{13}C resonance CP intensity build-up in *C. reinhardtii*'s cell wall extract. Tentative assignments are given but one-dimensional experiments involve peak overlapping compared to 2D spectra.

	Assignment	^{13}C δ (ppm) \ CP (ms)	**0.001**	**0.01**	**0.05**	**0.1**	**0.2**	**0.3**	**0.5**	**0.75**	**1**	**1.5**	**2**	**3**	**4**	**5**	**7.5**	**10**
amino acids	Ile C_γ	15.4	0.00	0.05	0.21	0.44	0.86	0.89	1.00	0.92	0.93	0.89	0.86	0.78	0.70	0.63	0.51	0.41
	Ile C_γ	16.3	0.00	0.02	0.23	0.45	0.88	0.87	1.00	0.89	0.95	0.88	0.85	0.76	0.69	0.61	0.52	0.42
	Met C_δ/Val C_γ/Ala C_β	19.2	0.01	0.03	0.20	0.32	0.85	0.93	1.00	0.95	0.98	0.93	0.89	0.81	0.73	0.66	0.51	0.42
	Leu C_δ	21.7	0.01	0.04	0.29	0.39	0.83	0.93	1.00	0.99	0.98	0.95	0.90	0.81	0.74	0.64	0.51	0.30
	Arg C_γ/Pro C_γ	24.9	0.01	0.08	0.42	0.50	0.96	0.96	1.00	0.99	0.97	0.92	0.87	0.76	0.67	0.61	0.48	0.28
	Val C_β/Met C_γ	29.7	0.01	0.11	0.27	0.47	0.84	0.95	1.00	0.98	0.96	0.91	0.85	0.75	0.67	0.60	0.49	0.39
	Hyp C_β/Glu C_γ	35.0	0.01	0.19	0.34	0.62	0.88	0.96	1.00	0.95	0.90	0.84	0.78	0.70	0.63	0.57	0.46	0.36
	Arg C_δ/Ile C_β	37.9	0.02	0.16	0.39	0.61	0.77	0.93	1.00	0.96	0.91	0.85	0.78	0.67	0.60	0.54	0.43	0.36
	Ala C_α	50.0	0.01	0.16	0.29	0.59	0.78	0.92	1.00	0.94	0.88	0.85	0.80	0.72	0.65	0.58	0.47	0.40
	Val C_α/Pro C_α	61.4	0.01	0.05	0.30	0.32	0.65	0.75	0.81	0.89	0.94	0.99	1.00	0.94	0.85	0.79	0.64	0.53
	Phe C_ε	128.6	0.01	0.05	0.45	0.60	0.82	0.95	1.00	0.96	0.88	0.84	0.77	0.63	0.58	0.54	0.43	0.31
	C_o	172.2	0.00	0.01	0.10	0.33	0.50	0.66	0.78	0.92	0.97	0.97	1.00	0.97	0.90	0.79	0.64	0.49
Glycans	glycan C_6	63.2	0.01	0.06	0.37	0.52	0.82	0.94	1.00	0.97	0.98	0.99	0.97	0.95	0.89	0.83	0.73	0.66
	Glc C_2/Rha C_5/Man C_2	69.7	0.01	0.09	0.47	0.64	0.85	0.91	0.97	1.00	1.00	0.99	0.97	0.90	0.82	0.76	0.63	0.54
	Gal C_2	73.2	0.01	0.09	0.47	0.64	0.84	0.90	0.94	0.97	0.98	1.00	0.98	0.93	0.85	0.79	0.66	0.58
	Man C_3	76.4	0.01	0.07	0.35	0.48	0.62	0.75	0.83	0.89	0.93	0.99	1.00	0.97	0.88	0.82	0.67	0.57
	Ara C_2	82.1	0.02	0.10	0.57	0.78	0.88	0.98	1.00	0.97	0.96	0.93	0.91	0.83	0.77	0.71	0.60	0.51
	Ara C_2	83.9	0.01	0.11	0.57	0.73	0.91	0.99	1.00	0.95	0.93	0.90	0.87	0.82	0.73	0.67	0.54	0.45
	Man C_1	94.8	0.00	0.14	0.53	0.70	0.80	0.94	0.99	0.99	1.00	0.97	0.94	0.85	0.78	0.72	0.56	0.46
	Man/Xyl C_1	97.1	-0.01	0.05	0.33	0.46	0.53	0.69	0.79	0.88	0.96	1.00	0.98	0.86	0.79	0.71	0.53	0.43
	Gal C_1	98.2	0.00	0.12	0.58	0.80	0.83	1.00	1.00	0.97	0.96	0.95	0.91	0.83	0.75	0.69	0.57	0.49
	Man/Rha/Xyl/Rha/Glc C_1	100.2	0.02	0.09	0.47	0.63	0.74	0.87	0.92	0.96	0.98	1.00	0.98	0.90	0.84	0.79	0.65	0.56
	Man/Gal C_1	103.6	-0.01	0.04	0.29	0.37	0.62	0.79	0.88	0.99	0.98	1.00	0.94	0.82	0.70	0.62	0.46	0.32
	Ara C_1	109.4	-0.02	0.09	0.46	0.69	0.89	0.93	1.00	1.00	0.98	0.96	0.97	0.92	0.81	0.74	0.64	0.57
	Ara C_1	108.5	-0.01	0.08	0.45	0.66	0.82	0.96	1.00	0.94	0.94	0.93	0.88	0.79	0.73	0.65	0.52	0.43

Supplementary Table 19. ^{13}C resonance CP intensity build-up in *C. reinhardtii*'s starch. Resonance-specific ^{13}C intensity build-up as a function of cross-polarization (CP) time in starch purified from *C. reinhardtii* [15]. Assignments are given as described before[15].

		^{13}C δ (ppm) \ CP (ms)	**0.01**	**0.025**	**0.05**	**0.075**	**0.1**	**0.25**	**0.5**	**0.75**	**1**	**2**	**3**	**5**
C. reinhardtii A-type starch	C1 am	102.6	0.12	0.29	0.52	0.83	1.00	1.00	1.00	0.76	0.72	0.60	0.56	0.48
	C1a	101.2	0.13	0.36	0.60	0.92	0.97	0.94	1.00	0.97	0.96	0.92	0.86	0.80
	C1b	100.6	0.12	0.33	0.57	0.86	1.00	0.96	0.96	0.93	0.96	0.93	0.87	0.81
	C1c	99.5	0.12	0.33	0.55	0.87	1.00	0.93	0.98	0.89	0.88	0.87	0.82	0.76
	C4 am	80.8	0.14	0.34	0.53	0.80	0.98	1.00	0.90	0.84	0.71	0.60	0.54	0.47
	C3	75.4	0.12	0.33	0.56	0.85	1.00	0.97	0.99	1.00	0.97	0.87	0.77	0.71
	C3	74.1	0.11	0.30	0.54	0.82	1.00	0.97	0.97	0.94	0.91	0.80	0.72	0.68
	C5	72.1	0.10	0.28	0.48	0.76	0.92	1.00	0.99	0.92	0.93	0.86	0.81	0.74
	C6	61.7	0.12	0.31	0.53	0.80	0.93	0.97	1.00	0.93	0.93	0.86	0.77	0.69

Supplementary Table 20. List of experiments performed in this work and acquisition time. Key parameters used for acquisition are also presented.

	Interest	Technique	Temperature (K)	Spinning frequency (kHz)	Initial polarization	Experiment	Mixing time	Recycling delay (s)	Number of scans	Number of increments	Total time (h)
Cell-wall extract	Composition & Structure	ssNMR 800 MHz	283	13.5	DP	INADEQUATE + THALOS^{+}		2	64	350	12.6
	Dynamics & dynamic filters	ssNMR 600 MHz	293	15	CP	^{13}C $T_{1\rho}$ (us)		3	32	12	0.3
					CP	^{1}H $T_{1\rho}$ (us)		3	32	12	0.3
					DP	^{13}C T_{1} (us)		10	32	17	1.5
					CP	^{1}H T_{1} (us)		10	32	19	1.7
		ssNMR 800 MHz	283	13.5	DP	1D DP 30s		30	128		0.0
					DP	1D DP 2 s		2	128		0.0
					CP	1D CP		2	128		0.0
					INEPT	1D INEPT		4	128		0.0
					CP	INADEQUATE		1.5	64	200	5.4
					CP	DARR		1.75	32	600	9.4
		ssNMR 600 MHz	293	15	CP	DARR	25 ms	2.5	64	256	11.4
					CP	PDSD	250 ms	2.5	32	256	5.7
					CP	DARR	300 ms	3	32	256	6.9
					CP	PDSD	1 s	3	32	256	6.9
					long CP (10 ms)	PDSD	1 s	3	32	256	6.9
					long CP (10 ms)	DARR	300 ms	3	32	256	6.9
					CP + ^{13}C $T_{1\rho}$ filter	DARR	25 ms	3	64	256	13.7
					CP + ^{13}C $T_{1\rho}$ filter	PDSD	250 ms	3	69	256	14.8
		ssNMR 600 MHz at cryogenic temperature	98	8	CP	DARR	50 ms	2.86	16	512	6.6
	Deglycosylation	ssNMR 600 MHz	278	15	CP	DARR	50 ms	2.5	64	256	11.4

	Hydration	ssNMR 800 MHz	283	13.5	CP	DARR	50 ms	1.75	32	600	9.4
					CP & water edition	DARR	50 ms	1.75	32	600	9.4
	Protein-glycan contacts	MAS-DNP 600 MHz □w on	100	8	CP	DARR	50 ms	2.86	16	512	6.6
					CP	PDSD	1.5 s	2.86	16	400	5.1
					DP	INADEQUATE		2.99	16	533	7.1
					CP	NCa	0	2.8	16	533	6.7
					CP	NCaCx	100 ms	2.8	16	533	6.7
		ssNMR 800 MHz	283	13.5	CP	NCa	0	1.5	48	180	3.6
					CP	NCaCx	100 ms	1.5	48	180	3.6
		ssNMR 600 MHz	278	15	CP	DARR	300 ms	3	32	256	6.9
					CP	PDSD	1 s	3	32	256	6.9
Whole cell	Composition	ssNMR 800 MHz	283	13.5	DP	INADEQUATE		2	64	350	12.6
	Dynamic filters				CP	INADEQUATE		1.5	64	200	5.4
	Structure				CP	DARR	50 ms	1.75	32	600	9.4
	Hydration				CP & water edition	DARR	50 ms	1.75	32	600	9.4
	Structure	MAS-DNP 600 MHz □w on	100	8	CP	DARR	50 ms	2.86	16	512	6.6

Supplementary Table 21. List of replicates used for ssNMR in this study. All the replicates showed identical overall composition and architecture based on 1D experiments (DP with 2 and 30 s recycling delay, CP and INEPT pulse sequences) that were ran on all the samples. Replicates consist in different cell culture leading to different cell-wall extracts. It must be noted that part of each culture was kept before cell-wall extraction for whole cell monitoring. Interestingly, cell-wall extraction done on cw15 cell-wall deficient strain did not give any material after dialysis.

Strain used for cell-wall extracts	Number of biological replicates
Wild-type (CC-124)	6
Wild-type - deglycosylated	2
Flagella deficient bald2	6
Flagella deficient bald2 - deglycosylated	2
Cell-wall deficient cw15	2 (no cw extract)
Mating types CC-124 (“mt+”)	2
Mating types CC-125 (“mt-”)	2
Starchless sta 6-1	2

References

1. Vila, J. A. & Arnautova, Y. A. in *Computational Methods to Study the Structure and Dynamics of Biomolecules and Biomolecular Processes: From Bioinformatics to Molecular Quantum Mechanics* (ed Adam Liwo) 659-698 (Springer International Publishing, 2019).
2. Fujiwara, K., Toda, H. & Ikeguchi, M. Dependence of α-helical and β-sheet amino acid propensities on the overall protein fold type. *BMC Struct. Biol.* **12**, 18 (2012).
3. Ferris, P. J. *et al.* Glycosylated polyproline II rods with kinks as a structural motif in plant hydroxyproline-rich glycoproteins. *Biochemistry* **40**, 2978-2987 (2001).
4. Homer, R. B. & Roberts, K. Glycoprotein conformation in plant cell walls : circular dichroism reveals a polyproline II structure. *Planta* **146**, 217-222 (1979).
5. Voigt, J. & Frank, R. 14-3-3 proteins are constituents of the insoluble glycoprotein framework of the *Chlamydomonas* cell wall. *Plant Cell* **15**, 1399-1413 (2003).
6. Shen, Y., Delaglio, F., Cornilescu, G. & Bax, A. TALOS+: a hybrid method for predicting protein backbone torsion angles from NMR chemical shifts. *J. Biomol. NMR* **44**, 213-223 (2009).
7. Schäler, K. *Low-fiield NMR studies of structure and dynamics of semicrystalline polymers* Doctoral thesis thesis, Martin-Luther-Universität Halle-Wittenberg, (2013).
8. Mathieu-Rivet, E., Mati-Baouche, N., Walet-Balieu, M.-L., Lerouge, P. & Bardor, M. N- and O-glycosylation pathways in the microalgae polyphyletic group. *Front. Plant Sci.* **11** (2020).
9. Lesage, A., Sakellariou, D., Steuernagel, S. & Emsley, L. Carbon−proton chemical shift correlation in solid-state NMR by through-bond multiple-quantum spectroscopy. *J. Am. Chem. Soc.* **120**, 13194-13201 (1998).
10. Gao, Y., Lipton, A. S., Wittmer, Y., Murray, D. T. & Mortimer, J. C. A grass-specific cellulose–xylan interaction dominates in sorghum secondary cell walls. *Nat. Commun.* **11**, 6081 (2020).
11. Simmons, T. J. *et al.* Folding of xylan onto cellulose fibrils in plant cell walls revealed by solid-state NMR. *Nat. Commun.* **7**, 13902 (2016).
12. Zhao, W. *et al.* Solid-state NMR of unlabeled plant cell walls: high-resolution structural analysis without isotopic enrichment. *Biotechnol. Biofuels* **14**, 14 (2021).
13. Kirui, A. *et al.* Carbohydrate-aromatic interface and molecular architecture of lignocellulose. *Nat. Commun.* **13**, 538 (2022).
14. Kang, X. *et al.* Molecular architecture of fungal cell walls revealed by solid-state NMR. *Nat. Commun.* **9**, 2747 (2018).
15. Poulhazan, A., Arnold, A. A., Warschawski, D. E. & Marcotte, I. Unambiguous *ex situ* and in Cell 2D ^{13}C solid-state NMR characterization of starch and its constituents. *Int. J. Mol. Sci.* **19**, 3817 (2018).
16. Poulhazan, A. *et al.* Identification and quantification of glycans in whole cells: architecture of microalgal polysaccharides described by solid-state nuclear magnetic resonance. *J. Am. Chem. Soc.* **143**, 19374-19388 (2021).
17. Gorin, P. A. J. & Mazurek, M. Further Studies on the Assignment of Signals in ^{13}C Magnetic Resonance Spectra of Aldoses and Derived Methyl Glycosides. *Can. J. Chem.* **53**, 1212-1223 (1975).
18. Bradbury, J. H. & Jenkins, G. A. Determination of the structures of trisaccharides by ^{13}C-n.m.r. spectroscopy. *Carbohydr. Res.* **126**, 125-156 (1984).
19. Lundborg, M. & Widmalm, G. Structural analysis of glycans by NMR chemical shift prediction. *Anal. Chem.* **83**, 1514-1517 (2011).
20. Hwang, J.-H. *et al.* Photoautotrophic hydrogen production by eukaryotic microalgae under aerobic conditions. *Nat. Commun.* **5**, 3234 (2014).
21. White, P. B., Wang, T., Park, Y. B., Cosgrove, D. J. & Hong, M. Water–polysaccharide interactions in the primary cell wall of *Arabidopsis thaliana* from polarization transfer solid-state NMR. *J. Am. Chem. Soc.* **136**, 10399-10409 (2014).
22. Phyo, P. *et al.* Gradients in wall mechanics and polysaccharides along growing inflorescence stems. *Plant Physiol.* **175**, 1593 (2017).
23. Rondeau-Mouro, C., Buléon, A. & Lahaye, M. Caractérisation par RMN des biopolymères d'origine végétale, de la molécule à l'organisation supramoléculaire. *Comptes rendus Chimie* **11**, 370-379 (2008).
24. King, C., Stein, R. S., Shamshina, J. L. & Rogers, R. D. Measuring the purity of chitin with a clean, quantitative solid-state NMR method. *ACS Sustain. Chem. Eng.* **5**, 8011-8016 (2017).
25. Habibi, Y., Heyraud, A., Mahrouz, M. & Vignon, M. R. Structural features of pectic polysaccharides from the skin of *Opuntia ficus*-indica prickly pear fruits. *Carbohydr. Res.* **339**, 1119-1127 (2004).

26. Laguri, C. *et al.* Solid State NMR Studies of Intact Lipopolysaccharide Endotoxin. *ACS Chem. Biol.* **13**, 2106-2113 (2018).
27. Pfeffer, P. E., Hicks, K. B., Frey, M. H., Opella, S. J. & Earl, W. L. Complete solid state ^{13}C NMR chemical shift assignments for α-D-glucose, α-D-glucose-H_2O and β-D-glucose. *J. Carbohydr. Chem.* **3**, 197-217 (1984).